

Theses and dissertations

1-1-2003

Energy absorption of composite materials under high velocity impact

Ramin Amid
Ryerson University

Follow this and additional works at: <http://digitalcommons.ryerson.ca/dissertations>



Part of the [Mechanical Engineering Commons](#)

Recommended Citation

Amid, Ramin, "Energy absorption of composite materials under high velocity impact" (2003). *Theses and dissertations*. Paper 34.

In compliance with the
Canadian Privacy Legislation
some supporting forms
may have been removed from
this dissertation.

While these forms may be included
in the document page count,
their removal does not represent
any loss of content from the dissertation.

ENERGY ABSORPTION OF COMPOSITE MATERIALS UNDER HIGH VELOCITY IMPACT

By

Ramin Amid
Bachelor of Mechanical Engineering
Ryerson University, Canada, May 2001

A thesis
Presented to Ryerson University
In partial fulfillment of the
Requirement for the degree of
Master of Applied Science
In the program of
Mechanical Engineering

Toronto, Ontario, Canada, 2003

©(Ramin Amid) 2003



National Library
of Canada

Acquisitions and
Bibliographic Services

395 Wellington Street
Ottawa ON K1A 0N4
Canada

Bibliothèque nationale
du Canada

Acquisitions et
services bibliographiques

395, rue Wellington
Ottawa ON K1A 0N4
Canada

Your file Votre référence

ISBN: 0-612-87148-7

Our file Notre référence

ISBN: 0-612-87148-7

The author has granted a non-exclusive licence allowing the National Library of Canada to reproduce, loan, distribute or sell copies of this thesis in microform, paper or electronic formats.

L'auteur a accordé une licence non exclusive permettant à la Bibliothèque nationale du Canada de reproduire, prêter, distribuer ou vendre des copies de cette thèse sous la forme de microfiche/film, de reproduction sur papier ou sur format électronique.

The author retains ownership of the copyright in this thesis. Neither the thesis nor substantial extracts from it may be printed or otherwise reproduced without the author's permission.

L'auteur conserve la propriété du droit d'auteur qui protège cette thèse. Ni la thèse ni des extraits substantiels de celle-ci ne doivent être imprimés ou autrement reproduits sans son autorisation.

Canada

I hereby declare that I am the sole author of this thesis.

I authorize Ryerson University to lend this thesis to other institutions or individuals for the purpose of scholarly research.

Signature

I further authorize Ryerson University to reproduce this thesis by photocopying or by other means, in total or in part, at the request of other institutions or individuals for the purpose of scholarly research.

Signature

Ryerson University requires the signatures of all persons using or photocopying this thesis. Please sign below, and give address and date.

ABSTRACT

Energy Absorption of Composite Materials Under High Velocity Impact

©Ramin Amid, 2003

Master of Applied Science

In the program of

Mechanical Engineering

Ryerson University

Many studies were directed toward understanding damage patterns in composite laminates and determining the damage development sequence upon high velocity impact. Damage accumulation depends on projectile velocity and on a number of other parameters, so that it is not possible to set strict limits between the different regimes. However, experiments show that, for a given set of experimental conditions where the impact speed is the only variable, there is a certain threshold velocity below which no detectable damage occurs. Above the threshold velocity, no surface damage is observed except for a small indentation at the contact point, but significant internal damage consisting of delamination and matrix cracks is introduced. As the impact velocity increases further, surface damage due mainly to fiber breakage is introduced. For very high speeds, the target does not have time to deform, and perforation occurs, leaving a clean hole in the sample.

The objective of this study is to develop a mathematical model that corresponds to the deformed geometry under high velocity impact applications for composite laminates. A total of 100 tests were conducted on composite laminates, struck by cylindro-hemispherical projectiles at normal incidents with velocities up to about 100 m/s. The

types of materials, used in this study, are AS4/3051, IM7/5250 Carbon/Epoxy and T1003 Glass/Epoxy. The strain energy was obtained by derivation of the proposed deflection function. The strain energy was plotted with respect to the deflection of the mid-plane and, then correlated through dynamic correlation factors to the actual kinetic energy during the impact. The dynamic correlation factors were determined using a genetic algorithm regression analysis. Two types of materials were tested, namely plain graphite composites and hybrid composites. The growth of the delamination and also the effect of varying the stacking sequence were investigated for the different type of materials and various orientations.

The mathematical model appears to provide a reasonable representation of the deformation of composite laminates during the penetration by a cylindro-hemispherical projectile. Furthermore, hybrid composites appear to provide more resistance to the impact, whereas plain composites have less resistance with respect to the higher velocities. It was concluded that, the change of the material in a hybrid composite affects the growth of the damaged area and also reduces the impact penetration resistance. Hence, IM7/E-Glass hybrid has a higher resistance to the penetration. Measurements of the energy levels of the hybrid composites indicated that they offer the highest resistance to ballistic perforation. The hybrid composites perforated at velocities between 77 m/s and 83 (m/s), whereas the graphite composites perforated at velocities between 48 m/s and 59 (m/s). The higher perforation resistance is attributed to the reduced level of delamination generated during the impact, and also the addition of the E-Glass, which was capable of absorbing more energy during the impact.

In studying the graphite composites, the best orientation in terms of the stacking sequence was found to be $[(45, -45, 0, 90)_2]_S$, which indicates that this stacking sequence withstand higher velocity and hence absorbs more energy during the impact. . Therefore, the quasi-isotropic orientation $[(45, -45, 0, 90)_2]_S$ is best for impact resistance if a laminate is not combined with E-Glass. The ballistic-limit velocity prior to perforation for the Quasi-isotropic laminate was measured as 58.9 m/s. This is a significant increase compared to the other plain graphite samples. The energy required for the complete perforation is approximately 48 % higher in this stacking sequence as compared to other plain Graphite specimens. It was also found that the energy absorption capability is reduced significantly in the cross-ply laminates. The penetration resistance of the $[(0,90,0,90)_2]_S$ laminate and the energy required for perforation are approximately 50 % less than the other plain graphite specimens.

ACKNOWLEDGMENTS

I would like to express my sincere thanks to all of the people who have assisted me in my efforts towards receiving a Master's degree at Ryerson University.

I am grateful to Dr. Fawaz, my advisor, for his support and for giving me the opportunity to perform this work. I wish to thank him for his confidence in me which was reflected in his flexibility, his willingness to let me decide the direction of this research, and to pursue it in a manner that I felt most suitable. I would also like to express my gratitude towards my co-advisor, Dr. Behdinan. I appreciate the time, useful suggestions and comments he gave me that helped me performing the work that led to this study.

I owe so many thanks to Mr. Ghaemi who has always been willing to provide assistance, give advice, and be a friend. I appreciate the time he invested in advising me and for his openness, honesty, and sincerity. I am especially indebted to him for his support and willingness to create a suitable test facility, for this study.

TABLE OF CONTENTS

page

AUTHOR'S DECLARATION.....	ii
BORROWER'S PAGE.....	iii
ABSTRACT.....	iv
ACKNOWLEDGEMENT.....	vii
TABLE OF CONTENTS.....	viii
LIST OF TABLES	xii
LIST OF FIGURES.....	xiii
NOMENCLATURE.....	xv
CHAPTER 1.....	1
INTRODUCTION.....	1
1.1 Motivation.....	1
1.2 Objective.....	4
CHAPTER 2	5
HIGH/LOW VELOCITY IMPACT REVIEW.....	5
2.1 Low Velocity Impact of Graphite Composites.....	5
2.1.1 Low Velocity Damage Mechanisms.....	5
2.1.2 Low Velocity Impact Test Methods.....	6
2.1.2.1 Charpy and Izod Pendulum Impact Tests.....	6
2.1.2.2 Drop weight Impact Tests.....	7
2.1.2.3 Hydraulic Test Machines.....	7
2.2 Improving Low Velocity Impact Damage Resistance.....	7
2.3 High Velocity and Ballistic Impact of Graphite Composites.....	9
2.3.1 Localization Effect.....	10
2.3.2 Damage Mechanism and Penetration Process.....	10
2.3.3 Effect of Stacking Sequence.....	11
2.3.4 Projectile Effects at High and Ballistic Velocities.....	11
2.3.5 Residual Strength vs. Resistance Penetration.....	12

2.3.6 Failure Modes.....	13
2.3.7 Prediction of Ballistic Limit.....	14
2.3.8 High and Ballistic Velocity Impact Test Methods.....	15
2.3.8.1 Projectile Acceleration Devices.....	15
2.3.8.2 Type of Projectiles.....	16
2.3.8.3 Method of Analysis.....	17
2.4 Improving High and Ballistic Velocity Impact Damage Resistance.....	18
 CHAPTER 3.....	21
MECHANICS OF COMPOSITE MATERIAL.....	21
3.1 Classical Lamination Theory.....	21
3.1.1 Introduction.....	21
3.1.2 Development of the Theory.....	21
3.1.3 Notation.....	22
3.1.4 Stiffness of Specific Laminate Configuration.....	26
3.1.5 Mid plane Symmetric Laminates.....	27
3.1.6 Aligned and Off-Axis Parallel-Ply Laminates.....	27
3.1.7 Cross-Ply Laminates.....	28
3.1.8 Angle-Ply Laminates.....	28
3.1.9 Quasi-Isotropic Laminates.....	29
3.1.10 $[0_m / \pm \theta_n]_s$ Laminates.....	29
 DYNAMICS OF COMPOSITE MATERIAL.....	30
3.2 Introduction.....	30
3.2.1 Energy Balanced Models.....	30
3.2.2 Assumed Force or Initial Condition.....	32
3.2.3 Wave Propagation.....	33
 EFFECT OF MATERIAL PROPERTIES.....	34
3.3.1 Effect of Matrix Properties.....	35
3.3.2 Effect of Fiber Properties.....	35
3.3.3 Effect of Fiber-Matrix Interface.....	36
3.3.4 Effect of Stacking Sequence.....	36

CHAPTER 4.....	38
FABRICATION AND TESTING APPARATUS	38
4.1 Fabrication of Composite Plate.....	38
4.2 Step-by-step Laminate Lay-up.....	40
4.3 Curing Laminated Plates.....	42
4.4 Manufacturing, Calibration and Testing of Projectile Machine.....	44
CHAPTER 5.....	48
EXPERIMENTAL PROCEDURE.....	48
5.1 Introduction.....	48
5.2 Experimental Setup and Test Procedure.....	48
5.3 High -Speed Camera.....	51
5.4 Experimental Measurements.....	54
5.5 Projectiles.....	54
CHAPTER 6.....	55
EXPERIMENTAL RESULTS.....	55
6.1 Introduction.....	55
6.2 AS-4 Results.....	55
6.3 HYBRID Results.....	60
CHAPTER 7.....	66
DEVELOPMENT OF THE MATHEMATICAL MODEL.....	66
7.1 Mathematical Model of Deformed Geometry.....	66
7.2 Dynamic Correlation to Static Properties.....	71
CHAPTER 8.....	81
DISCUSSION AND RECOMMENDATIONS.....	81
8.1 Discussion.....	81
8.2 Recommendations.....	84

REFERENCES.....	85
APPENDIX A Matlab Program.....	92
APPENDIX B Derivation of Deflection Function.....	94
APPENDIX C Classical Lamination Theory.....	102

LIST OF TABLES	page
Table 4.1: Specified loads and pressures for fabrication.....	40
Table 4.2: Stacking Sequence and Orientation.....	41
Table 4.3: Bursting Pressure of Diaphragm.....	45
Table 6.1: Experimental results for $[(45, -45, 0, 0)_2]_S$ laminate.....	56
Table 6.2: Experimental results for $[(0, 0, 45, -45)_2]_S$ laminate.....	56
Table 6.3: Experimental results for $[(0, 45, -45, 0)_2]_S$ laminate.....	57
Table 6.4: Experimental results for $[(45, -45, 0, 90)_2]_S$ laminate.....	57
Table 6.5: Experimental results for $[(45, -45, 90, 0)_2]_S$ laminate.....	58
Table 6.6: Experimental results for $[(0, 90, 0, 90)_2]_S$ laminate.....	58
Table 6.7: Experimental results for $[(45, -45, 45, -45)_2]_S$ laminate.....	59
Table 6.8: Experimental results for $[(45, -45, 0, 90)_2]_S$ laminate.....	60
Table 6.9: Experimental results for $[(45, -45, 90, 0)_2]_S$ laminate.....	61
Table 6.10: Experimental results for $[(-45, 45, 90, 0)_2]_S$ laminate.....	61
Table 6.11: Experimental results for $[(0, 90, 0, 90)_2]_S$ laminate.....	62
Table 6.12: Experimental results for $[(0, 90, 0, 90)_2]_S$ laminate.....	63
Table 6.13: Experimental results for $[(90, 0, 45, -45)_2]_S$ laminate.....	63
Table 6.14: Experimental results for ballistic limit velocity.....	65
Table 7.1: Comparisons of the strain energy and kinetic energy for AS4 Plain Graphite.....	69
Table 7.2: Comparisons of the strain energy and kinetic energy for AS4/E-Glass.....	70
Table 7.3: Comparisons of the strain energy and kinetic energy for IM7/E-Glass.....	71
Table 7.4: Correlation factors for different stacking sequences.....	73

LIST OF FIGURES	page
Figure 3.1: Laminate coordinates	22
Figure 4.1: Compression mold setup.....	39
Figure 4.2: Laminate manufacturing assembly.....	39
Figure 4.3: Cure-cycle for composite laminate.....	43
Figure 4.4: Gas gun.....	47
Figure 5.1: Holding fixture.....	49
Figure 5.2: Target laminate and impact point.....	50
Figure 6.1: AS4 Laminated plate after impact.....	59
Figure 6.2: AS4/E-Glass Laminated plate after impact.....	62
Figure 6.3: IM7/E-Glass Laminated plate after impact.....	64
Figure 7.1: The assumed deform geometry.....	66
Figure 7.2: Energy comparisons for analytical and experimental for AS4 Plain graphite	74
Figure 7.3: Energy comparisons for analytical and experimental for AS4 Plain graphite	74
Figure 7.4: Energy comparisons for analytical and experimental for AS4 Plain graphite	75
Figure 7.5: Energy comparisons for analytical and experimental for AS4 Plain graphite	75
Figure 7.6: Energy comparisons for analytical and experimental for AS4 Plain graphite	76
Figure 7.7: Energy comparisons for analytical and experimental for AS4 Plain graphite composite.....	76
Figure 7.8: Energy comparisons for analytical and experimental of AS4 Plain graphite.....	77
Figure 7.9: Energy comparisons for analytical and experimental for AS4/Eglass hybrid	78
Figure 7.10: Energy comparisons for analytical and experimental for AS4/Eglass hybrid	78
Figure 7.11: Energy comparisons for analytical and experimental for	

AS4/Eglass hybrid 78

Figure 7.12: Energy comparisons for analytical and experimental for
AS4/Eglass hybrid 79

Figure 7.13: Energy comparisons for analytical and experimental for
IM7/Eglass hybrid 79

Figure 7.14: Energy comparisons for analytical and experimental for
IM7/Eglass hybrid 80

NOMENCLATURE

θ : Fiber angular orientation

t : Thickness of the layer

$2h$: Total laminate thickness

$\varepsilon_1, \varepsilon_2$: Normal in-plane strains

ε_6 : Shear in-plane strain

$\varepsilon_1^0, \varepsilon_2^0$: Normal mid-plane strains

ε_6^0 : Shear mid-plane strain

κ_1, κ_2 : Bending curvatures

κ_6 : Twisting curvatures

σ_k : Component of stress tensor

$\overline{Q_{ij}}$: Transformed reduced stiffness matrix

C_{ij} : Components of the reduced stiffness matrix

ν_{ij} : Poisson's ratios

N_1, N_2 : In-plane normal forces

N_6 : In-plane shear force

M_1, M_2 : Bending moments

M_6 : Twisting moment

A_{ij} : Components of stretching stiffness

B_{ij} : Components of bending-stretching coupling stiffness

D_{ij} : Components of bending stiffness

N^T : Thermal stretching

M^T : Thermal bending

N^M : Moisture-induced stretching

M^M : Moisture-induced bending

$\bar{\alpha}$: Transformed thermal-expansion coefficient

$\bar{\beta}$: Moisture-expansion coefficient
 ΔC : Moisture change
 ΔT : Temperature change
 n : Total number of layers for the laminated plate
 V : Velocity of the projectile
 m : Mass of the projectile
 E_b : Energy absorbed due to bending
 E_s : Energy absorbed due to shear
 E_m : Energy absorbed due to membrane
 E_c : Energy stored during contact
 P : Contact force during impact
 K_{bs} : Linear stiffness including bending and shear
 K_m : Membrane stiffness
 W : Deflection at the impact point
 α : Relative motion or indentation of structure by the projectile
 W_{\max} : Maximum displacement at the impact location
 α_{\max} : Maximum indentation
 F_0 : Maximum force due to impact
 t_0 : Time at which force becomes maximum
 T : Contact time duration
 G : Shear modulus
 p : Concentrated load
 w : Deflection of the clamped plate
 w_o : Mid-plane deflection of the clamped plate
 a : Semi-major axis for the ellipse
 b : Semi-minor axis for the ellipse
 U : Strain energy of the clamped plate
 c_1, c_2 : Dynamic correlation factors

[A]: Extensional stiffness matrix

[D]: Bending stiffness matrix

[B]: Coupling between extensional and bending stiffness matrix

CHAPTER 1

INTRODUCTION

1.1 MOTIVATION

As composite materials are used more extensively, a constant source of concern is the effect of foreign object impacts. Such impacts can reasonably be expected during the life of the structure and can result in internal damage that is often difficult to detect and can cause severe reductions in the strength and stability of the structure. Internal damage is more difficult to detect when low velocity impact has occurred. This concern provided the motivation for intense research resulting in hundreds of journals and conference articles. Important advances have been made, and many aspects of the problem have been investigated.

During the life of the structure, impacts by foreign objects can be expected to occur during manufacturing, service, and maintenance operations. During the manufacturing process or during maintenance, tools can be dropped on the structure. In this case, impact velocities are small but the mass of the projectile is relatively large. Laminated composite structures are more susceptible to impact damage than similar metallic structures. In composite structures, impacts create internal damage that often cannot be detected by visual inspection. This internal damage can cause severe reductions in strength and can grow progressively under load. Therefore, the effects of foreign object impacts on composite structures must be understood, and proper measures should be taken in the design process to account for these unexpected events.

Different test apparatuses are used to simulate various types of impact. Drop-weight testers are used to simulate low-velocity impacts typical of tool-drop problems in which a large object falls onto the structure with a relative low velocity. Air-gun systems, in which a small projectile is propelled at high speeds, are used to simulate the type of impacts encountered during the aircraft takeoffs and landings. Testing conditions should replicate the actual impact

that the structure is designed to withstand, and so the choice of the proper test apparatus procedures is important.

Sometimes the expression "high velocity impact" refers to impact resulting in complete perforation of the target. However, it must be recognized that complete perforation can be achieved both under low-velocity impacts when overall deflections of the target are taking place and under high-velocity impacts when the deformations of the target are localized in a small region near the point of the impact. Here, high-velocity impacts are defined so that the ratio between impact velocity and the velocity of compressive waves propagating through the thickness is larger than the maximum strain to failure in that direction. Thus, within the context of high-velocity impact, this implies that damage is introduced during the first few travels of the compressive wave through the thickness when overall plate motion is not yet established (Abbate) [1]. In addition, for high-velocity impact, the ballistic limit is defined as the initial velocity of the projectile that results in complete penetration of the target with zero residual velocity. For impact velocities above the ballistic limit, the residual velocity of the projectile is also of interest. General trends for ballistic impacts (including the effect of several important parameters) are obtained from experimental results, and models for predicting the ballistic limit are available.

Impact damage consists of delaminations, matrix cracking, and fiber failure for both high and low velocity impacts. Extensive experimental investigations have revealed definite patterns for the shape of the damage and its initiation and growth. It is generally accepted that during low-velocity impacts, damage is initiated by matrix cracks, which create delaminations at interfaces between plies with different fiber orientations. For low velocity impact situations involving stiff structures, matrix cracks start on the impacted face of the specimen due to high contact

stresses. Damage propagates downward by a succession of intra-ply cracks and interface delaminations to give what is called a pine-tree pattern. For thin specimens, bending stresses cause matrix cracking in the lowest ply, and damage progresses from the non impacted face up toward the projectile giving a reverse pine-tree appearance. The delaminated area at an interface depends on the fiber orientations in the plies adjacent to the interface. Of the large number of experimental methods that have been developed for damage assessment, some result in the complete destruction of the specimen and others are nondestructive, but most methods are used to determine the state of the damage after impact. Once the failure modes involved are known and methods to assess the damage are available, the next task is to determine what the governing parameters are. The properties of the matrix, the reinforcing fibers, and the fiber-matrix interfaces affect impact resistance in several ways, along with effects of lay-up, thickness, size, boundary conditions, and the shape, mass, and the velocity of the projectile. The prediction of impact damage is a difficult task for which complete success may not be possible and is probably not necessary. A large number of matrix cracks and delaminations are created in the impact zone, and the introduction of each new crack creates a redistribution of stresses. Thus it is not realistic to attempt to track every detail of damage development during the dynamic analysis of the impact event. In low velocity impact, purely qualitative models explain the orientation and size of delaminations at the various interfaces through the thickness of the laminates. In high velocity impact, models predict the onset of delaminations by predicting the appearance of the first matrix crack.

1.2 OBJECTIVE

The primary objective of this research is to investigate methods for improving the high velocity impact penetration resistance of advanced composite laminates. In particular, this study examines the high-energy impact resistance of such laminates as a function of their stacking sequence. For this purpose, three types of materials were used and their behaviors with respect to impact resistance were investigated. The two types of carbon fiber materials were AS4/3051 and IM7/5250 manufactured by HEXCEL. In addition, E-Glass/epoxy T1003 manufactured by 3M was also considered in this study. The primary use of the Glass epoxy was to fabricate hybrid laminates with the AS4 or IM7 laminates.

To partially fulfill the above objective, this study aims to develop a mathematical model that simulates the deformed geometry of the composite laminates as they undergo the high velocity impact. The proposed mathematical model aims to simulate the geometry of deformation of the impacted laminate, although the actual configuration is more complex due to the high degree of anisotropy in laminated composite plates. The strain energy associated with the impact will be obtained by derivation of the proposed model, calculated with respect to the deflection of the laminates, and then correlated to the actual kinetic energy during impact by introducing dynamic correlation factors for each laminate orientation. The effect of varying stacking sequences will also be investigated on the basis of sub-laminate delamination, mid-plane deflection, and energy absorption capability of the aforementioned materials.

CHAPTER 2

HIGH/LOW VELOCITY IMPACT REVIEW

2.1 LOW VELOCITY IMPACT OF GRAPHITE COMPOSITES

Considerable attention in the composite community has been given towards the effects of low velocity non-penetrating impact similar to that of a dropped tool, careless handling, or runway debris. This type of damage is most often undetectable by visual surface inspection (Choi and Chang) [2], and can cause a significant reduction of the compression strength. In previous studies, it has been shown that low energy impacts may significantly reduce the load carrying capability of composite component by as much as 50% (Cantwell et al., Cantwell et al., Dorey) [3,4,5].

2.1.1 LOW VELOCITY DAMAGE MECHANISMS

When traditional engineering materials such as steel and aluminum experience low velocity impact, the energy is typically absorbed through plastic deformation. Although this deformation is permanent, it usually does not significantly reduce the load carrying capability of the structure (Bradshaw et al.) [6].

Graphite composites however experience very little or no plastic deformation during low velocity impact because of the low strain to failure of the fiber and brittle nature of the epoxy matrix. Therefore, the impact energy is absorbed through various fracture processes. It has been well documented that the principal mechanisms for dissipating low velocity impact is through matrix cracking, delamination and fiber failure (Lagace and Wolf, Cantwell and Morton, Sierakowski and Chaturvedi) [7,8,9]. The extent of damage imposed by low velocity impact may be affected by the geometry and laminate configuration of the composite. Cantwell

and Morton [10] found a top surface contact initial failure in short thick composites and a lower surface flexural initial failure in long thin laminates. Based on a study by Choi et al. [11], it was concluded that a change of stacking sequence has a more significant influence on the impact damage than a change of thickness.

2.1.2 LOW VELOCITY IMPACT TEST METHODS

A wide variety of test methods for low velocity impact of composites have been used in the literature. Since most studies were for specific applications, it is often difficult to make adequate comparisons of results. The test methods most widely used include the Charpy pendulum, the Izod pendulum, the drop weight, and the hydraulic test machine.

2.1.2.1 CHARPY AND IZOD PENDULUM IMPACT TEST

The earliest methods used for low velocity impact testing were the Charpy pendulum (Novak and De Crescente) [12] and the Izod pendulum (Chamis et al.) [13]. Both methods were originally designed for the testing of metallic materials. The Charpy test consists of a swinging pendulum impacting the center of a thick beam supported at both ends with a notch at the mid-plane.

The Izod test is similar to the Charpy test except that the notch is near the fixed end of the specimen while the impactor strikes the free end of the specimen. The energy absorbed by the specimen is measured by the height of the swinging pendulum. The Charpy and Izod tests can provide a simple method to gain insight to a materials performance. It has been suggested that these two tests are suitable for the ranking the impact performance of various continues fiber

composites and as a first step in determining the dynamic toughness of these materials (Cantwell and Morton, Chamis et al.) [8,13].

2.1.2.2 DROP WEIGHT IMPACT TESTS

Another type of test used frequently is the drop weight impact test (Cantwell and Morton, a, b, c, a, b; Wang and Jang, Paine and Rogers) [10,14,15, 16,17,18,19]. As its name suggests, an impactor of specific weight is dropped from a predetermined height. Instrumented drop weight test machines that can measure the force versus time response make possible the study of the energy absorption through the different stages of specimen fracture. Also the drop weight test allows for a greater variety of specimen geometries, which is an advantage over the Charpy and Izod impact tests.

2.1.2.3 HYDRAULIC TEST MACHINES

More recently, composite material properties have been studied with hydraulic test machines (Gillespie et al.) [20]. Although an actual impact event does not occur, testing the specimen at high strain rates can be simulated. Extreme care must be taken when preparing the specimen and mounting it in the grips of the machine to prevent slippage at the clamped ends.

2.2 IMPROVING LOW VELOCITY IMPACT DAMAGE RESISTANCE

Since the early 1970's, researchers have been looking at various methods for improving the low velocity impact response of graphite composites. Oplinger and Slepetz [21] concluded that any attempt to improve impact behavior must confront the low strain capability of graphite composites. Either graphite fibers with higher strain to fracture must be developed, or

ways to reduce the local strain under the impacting object must be contrived'. The methods of improving the damage resistance of graphite composites due to low velocity impact can be divided into five major areas; fiber toughening, matrix toughening, interface toughening, through-the thickness reinforcement, and hybridizing.

Fiber toughening involves the use of graphite fibers developed with the higher strain to failure. The impact performance of this type of fiber has been evaluated with moderate success (Cantwell et al., Curtis) [4,22].

Several different approaches have been taken to toughen the matrix material. Although the stiffness of the composite is slightly reduced, one method of toughening the epoxy matrix is through the addition of rubber or thermoplastic compounds (Hedrick et al., Haung et al., Hunston et al., Williams and Rhodes) [23,24,25,26]. Replacing the epoxy with a high performance thermoplastic matrix with stiffness comparable to epoxy material known as polyetheretherketone (PEEK) has also exhibited a higher resistance to impact (Wang and Vukhanh) [27].

Since impact induced delamination occurs due to the graphite composites relatively low interlaminar strength, interface toughening through the use of adhesive layers has found success (Chan et al., Sun and Rechak, Bascom et al., Hoisington and Seferis) [28,29,30,31]. Because the additional adhesive layers may cause a great weight penalty, Rechak and Sun [32] demonstrated how the placement of adhesive layers can be optimized to obtain the greatest benefit in improving impact resistance.

Another method for decreasing the amount of delamination caused by low velocity impact is through-the-thickness reinforcements such as braiding, three dimensional weaving, and stitching (Jang and Chung, Su, Kang and Lee) [33,34,35]. Although significant delamination

reductions are achieved, these techniques are costly and degrade the in-plane properties due to fiber impalement.

Hybridizing graphite composites with additional tough high strain energy fibers have been shown to improve the damage tolerance due to low velocity impact (Jang et al., Wang and Jang) [36,18]. Fibers used in hybridizing include; S-Glass (Adams and Miller, Harris and Bunsell, Manders and Bader) [37,38,39], aramid known as Kevlar (Dorey et al., Wardle, Marom et al.) [40,41,42], and extended chain polyethylene known as Spectra (Cordova and Bhatnager, Poursartip et al.) [43,44]. The high strain capabilities of these fibers allow the impact energy to be spread over a wider area allowing the load to be shared by a greater volume of material. In most cases, however, the improved impact damage resistance is achieved at the expense of a reduction in the intended load bearing ability of the composite.

2.3 HIGH VELOCITY AND BALLISTIC IMPACT OF GRAPHITE COMPOSITES

Although some of the high and ballistic velocity impact damage mechanisms are similar to those at low velocity, the response of structure graphite composite is different and more complex. Furthermore, it is also more difficult to test at high and ballistic velocities. While most of the literature on the ballistic impact of composites is related to tougher, high strain materials such as aramids (Kevlar), S-glass, and high performance polyethylene (Spectra). A few important studies have been performed on graphite composites (Cantwell and Morton, a; Cantwell and Morton, b; Hsieh et al., Jenq et al.) [10,14,45,46]. An over view of the issue that makes the high and ballistic velocity impact different from low velocity impact will be presented.

2.3.1 LOCALIZATION EFFECT

As discussed previously, some of the low velocity impact energy may be absorbed through global bending of the composite allowing energy transfer to locations away from the point of impact. Since the contact time between the projectile and composite is considerably less at higher velocities, the impact loading includes a localized response with no global deformation. These two different types of impact suggested by (Cantwell and Morton) [14]. Cantwell and Morton [14] demonstrated this concept by looking at delaminations in beams of various lengths impacted at low and high velocities. It was found that the damage size decreased as the length of the beam increased when impacted at low velocities. At high impact velocities, the level of damage was independent of the length of the beam. It was also found that with a high specimen to mass ratio, the specimen boundary conditions have negligible effects on ballistic impact results. (Dikshit and Sundararajan) [47].

2.3.2 DAMAGE MECHANISM AND PENETRATION PROCESS

The entire high velocity projectile penetration process at higher impact velocities involves a combination of fiber shear (shear plug), matrix crack growth, delamination, and tensile fiber failure. The sequence of events for a cross-ply lay-up is described in great detail by Cristescu et al. [48], which will be summarized here. As discussed, upon impact of the first ply, the projectile energy is sufficient to cut the fibers in shear. This shear process continues in successive plies until the impact energy of the projectile is lowered to the point that the fibers can provide some resistance to shear. When this occurs, the fibers in contact with the projectile are pushed forward and this causes a line of matrix cracks within that ply to generate outward between fibers on either side of the projectile.

2.3.3 EFFECTS OF STACKING SEQUENCE

Several researchers have attempted to gain better understanding of the effects of stacking sequence on damage resistance. Hong and Liu [49] examined changes in the relative angle between fiber orientations of adjacent plies, for various ply angles. Hong and Liu [49] found that the delamination area would increase significantly with increasing ply angle. Strait et al. [50] compared the impact energy against the measured damage area for various woven, cross-ply and quasi-isotropic lay-ups. This work found that quasi-isotropic lay-ups contained the highest damage resistance capability. Hitchen and Kemp [51] performed a more systematic study of stacking sequence involving plies oriented at 0° , $\pm 45^\circ$, and 90° . The major conclusion was that placing the $\pm 45^\circ$ plies in the surface layers and increasing the number of interfaces within the laminate resulted in an increase in damage initiation energy. Finn et al. [52] studied the above effects as well as the effect of increasing the number of plies in the back-face ply group, and found that increasing the back-face ply group also increased the delamination size. In general, the laminate stacking sequence had two main effects: laminates with 0° outer plies were more weakened by delaminations than laminates with $\pm 45^\circ$ plies (Baker et al.) [53]; and generally, laminates woven $\pm 45^\circ$ plies showed improved delamination resistance from laminates unidirectional $\pm 45^\circ$ plies (Baker et al., Curtis and Bishop) [53,54].

2.3.4 PROJECTILE EFFECTS AT HIGH AND BALLISTIC VELOCITIES

At high and ballistic velocities, the action and characteristics of the penetrator have significant effects on test results. New issues that arise when testing at higher velocity schemes include; the shape and mass of the penetrator, the projectile deformation, and the spinning effects. Although the shape of penetrator can affect the degree of damage at all velocity ranges, the

shape effect is greater at high velocities. A sharp shape pointed projectile is going to penetrate further into a composite than a more relative rounded blunt projectile of larger diameter but equal mass. The blunt projectile, however, may cause significantly more damage to the composite whereas the pointed projectile may just pierce entirely through leaving only small hole. Jenq et al. [46] found that the momentum transfer to graphite/epoxy targets by blunt impactors is about four times greater than that of a tip ended penetrator when the penetrator is fired at ballistic velocities. The effect of varying the mass of the projectile while maintaining the same size and shape has been studied by Cantwell and Morton [15]. It was found that varying the mass of the projectile had a significant effect on the resulting damage to the composite. Cantwell and Morton [15] suggest that lighter projectiles are more damaging to the overall load-bearing capability of the composite because the incident energy is dissipated over a very small area immediately adjacent to the point of impact. Finally, for ballistic testing, most projectiles are fired from some type of test barrel. For stability reasons, the barrel is designed so that the projectile is spinning as it leaves the device. This causes a type of drilling action as the projectile impacts the specimen. Also, if the test barrel is close to the specimen, the projectile may not have time to stabilize causing its tip to penetrate at an angle.

2.3.5 RESIDUAL STRENGTH VS. RESISTANCE TO PENETRATION

A few high and ballistic velocity impact studies have been performed to characterize the structural strength after impact (also known as residual strength) of graphite/epoxy composites (Husman et al., Cantwell and Morton, Suarez and Whiteside) [55,17,56]. It has been found that for a given impactor type, the level of damage increases with increasing impact energy up to the penetration velocity (also known as the ballistic limit), at which point the projectile barely

perforates the target (Cantwell and Morton) [15]. It can be concluded that as the level of the damage increases, the structural strength of the composite after impact also decreases. However, at increasing impact energy levels greater than the penetration velocity, the level of damage decreases. It has been found that at velocities much greater than the perforation velocity, the hole in the material inflicted by the projectile produces the same reduction in residual strength as a hole with the same diameter that is cut or drilled out of the same material (Husman et al.) [55]. Therefore, when designing for greater strength after impact where projectile containment is not of a concern, a material formulated with the least resistance to penetration while maintaining the structural strength requirements would be desired.

2.3.6 FAILURE MODES

Failure during laminate penetration depends largely on the shape of the projectile, which strongly affects the perforation energy. In general, shear plugging occurs near the impacted side, followed by a region in which failure occurs by tensile fiber fracture, and near the exit, delaminations occurs. Depending on the target rigidity, impactor mass, and velocity, only a shear failure mode is observed, while in other cases, the first two modes are present, and for thicker targets all three modes are present. The penetration energy can be estimated by adding the energies required to produce each type of failure involved in the penetration process: fiber failure, matrix cracking, delamination, and friction between the projectile and the target. Which failures modes occur in a particular case depend on the laminate thickness and impact velocity and cannot yet be predicted.

Zee and Hsieh [57] designed experiments to determine how the energy lost during penetration of the laminate is partitioned into energy of penetration, and frictional energy. The contribution

of fiber failure, matrix cracking, delaminations, and friction between the projectile and the laminate are evaluated for several material systems. Delamination was a major factor for graphite/epoxy laminates but had only a minimum effect for laminates with Kevlar and polyethylene fibers. Sykes and Stoakley [58] showed that with graphite-epoxy laminates; cure conditions had a significant effect on the force-displacement relations during perforation. Initial fracture occurred at the same force level, but for specimens cured at 450° K, the force decreased linearly down to zero, which for a specimen cured at 394° K, the force continued to increase to about twice the value required for damage initiation and then decreased. The penetration energy, which is the area under the force-displacement curve, was obviously very different in the above two cases.

2.3.7 PREDICTION OF BALLISTIC LIMIT

Failure modes involved during the penetration of the target by the projectile can be different at different locations through the thickness. For simple cases where failure modes are known, simple energy consideration allows estimation of the ballistic limit. When perforation occurs in thin laminates, a conical-shaped perforation zone is observed (Cantwell) [14], starting with a diameter equal to that of the ball. The cone makes a 45° angle with respect to the impact direction, and extensive delaminations are observed. Zhu et al. [59] presented simple models to estimate the resistance to striker motion and to predict the ballistic limit of Kevlar-polyester plates. The event was divided into three consecutive phases: indentation, perforation, and exit. The global deflections were determined using laminated plate theory, and dissipative mechanism included the indentation of the striker tip, bulging at the back surface, fiber failure, delamination, and friction. Good agreement between predictions and experimental results was

obtained. Czarnecki [60] measured the transverse normal stress during high velocity impact of graphite-epoxy laminates at different locations through the thickness. These results indicated the presence of two pulses propagating at different velocities. Experiments by Zhu et al. [61] and others indicated that in the through-the-thickness direction, laminated composites have a non-linear stress-strain behavior for the strain levels obtained during impact. Prevorsek et al. [62] used a finite element model for simulating the deformation of a composite plate during ballistic impact, and a finite difference model for determining the temperature rise during the event. The analysis showed that a significant temperature rise occurs at the projectile-composite interface, but because of the short duration of the impact and the low thermal conductivity of the composite. This temperature rise is confined to a very small region around the interface and the volume of material affected is too small to have any effect on performance.

2.3.8 HIGH AND BALLISTIC VELOCITY IMPACT TEST METHODS

Several different approaches have been taken for the testing, evaluating of materials with respect to the impact at high and ballistic velocities. These aspects of ballistic evaluation testing include, projectile acceleration devices, types of projectiles used, and methods of analysis are presented.

2.3.8.1 PROJECTILE ACCELERATION DEVICES

In order to achieve speeds above 300 m/sec, a projectile is propelled through a device (gun) having a cylinder (barrel) slightly larger than its diameter. A compressed gas or a burning powder has been used as propellants. Projectiles fired from a gas gun are accomplished by

pressurizing a chamber containing a plastic diaphragm restricting gas flow (usually nitrogen) into the barrel. When a predetermined pressure is reached, the diaphragm is burst by electrical heating and the projectile is accelerated. Gas guns are generally used for high velocity testing at typical speeds ranging from 60 m/sec to 240 m/sec. However, velocities as high as 700 m/sec have been achieved with more sophisticated systems (Cantwell and Morton) [15].

Ballistic velocities of 340 m/sec or more is usually accomplished through use of a burning powder gun. The projectile is propelled using a powder that is explosive upon ignition. Velocity is controlled by using a pre-determined amount of charge. Extreme velocities as high as 2700 m/sec can be obtained (Husman et al.) [55].

2.3.8.2 TYPES OF PROJECTILES

As discussed previously, the characteristic of the projectile used may have significant effects on impact results. Projectiles used for high and ballistic velocity testing include machine steel cylinders and spheres, fragment simulated projectiles, and commercial ammunition.

Machined steel cylinders and spheres are often used for gas gun testing (Cantwell and Morton, b, c, a, b; Cristescu et al., Jenq et al.) [14,15,16,17,48,46]. They are used because they can easily be purchased or fabricated in machine shop to fit the dimensions of the test barrel. Projectile deformation is minimal, thus avoiding an additional test variable. The disadvantage of a machined steel projectile is that it may not adequately represent foreign threats one might be designing for.

As its name suggests, the fragment-simulated projectile (FSP) was developed by the U.S army in order to simulate metal fragments encountered in war. This type of projectiles usually fired from a powder-burning gun. This type of projectile has been used widely by military agencies

and personal armor manufactures for ballistic performance studies (Bhatnager et al., Kang and Lee, Lin and Bhatnager, Bless and Hartman) [63,64,65,66].

Commercially available ammunition is used for testing at ballistic velocities with a burning powder firing device (Lin et al.) [67]. Projectiles of this type are used because they are inexpensive, can be easily obtained, and in some cases may represent the exact type of threat one may be designing for. However, since most commercial ammunition is made of lead, projectile deformation and breakup may be of concern.

2.3.8.3 METHOD OF ANALYSIS

Several different methods of analysis have been used for impact testing at high and ballistic velocities, depending on the type of response desired for the particular threat one is designing for. The large variety of test methods presented in the literature is due to a lack of unified official testing standards, which can make the comparison of various results difficult. Test schemes to measure ballistic performance includes residual velocity, ballistic limit velocity, penetration depth, and instrumented techniques.

For residual velocity testing, the specimen completely perforated (Heatherington and Rajagopalan, Gupta and Madhu, Jenq et al.) [68,69,70]. They indicated the amount of energy absorbed by the composite can be calculated, via measuring the velocity of the projectile entering and exiting the composite.

Ballistic limit velocity testing involves determining the velocity at which there is a 50% probability of specimen penetration (Cunniff et al., Kang and Lee, Heatherington, Wright et al.) [71,64,72,73]. This can be seen as the velocity at which the projectile just penetrates the composite. Testing involves taking a certain number of shots where the projectile penetrates

the specimen and that same number of shots where no penetration occurs. If all shots are within a specified velocity range (usually 125 m/sec) then the ballistic limit is calculated from the average of these measurements. This type of testing has been widely used by government agencies and armor manufacturers for acceptance testing and material rating.

Another method for analyzing resistance to ballistic impact is to measure the depth of projectile penetration (Walters and Scott, Dikshit et al., Pageau et al.) [74,75,76]. When impacting metal armor, characteristics of the penetration cavity are observed to gain insight into the materials impact absorption mechanism. The method is also useful when comparing several materials to be used in applications where penetration resistance is required.

In order to gain a force vs. time curve, Azzi et al. [77] created a reverse impact technique where the composite specimen was accelerated to impact a stationary impactor instrumented with a piezoresistive gauge. In another study, Zee et al. [78] inserted a small magnet on the projectile. The changing magnetic flux in coils placed around the specimen gave a real-time velocity profile during the specimen penetration.

2.4 IMPROVING HIGH AND BALLISTIC VELOCITY IMPACT DAMAGE RESISTANCE

Due to the low strain to failure and low transverse shear strength of the graphite fiber coupled with the brittle nature of the epoxy matrix, graphite epoxy composites have very poor resistance to high-energy impact. To date, only limited work has been done in the area of impact resistance improvement of graphite composites subjected to high and ballistic velocity impact.

Some of the methods used to improve low velocity impact resistance are not appropriate in improving the high and ballistic velocity impact resistance. For the fiber and matrix toughening approach to improved impact resistance, the large amount of material needed for high velocity applications would result in a significant reduction in the structural stiffness of the composite. As for interface toughening and through-the-thickness reinforcements, which are designed to reduce delamination, these methods are effective at higher velocities if penetration resistance is not required, and improved structural strength after impact is desired. However, if penetration resistance required, prohibiting delamination may be counter-effective since delamination plays an important role in energy absorption and stopping the motion of the projectile. Dorey [79] concluded that the carbon fiber matrix bond strength should be high for good threshold impact performance, but low for projectile containment.

Under conditions of high velocity impact the mode of target response is more complex, with deformation tending to occur in localized region around the point of impact (Cantwell, and Morton) [80]. Ross and Sierakowski [81], following high velocity impact tests on glass fiber reinforced plastic (GFRP), showed that laminates possessing multiple-ply interfaces offer superior resistance to ballistic perforation. It has been shown that increasing the flexural stiffness of a target by varying the fibers stacking sequence or increasing its thickness changes the mode of initial fracture from a lower surface flexural failure to a top surface contact failure (Cantwell) [82]. For a given incident energy, increasing the target thickness results in a lower level of damage as detected by ultrasonic inspection.

Hybridizing graphite composites with high strain materials is effective for high velocity applications. Through hybridizing, a portion of the energy imparted by the projectile is transferred to the high strain component reducing the amount of energy causing damage to the

base composite. Various high strain materials, such as aramid fibers (Kevlar), S-glass, and high performance polyethylene (Spectra), have been shown to be effective ballistic resistance materials, which make them good candidates for hybrid applications (Bless and Hartman, Lee et al., Zhu et al.) [66,83,59]. Dorey [79] found that hybrid composites faced with Kevlar performed better than all carbon composites when impacted by a steel ball traveling at ballistic velocities.

CHAPTER 3

MECHANICS OF COMPOSITE MATERIAL

3.1 CLASSICAL LAMINATION THEORY

3.1.1 INTRODUCTION

In a typical structural application of a composite, multiple layers (or laminate) of unidirectional composites are stacked together at various angles to form a laminate. The stacking sequence and orientations of the individual layers give the laminate designer additional ‘degrees of freedom’ to ‘tailor’ or optimize the design with respect to strength, stiffness, buckling load, vibration response, panel flutter or other desired performance objective. The purpose of lamination theory is to predict the behavior of the laminate from knowledge of the material properties of the individual layers and the laminate geometry.

3.1.2 DEVELOPMENT OF THE THEORY

Classical lamination theory is based upon the following simplifying engineering assumptions:

- 1) The laminate consists of perfectly bonded layers (laminates).
- 2) Each layer is a homogeneous material with known effective properties.
- 3) Individual layer properties can be isotropic, orthotropic, or transversely isotropic.
- 4) Each layer in a state of plane stress.
- 5) The laminate deforms according to the following Kirchhoff (1850) assumptions for bending and stretching the thin plates:
 - a) Normal to the mid plane remain straight and normal to the deformed mid plane after deformation.
 - b) Normal to the mid plane do not change length.

3.1.3 NOTATION

For the laminate in Fig.3.1, we take a global x-y-z coordinate system with z perpendicular to the plane of the laminate and positive downward. The origin of coordinate system is located on the laminate mid plane, centered between the top and bottom surfaces. The laminate has n layers numbered from top to bottom. Each layer has a distinct fiber orientation denoted θ_k . As indicated in Fig3.1, the z-coordinate of the bottom of the k^{th} layer is designated z_k with the top of the layer being z_{k-1} . The thickness t_k of any layer is then $t_k = z_k - z_{k-1}$. The top surface of the laminate is denoted z_o and the total thickness is $2h$.

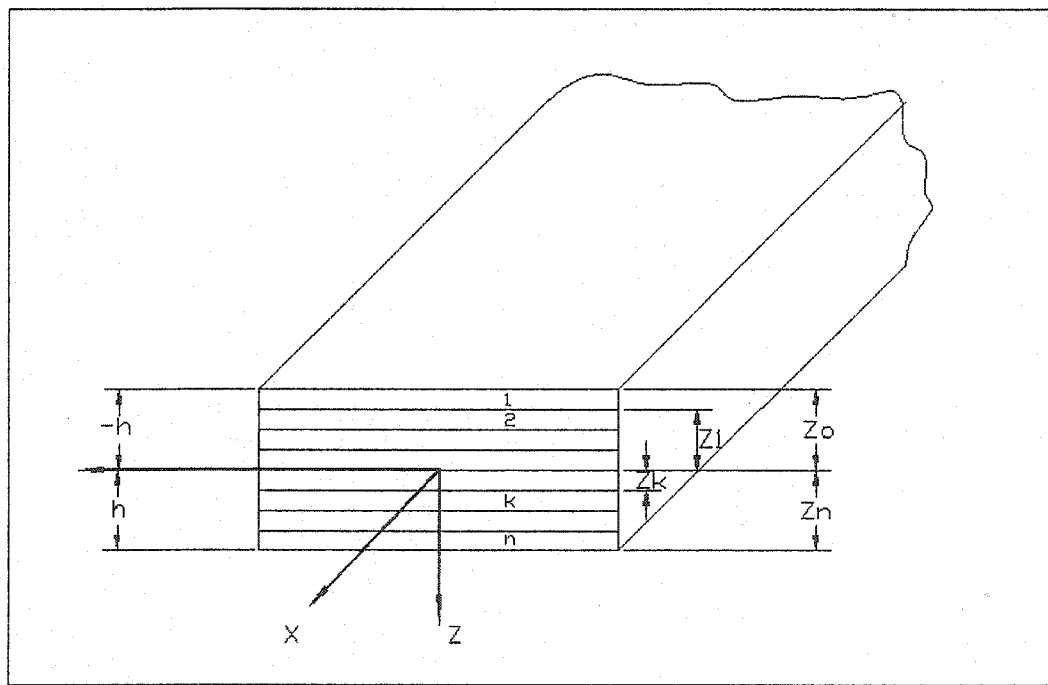


Figure 3.1 Laminate Coordinates

The in-plane displacements vary linearly through the entire thickness of the laminate, while the normal deflection is uniform through the thickness. Thus, the thickness-shear (transverse shear) strains and the thickness-normal strain are all zero. The only nonzero strains are the in-plane

strains (two normal strains ε_1 and ε_2 and one shear strain ε_6), which vary linearly through the thickness:

$$\begin{Bmatrix} \varepsilon_1 \\ \varepsilon_2 \\ \varepsilon_6 \end{Bmatrix} = \begin{Bmatrix} \varepsilon_1^0 \\ \varepsilon_2^0 \\ \varepsilon_6^0 \end{Bmatrix} + z \begin{Bmatrix} K_1 \\ K_2 \\ K_6 \end{Bmatrix} \quad (3.1)$$

Here, ε_1^0 and ε_2^0 are the mid-plane normal strains, ε_6^0 is the mid-plane shear strain, K_1 and K_2 are the bending curvatures, K_6 is the twisting curvature, and z is the thickness-direction position coordinate, measured from the mid-plane.

The stress in a typical layer (denoted by the subscript k), with the fibers oriented at an angle θ_k from the reference axes, can be expressed as:

$$\begin{Bmatrix} \sigma_1 \\ \sigma_2 \\ \sigma_6 \end{Bmatrix} = \begin{bmatrix} \bar{Q}_{11} & \bar{Q}_{12} & \bar{Q}_{16} \\ \bar{Q}_{12} & \bar{Q}_{22} & \bar{Q}_{26} \\ \bar{Q}_{16} & \bar{Q}_{26} & \bar{Q}_{66} \end{bmatrix}_K \begin{Bmatrix} \varepsilon_1 \\ \varepsilon_2 \\ \varepsilon_6 \end{Bmatrix} \quad (3.2)$$

For laminates, as in plate and shell structures, it is usually more convenient to work with the resultant forces and moments, expressed per unit width, than it is to deal with stress components in each individual layer. The in-plane forces per unit width for a general laminate consisting of n plies can be determined by:

$$\begin{Bmatrix} N_1 \\ N_2 \\ N_6 \end{Bmatrix} = \int_{-h/2}^{h/2} \begin{Bmatrix} \sigma_1 \\ \sigma_2 \\ \sigma_6 \end{Bmatrix} dz = \sum_{k=1}^n \int_{h_{k-1}}^{h_k} \begin{Bmatrix} \sigma_1 \\ \sigma_2 \\ \sigma_6 \end{Bmatrix} dz \quad (3.3)$$

Here N_1 and N_2 are in-plane normal forces per unit width, and N_6 is the in-plane shear force per unit width.

Similarly, the moment resultants or stress couples can be expressed as:

$$\begin{Bmatrix} M_1 \\ M_2 \\ M_6 \end{Bmatrix} = \int_{-h/2}^{h/2} z \begin{Bmatrix} \sigma_1 \\ \sigma_2 \\ \sigma_6 \end{Bmatrix} dz = \sum_{k=1}^n \int_{h_{k-1}}^{h_k} z \begin{Bmatrix} \sigma_1 \\ \sigma_2 \\ \sigma_6 \end{Bmatrix} dz \quad (3.4)$$

Here, M_1 and M_2 are the bending moments per unit width, and M_6 is the twisting moment per unit width. Substituting equations (3.1) and (3.2) into equation (3.3), one can obtain:

$$\begin{Bmatrix} N_1 \\ N_2 \\ N_6 \end{Bmatrix} = \begin{Bmatrix} A_{11}A_{12}A_{16} \\ A_{12}A_{22}A_{26} \\ A_{16}A_{26}A_{66} \end{Bmatrix} \begin{Bmatrix} \varepsilon_1^0 \\ \varepsilon_2^0 \\ \varepsilon_6^0 \end{Bmatrix} + \begin{Bmatrix} B_{11}B_{12}B_{16} \\ B_{12}B_{22}B_{26} \\ B_{16}B_{26}B_{66} \end{Bmatrix} \begin{Bmatrix} \kappa_1 \\ \kappa_2 \\ \kappa_6 \end{Bmatrix} \quad (3.5)$$

Where the stretching stiffness are given by:

$$A_{ij} = \int_{-h/2}^{h/2} z \bar{Q}_{ij} dz = \sum_{k=1}^n (h_k - h_{k-1}) (\bar{Q}_{ij})_k \quad (i, j = 1, 2, 6) \quad (3.6)$$

And the bending-stretching coupling stiffness is:

$$B_{ij} = \int_{-h/2}^{h/2} z^2 \bar{Q}_{ij} dz = \frac{1}{2} \sum_{k=1}^n (h_k^2 - h_{k-1}^2) (\bar{Q}_{ij})_k \quad (i, j = 1, 2, 6) \quad (3.7)$$

In a similar fashion, substitution of equations (3.1) and (3.2) into equation (3.4) yields:

$$\begin{Bmatrix} M_1 \\ M_2 \\ M_6 \end{Bmatrix} = \begin{Bmatrix} B_{11}B_{12}B_{16} \\ B_{12}B_{22}B_{26} \\ B_{16}B_{26}B_{66} \end{Bmatrix} \begin{Bmatrix} \varepsilon_1^0 \\ \varepsilon_2^0 \\ \varepsilon_6^0 \end{Bmatrix} + \begin{Bmatrix} D_{11}D_{12}D_{16} \\ D_{12}D_{22}D_{26} \\ D_{16}D_{26}D_{66} \end{Bmatrix} \begin{Bmatrix} \kappa_1 \\ \kappa_2 \\ \kappa_6 \end{Bmatrix} \quad (3.8)$$

Here, the B 's are as defined in equation (3.7) and the bending stiffness are given by:

$$D_{ij} = \int_{-h/2}^{h/2} z^3 \bar{Q}_{ij} dz = \frac{1}{3} \sum_{k=1}^n (h_k^3 - h_{k-1}^3) (\bar{Q}_{ij})_k \quad (i, j = 1, 2, 6) \quad (3.9)$$

Equations (3.5) and (3.8) can be combined into the following single 6*6 matrix equation:

$$\begin{Bmatrix} N_1 \\ N_2 \\ N_6 \\ M_1 \\ M_2 \\ M_6 \end{Bmatrix} = \begin{Bmatrix} A_{11}A_{12}A_{16}B_{11}B_{12}B_{16} \\ A_{12}A_{22}A_{26}B_{12}B_{22}B_{26} \\ A_{16}A_{26}A_{66}B_{16}B_{26}B_{66} \\ B_{11}B_{12}B_{16}D_{11}D_{12}D_{16} \\ B_{12}B_{22}B_{26}D_{12}D_{22}D_{26} \\ B_{16}B_{26}B_{66}D_{16}D_{26}D_{66} \end{Bmatrix} \begin{Bmatrix} \varepsilon_1^0 \\ \varepsilon_2^0 \\ \varepsilon_6^0 \\ \kappa_1 \\ \kappa_2 \\ \kappa_6 \end{Bmatrix} \quad (3.10)$$

Equation (3.10), which is known as the laminate constitutive equation, can be written in a much more compact form as:

$$\begin{Bmatrix} N \\ M \end{Bmatrix} = \begin{Bmatrix} A & B \\ B & D \end{Bmatrix} \begin{Bmatrix} \varepsilon^0 \\ \kappa \end{Bmatrix} \quad (3.11)$$

It is emphasized that equation (3.10) exhibits a variety of different kinds of coupling. First, all of the B 's represents bending-stretching coupling in general. Further, all quantities with subscript 12 involve Poisson coupling due to the presence of nonzero Poisson's ratio. Finally, all quantities with subscript 16 and 26 involve normal-shear coupling (often called simply 'shear coupling' in the literature). The form of the array of stiffnesses (A, B and D) appearing in equation (3.10) simplifies for many common laminate configurations.

In developing the preceding equations, thermal and hygrothermal effects were neglected, i.e., it was assumed that the isothermal and isomoiiture conditions existed. If the temperature and the moisture concentration change, equation (3.1) must be replaced by:

$$\begin{Bmatrix} N \\ M \end{Bmatrix} = \begin{Bmatrix} A & B \\ B & D \end{Bmatrix} \begin{Bmatrix} \varepsilon^0 \\ \kappa \end{Bmatrix} + \begin{Bmatrix} N^T \\ M^T \end{Bmatrix} + \begin{Bmatrix} N^M \\ M^M \end{Bmatrix} \quad (3.12)$$

Here, N^T and M^T represent thermal stretching and thermal bending, respectively, while N^M and M^M represent moisture-induced stretching and moisture-induced bending, respectively. They may be calculated in terms of the individual-layer properties as:

$$\begin{Bmatrix} N_1^T \\ N_2^T \\ N_6^T \end{Bmatrix} = \int_{-h/2}^{h/2} \begin{Bmatrix} \bar{Q}_{11}\bar{\alpha}_1 + \bar{Q}_{12}\bar{\alpha}_2 + \bar{Q}_{16}\bar{\alpha}_6 \\ \bar{Q}_{12}\bar{\alpha}_1 + \bar{Q}_{22}\bar{\alpha}_2 + \bar{Q}_{26}\bar{\alpha}_6 \\ \bar{Q}_{16}\bar{\alpha}_1 + \bar{Q}_{26}\bar{\alpha}_2 + \bar{Q}_{66}\bar{\alpha}_6 \end{Bmatrix} \Delta T dz \quad (3.13)$$

$$\begin{Bmatrix} M_1^T \\ M_2^T \\ M_6^T \end{Bmatrix} = \int_{-h/2}^{h/2} z \begin{Bmatrix} \bar{Q}_{11}\bar{\alpha}_1 + \bar{Q}_{12}\bar{\alpha}_2 + \bar{Q}_{16}\bar{\alpha}_6 \\ \bar{Q}_{12}\bar{\alpha}_1 + \bar{Q}_{22}\bar{\alpha}_2 + \bar{Q}_{26}\bar{\alpha}_6 \\ \bar{Q}_{16}\bar{\alpha}_1 + \bar{Q}_{26}\bar{\alpha}_2 + \bar{Q}_{66}\bar{\alpha}_6 \end{Bmatrix} \Delta T dz \quad (3.14)$$

and

$$\begin{Bmatrix} N_1^M, M_1^M \\ N_2^M, M_2^M \\ N_6^M, M_6^M \end{Bmatrix} = \int_{-h/2}^{h/2} (1, z) \begin{Bmatrix} \bar{Q}_{11}\bar{\beta}_1 + \bar{Q}_{12}\bar{\beta}_2 + \bar{Q}_{16}\bar{\beta}_6 \\ \bar{Q}_{12}\bar{\beta}_1 + \bar{Q}_{22}\bar{\beta}_2 + \bar{Q}_{26}\bar{\beta}_6 \\ \bar{Q}_{16}\bar{\beta}_1 + \bar{Q}_{26}\bar{\beta}_2 + \bar{Q}_{66}\bar{\beta}_6 \end{Bmatrix} \Delta C dz \quad (3.15)$$

Here, the $\bar{\alpha}$'s and $\bar{\beta}$'s are the transformed thermal-expansion and moisture-expansion coefficients, respectively, ΔT is the temperature change (from a strain-free temperature) and ΔC is the moisture change (from a strain-free moisture), see Herakovich, C.T. [91].

3.1.4 STIFFNESS OF SPECIFIC LAMINATE CONFIGURATION

Before listing the simplifications of applying the theory of the preceding subsection to specific laminate configuration, the standard code or abbreviation used to designate stacking sequence will be illustrated by several examples. First, consider $[0_2/90_3/30/-30]_S$ which means that the first 'ply group' or 'sub laminate' starting from the bottom of the laminate, consists of two plies at an orientation of 0 deg, followed by another ply group of three plies at 90 deg, a single layer at 30 deg, and finally another single layer at -30 deg. The subscript S at the closing bracket indicates that the laminate is symmetric about the laminate mid plane ($z=0$). Thus the upper half of the laminate has a stacking sequence exactly reverse in order of that of the bottom half. Other ways of designating the same laminate described in the preceding paragraph are:

$$[0_2 / 90_3 / 30 / -30 / -30 / 30 / 90_3 / 0_2]_T$$

Where the subscript T at the end denotes that this is the stacking sequence for the total laminate. If a laminate consists of layers of two different composites, i.e., graphite-epoxy (for high stiffness) and glass-epoxy (for low cost), it is called an interlaminar hybrid laminate.

3.1.5 MID PLANE-SYMMETRIC LAMINATES

A laminate is said to be mid plane symmetrically laminated, or simply symmetrically laminated, if, for each and every layer located a certain distance (z) above the mid plane of the laminate, there is an identical layer (same properties, orientation and thickness) located at the same distance below the mid plane (i.e., $-z$). From the definition of the bending-stretching coupling stiffnesses in equation (3.7), it is apparent that all of these B_{ij} are equal to zero for a symmetric laminate.

3.1.6 ALIGNED AND OFF-AXIS PARALLEL-PLY LAMINATES

A parallel-ply laminate is simply a laminate in which all of the major material-symmetry axes (fiber directions) of the individual layers have the same orientation. The plies do not have to be identical in thickness. However, since commercially available Prepreg composites come in certain standard ply thickness, the layers usually are all of the same nominal thickness.

A parallel-ply laminate is considered to be aligned, when the material-symmetry axes of the layers coincide with the reference axes of the laminated plate (such as the sides of the rectangular plate), i.e., $\theta = 0$. Such a plate is called especially orthotropic, since the $\bar{Q}_{ij} = Q_{ij}$ and thus, $\bar{Q}_{16} = \bar{Q}_{26} = 0$. Therefore, all elements of the stiffness sub matrices ($[A]$, $[B]$, $[D]$) with subscripts 16 and 26) are equal to zero. In the case of $\theta \neq 0$, a parallel ply-laminate is said

to be an off-axis one. In this case, the stiffness-matrix elements with subscripts 16 and 26 are not zero and the plate is called generally orthotropic.

3.1.7 CROSS-PLY LAMINATES

A cross-ply laminate is one consisting of an arbitrary number of plies, some of which are oriented at 0 deg and the rest at 90 deg. A regular cross-ply laminate is one having an arbitrary number of plies of the same material and thickness, but with alternating orientations of 0 and 90 deg to the geometric reference axes (plate edges). Thus, by definition, each ply is especially orthotropic; thus, $\bar{Q}_{16} = \bar{Q}_{26} = 0$ for all layers and all elements of the stiffness matrices having subscripts 16 and 26 are equal to zero.

3.1.8 ANGLE-PLY LAMINATES

An angle-ply laminate consists of layers oriented at one or more sets of angles, say $+θ_1, -θ_1$ and $θ_2, -θ_2$. A regular angle-ply laminate consists of an arbitrary number of layers (n), identical in thickness and material but having alternating orientations of $-θ$ and $+θ$. If a regular angle-ply laminate has an odd number of layers, it is symmetric laminate, so that all of the B 's are equal to zero. Unfortunately, however, A_{16}, A_{26}, D_{16} and D_{26} are not zero; thus, there is in-plane shear-normal coupling and bending-twisting coupling. A regular angle-ply laminate with an even number of layers has $A_{16} = A_{26} = D_{16} = D_{26} = 0$; but unfortunately it is not symmetric.

3.1.9 QUASI-ISOTROPIC LAMINATES

In certain applications, such as thermally loaded structures and balanced-biaxial-stressed structures, it is desirable that the in-plane behavior of the laminate is isotropic, i.e., the stretching stiffness matrix contains only two independent parameters. If these two are taken to be A_{11} and A_{12} then the in-plane isotropy requires that these three conditions be meet:

$$A_{22} = A_{11} \quad A_{66} = \frac{1}{2}(A_{11} - A_{12}) \quad A_{16} = A_{26} = 0 \quad (3.16)$$

The conditions of equations (3.16) can be met by a laminate configuration first suggested by Werren and Norris: (1) The total number of layers n must be at least three. (2) The individual layers must have identical orthotropic elastic coefficients (Q_{ij}) and thickness. (3) Each layer in a ply group (or set), denoted by index k , must be oriented at an angle $\theta_k = \pi(k-1)/S$ radians with respect to a reference direction, where S is the number of such a ply groups. Since a laminate made according to the Werren-Norris configuration is isotropic in regard to stretching only (sub matrix $[A]$) and not, in general, in regard to $[B]$ and $[D]$, such a laminate is called isotropic. A more popular quasi-isotropic laminate configuration is $[0/45/-45/90]_s$ or $[0/90/45/-45]_s$ which contains a total of eight layers.

3.1.10 $[0_m/\pm\theta_n]_s$ LAMINATES

A very popular lamination scheme for structural panels in the airframe industry is $[0_m/\pm\theta_n]_s$, where, of course, m and n is integers. There are several advantages of this configuration over other simpler ones: (1) Unlike a regular angle-ply laminate, there is a reserve of strength after first-ply failure. This reserve is analogous to the reserve of strength provided by plasticity in

isotropic materials. (2) It is possible to tailor the various properties continuously rather than in discrete steps as is required in cross-ply laminates.

DYNAMICS OF COMPOSITE MATERIAL

3.2 INTRODUCTION

Several types of mathematical models are used to study the impact of a structure by a foreign object. In certain cases, the contact force history can be accurately determined by modeling the structure by an equivalent spring-mass system. When the structure behaves quasi-statically, it is also possible to calculate the maximum contact force by assuming that when the contact force reaches its maximum, the sum of the strain energy in the structure and the energy required for indentation is equal to the initial kinetic energy of the projectile. This energy balance approach is useful when one is interested not in the complete contact force history but rather only in maximum contact force. When the dynamics of the structure must be more accurately accounted, more sophisticated models are needed.

3.2.1 ENERGY BALANCED MODELS

Another approach for analyzing the impact dynamics is to consider the balance of energy in the system. The initial kinetic energy of the projectile is used to deform the structure during impact. Assuming the structure behaves quasi-statically, when the structure reaches its maximum deflection, the velocity of the projectile becomes zero and all the kinetic energy has been used to deform the structure. The overall deformation of the structure usually involves bending, shear deformation, and for a large deformations, membrane stiffening effects. Local deformations in the contact zone also are to be considered. For impacts that induce only small

amounts of damage, the energy needed to create damage can be neglected. Therefore the energy-balance equation can be written as:

$$\frac{1}{2}mV^2 = E_b + E_s + E_m + E_c \quad (3.17)$$

Where the subscripts b, s and m refer to the bending, shear, and membrane components of the overall structural deformation, and E_c is the energy stored in the contact region during indentation. It is always possible to express the force-deflection relation in the form:

$$P = K_{bs}W + K_m W^3 \quad (3.18)$$

Where K_{bs} is the linear stiffness including bending and transverse shear deformation effects, K_m is the membrane stiffness, and W is the deflection at the impact point. Then

$$E_b + E_s + E_m = \frac{1}{2}K_{bs}W_{\max}^2 + \frac{1}{4}K_m W_{\max}^4 \quad (3.19)$$

Both experimental and analytical studies of contact between smooth indentors and laminated composites indicate that during the loading phase, the contact law can be written as:

$$P = n\alpha^{3/2} \quad (3.20)$$

Where α represents the relative motion or indentation of the structure by the projectile:

$$E_c = \int_0^{\alpha_{\max}} P d\alpha = \frac{2}{5}n\alpha_{\max}^{5/2} \quad (3.21)$$

The maximum indentation can be expressed in terms of the maximum displacement of the structure at the impact location:

$$\alpha_{\max} = \left(\frac{P}{n} \right)^{2/3} = n^{-2/3} (K_{bs}W_{\max} + K_m W_{\max}^3)^{2/3} \quad (3.22)$$

After substitution into (3.21), the contact energy becomes:

$$E_c = \frac{2}{5} n^{-2/3} (K_{bs} W_{\max} + K_m W_{\max}^3)^{5/3} \quad (3.23)$$

Using (3.19) and (3.23), the energy-balance equation becomes:

$$\frac{1}{2} M V^2 = \frac{1}{2} K_{bs} W_{\max}^2 + \frac{1}{4} K_m W_{\max}^4 + \frac{2}{5} n^{-2/3} (K_{bs} W_{\max} + K_m W_{\max}^3)^{5/3} \quad (3.24)$$

This equation can be solved numerically for W_{\max} , and the maximum contact force can be obtained after substitution into (3.18).

3.2.2 ASSUMED FORCE OR INITIAL CONDITION

In order to study the dynamic response of the composite structures to the impact, researchers assumed certain kinds of the contact force and the form of its distribution over the contact area. These assumptions are useful and efficient for studying the overall dynamic response of the composite structures under the impact. However, the models are not accurate enough to do the damage analysis based on these assumptions. The linear composite plate theories are usually used in modeling the impact response of rectangular, circular and cantilever composite plates under low velocity impact.

Sun and Grady [84] studied the impact of graphite-epoxy laminates by a rubber ball at high speeds. In this case, the rubber ball undergoes, large deformations, and the contact force cannot be modeled using Hertzian contact laws. Instead, the following approximation was used:

$$F(t) = \begin{cases} F_0 \sin[\pi t / t_0] \\ F_0 \cos[\pi(t - t_0) / 2(T - t_0)] \\ 0 \end{cases} \quad (3.25)$$

For $0 < t < t_0$, For $t_0 < t < T$, For $t > T$

Where F_0 is the maximum force, t_0 the time at which the force becomes maximum, and the contact time duration is T .

3.2.3 WAVE PROPAGATION

Experimental investigations for impact loaded structural materials can be broadly classified into three categories based upon wave shape and amplitude, these being:

1. Low-amplitude sinusoidal waves or ultrasonic waves
2. Low-amplitude transient waves
3. High-amplitude transient waves

Several experimental methods have been developed to study the wave motion in various composite systems. These methods include the generation and monitoring of waves under each of the above categories. Ultrasonic, for example, has been used successfully, for monitoring and characterizing the damage in composites.

The principal wave motions under transverse impact loading consist primarily of five waves: two waves related to in-plane motion and three related to flexural deformations. (Daniel, and Liber) [85], measured and calculated wave velocities for the various types of waves for two types of Boron/Epoxy specimens with different stacking sequence. The following significant observations can be made from their study:

1. The longitudinal in-plane wave along the fiber direction in a unidirectional laminate (0_{16}) travels, as expected, faster than any other in-plane or flexural wave.
2. There is a noticeable discrepancy between measured and computed values of wave velocities for both types of laminates. Several reasons have been suggested for this discrepancy. The measured value of the longitudinal wave along the fiber direction may

not be as accurate as expected, due in part to the fact that the measured time interval is not quite accurate. Similar discrepancies in the flexural wave velocities are attributed to the inaccuracies in the shear moduli G_{12} , G_{13} and G_{23} .

Further transient wave motion studies due to localized impact on composite laminated plates by (Takeda) [86], and (Takeda, Sierakowski, Malvern) [87]. These studies used cylindrical steel impactors of 3/8 in diameter and 1 in length with blunt ends impacting at the center of Glass/Epoxy cross-ply and angle-ply laminated plates with a plate geometry 6 in by 6 in and clamped along their four edges. They indicated the predominant wave appears to be the flexural in the direction of 45^0 ply. This indicates that the plate is in flexural motion during the impact, and the membrane effects are negligible. The transverse matrix cracks on the impacted surface are believed to be generated by the tensile stresses due to the leading part of the transient flexural wave generated immediately after impact.

EFFECT OF MATERIAL PROPERTIES

The damage in composites represents a combination of events including delamination, matrix cracking and fiber breakage. The first two types of damage are related to the matrix properties while the last is related to fiber properties. Improvements in the properties of the constituents leads, in general, to improved impact damage resistance of the laminate. However, defining a better material system for a particular application is difficult because of inadequate understanding of the micromechanics of damage formation.

3.3.1 EFFECT OF MATRIX PROPERTIES

It is generally recognized that an increase in strain to failure of the matrix will result in improved residual strength of the composite after impact, due to better resistance to delamination and matrix cracking. Testing neat resin specimens, Hirschbuehler [88] showed that high strain to failure resins were capable of resisting higher impact loads. When deflections become of the order of one half of the specimen thickness, a significant fraction of the load is carried by membrane action, and the maximum load or maximum energy to failure of the resin specimen is measure of the amount of in-plane stress that can be generated before failure.

It has been observed that thermoplastic matrix composites exhibit relatively higher toughness. In general thermoplastic composites produce less matrix cracking and exhibit less extensive damage. In addition to sustaining higher impact loads, toughened systems also demonstrate higher residual compression strength after impact, since there is less delamination.

3.3.2 EFFECT OF FIBER PROPERTIES

Fiber strain energy has been pinpointed as one of the fiber parameters that would most significantly improve the properties of the composite. Higher fiber failure strains, with the same elastic modulus, will result in higher energy absorption, especially since the strain energy absorbed by the matrix represents a large portion of strain energy. For the same impact energy, higher capacity to absorb energy results in less fiber breakage and a higher residual tensile strength. Cantwell et al. [3] has reported some results on the performance of such composites. His study indicated that replacing the $\pm 45^\circ$ plies in 0° , $\pm 45^\circ$ laminates with a woven fabric

improved the residual strength after impact by inhibition of delaminations and matrix shear cracks.

3.3.3 EFFECT OF FIBER-MATRIX INTERFACE

The fiber matrix-interface is as important as the matrix and fiber constituents in the control of composite damage. For short-fiber composites a critical fiber length embedded in a matrix is necessary to transfer load from the matrix to the fiber. For continuous composites, the introduction of a material interface can increase the impact resistance of the composites. Peiffer et al. [89] indicated that, for the case of Glass-Epoxy composites, the introduction of a rubber-like interface can be useful in improving the damage tolerance of composites.

3.3.4 EFFECT OF STACKING SEQUENCE

The ply stacking sequence in laminated composites has been shown to play an important role in the damage tolerance of composite Ross, and Sierakowski [81]. In particular, depending upon whether a rigid impactor strikes a rigid or flexible target, the damage initiated may represent a front to back or back to front damage development. Experimental evidence indicates that target stiffness represents a dominant parameter and controls the mode of fracture.

At impact energy levels, which result in local damage initiation, damage occurs from front to back, with damage spread from high tensile stresses generated in the vicinity of the impactor. Such stresses are sufficiently large to cause failure at the fiber-matrix interfaces resulting in crack transmission progressing from front to back, with corresponding delamination.

Studies by Cantwell [82], on impacted CFRP composites targets of varying thickness, with the same stacking sequence, indicate that the projected delamination area varies linearly with the impacted kinetic energy of the projectile. Malvern et al. [90], studied the effect of varying stacking sequence and relationship between the total delaminated area and the kinetic energy of the projectile. A systematic study of cross-ply Glass-Epoxy composite plates indicates that for the system studied, a sequential delamination process occurs which plays an important role in dispersing the absorbed energy.

The energy required to achieve complete penetration was shown to increase with plate thickness. Reploting the data from Cantwell [82] and Cantwell and Morton [14], the perforation energy was found to increase with the square of the plate thickness for both low and high velocity tests on the same laminate under the same condition. The energy level required for perforation by a small spherical impactor with high velocity was the same as that for a larger mass traveling at a smaller initial velocity.

CHAPTER 4

FABRICATION AND TESTING APPARATUS

4.1 FABRICATION OF COMPOSITE PLATE

The compression mould method was used to fabricate the composite plates. The set-up of compression mould consists of upper and lower part, and the intermediate space between these two parts. The total of 8 pressure plates of 20.48cm by 30.48cm by 0.635cm thickness was used to fabricate 4 composite plates at a time. The compression mould was manufactured of two 30.48 cm by 30.48 cm by 1.27 cm plate and four 2.54 cm by 1.27cm by 30.48cm rod. The plates and rods were welded together to form an open box. A total of five holes, one at the center and four at equal distances from the centerline of the plate were made on the top plate of the open box. The holes were tapped and lead screws were used to apply the required pressure on the composite samples, see figure 4.1. The objective was to obtain the uniform pressure over the entire specimens. Four composite specimens were sandwiched with 8 pressure plates and the entire assembly was placed inside of the open box, see figure 4.2.

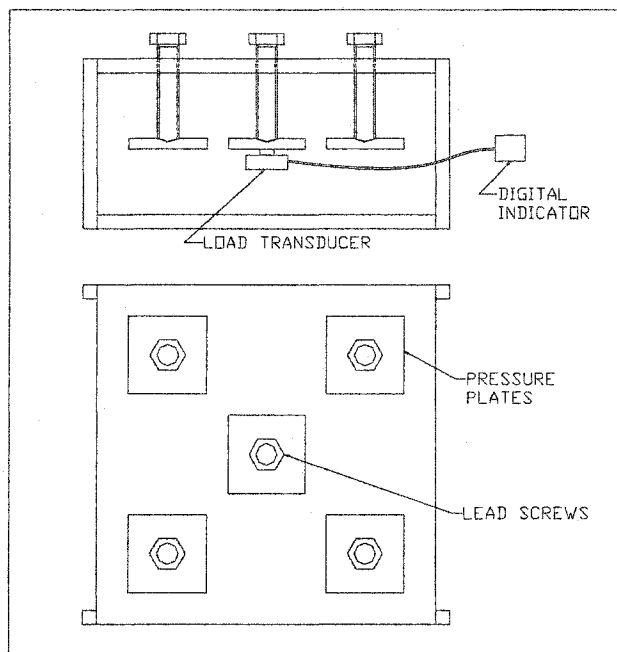


Figure 4.1 Compression mold setup

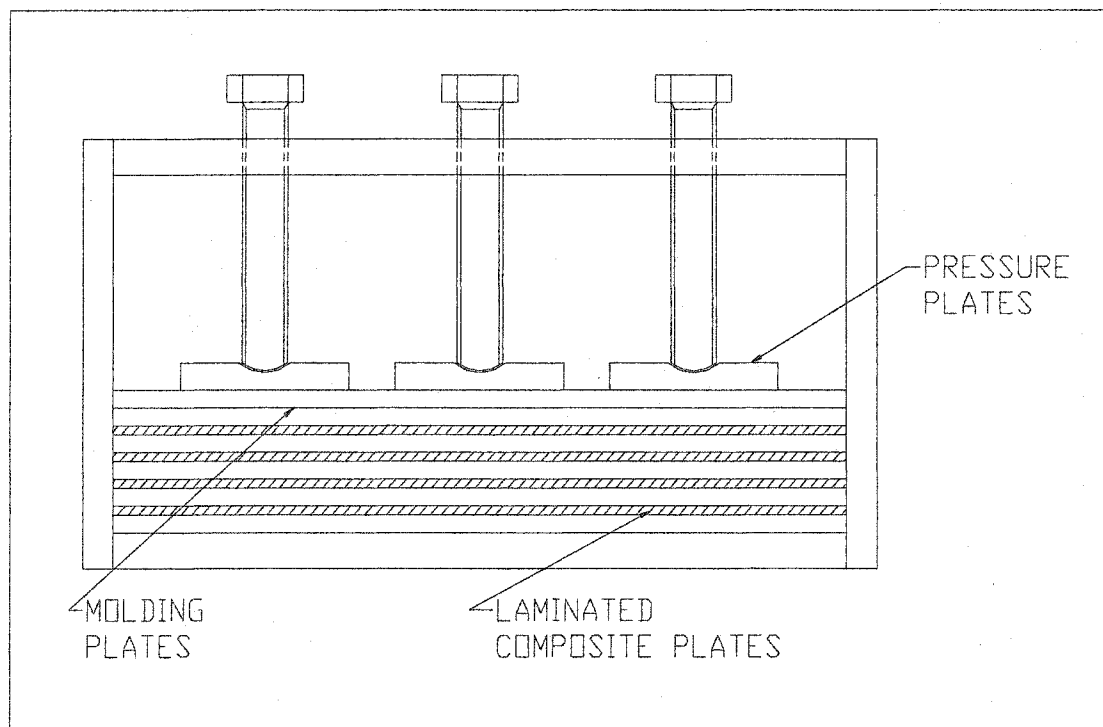


Figure 4.2 Laminate manufacturing assembly

A \pm 45KN load transducer was used to apply an equivalent load of required pressure outlined by pre-preg manufacturer at the center of specimens. The required load was applied to the center of the entire assembly when placed in the open box, and other lead screws were torqued equally, using a torque-rench, such that the load transducer would read 0 load. For different type of specimens, based on type of materials, specific loads were calculated and applied. The following table 4.1 shows the manufacturer recommended pressure and the applied equivalent load.

Table 4.1 Specified loads and pressures for fabrication

<i>Material Type</i>	<i>Pressure</i>	<i>Plate Area</i>	<i>Equivalent Load</i>
Carbon Fiber AS4	420 – 550 KPa	0.07456 m ²	38KN
Carbon Fiber IM7	420 – 550 KPa	0.07456 m ²	38KN
Hybrid	420 – 550 KPa	0.07456 m ²	31KN

4.2 STEP-BY- STEP LAMINATE LAY-UP

Three common Prepreg materials were used in this study, namely AS4/3051 carbon/epoxy by Hexcel, IM7/5250 carbon/epoxy by Hexcel and T1003 glass/epoxy by 3M. The materials were supplied as unidirectional tape of 30.48cm by 6583cm yard for AS4 and IM7 and 9144cm by 4389cm for T1003 respectively. These pre-preg tape come in roles with one side of the tape covered with a protective, peel able wax paper. The materials were removed from the freezer and allowed to warm up to near room temperature and the following procedures were taken in laying up the plies:

1. Templates were used to cut the pre-preg composite tape to the desired orientations.
2. The per-preg material was then measured and cut 0.5cm larger on each side. The panels were cut over size to allow further trimming of the panels to exact dimension.

3. The plies were tacked together one by one at the desired orientation. Each composite laminate was made up of 16 differently oriented layers. To reduce the possibility of having voids and air pockets between the plies, each top ply was rubbed gently along the fiber direction by a roller supplied by De-Comp Composite Inc.
4. When all the plies were cut and tacked together, the laminate was cut to the 27.3cm by 27.3cm Square.

The following table 4.2 shows different stacking sequence and orientation for different types of material:

Table 4.2 Stacking Sequence and Orientation

<i>Quantity</i>	<i>Materials</i>	<i>Stacking Sequence</i>
4	AS4	$[(45, -45, 0, 0)_2]_S$
4	AS4	$[(0, 0, 45, -45)_2]_S$
4	AS4	$[(0, 45, -45, 0)_2]_S$
4	AS4	$[(45, -45, 0, 90)_2]_S$
4	AS4	$[(45, -45, 90, 0)_2]_S$
4	AS4	$[(0, 90, 0, 90)_2]_S$
4	AS4	$[(45, -45, 45, -45)_2]_S$
4	E-GLASS/AS4	$[(45, -45, 0, 90)_2]_S$
4	E-GLASS/AS4	$[(45, -45, 90, 0)_2]_S$
4	E-GLASS/AS4	$[(-45, 45, 90, 0)_2]_S$
4	E-GLASS/AS4	$[(0, 90, 0, 90)_2]_S$
4	E-GLASS/IM7	$[(0, 90, 0, 90)_2]_S$
4	E-Glass/IM7	$[(90, 0, 45, -45)_2]_S$

4.3 CURING LAMINATED PLATES

Advanced composite materials have a unique cure cycle that has to be followed closely if reliable test samples are to be obtained. The cure cycle varies depending on the type of the material with the variables being the temperature, and processing time. The fabrication process is divided into three stages:

1. Pre-cure
2. Cure
3. Post-cure

During pre-curing the specimen is heated to a fixed maximum temperature up to the recommended manufacturer temperature. The recommended temperature rise is $2-5^{\circ}\text{F}$ per minute. In the curing stage, specimen is kept at the liquefying temperature for a specified period of time. The recommended constant temperature time is between 2 to 3 hours. Finally, in the post curing stage the specimen is cooled down to room temperature with a specified rate of 1°F per minute. The rate of temperature drop is such that no residual thermal stress would exist once the room temperature is reached, see figure 4.3. The above three stages are essential parts of the manufacturing process and, regardless of the method of fabrication; these steps need to be followed.

Post-cure is the most crucial step in the fabrication of composite materials. The importance of this particular stage is due to the variety of parameters, largely the thermal expansion coefficients, which contributes to the curing process. At this stage there is a difference between coefficients of thermal expansion between the individual constituents of composite laminate namely fiber and epoxy or glass and epoxy. The epoxy has the higher coefficient of thermal

expansion in comparison to the carbon or glass fiber. In the cooling stage, this difference can cause a large shrinkage in matrix compare to the carbon fiber as temperature decreases. The difference in shrinkage between matrix and carbon fiber creates the compressive stress on fibers by matrix, and tensile stresses on matrix by carbon fibers, which in result creates a warped panel. These internal stresses can contribute to the pre-mature failure of specimens during particular applications, such as impact testing. In this study manufacturers guideline followed closely to avoid any problem, namely the creation of matrix crack due to the residual thermal stresses, which can damage the sensitivity of these materials with respect to particular application.

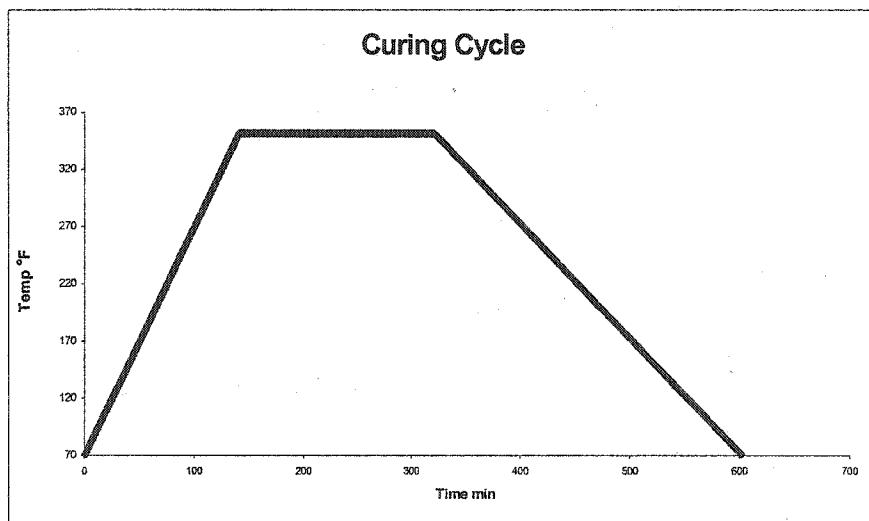


Figure 4.3 Cure-cycle for composite laminate

4.4 MANUFACTURING, CALIBRATION AND TESTING OF PROJECTILE MACHINE

The projectile machine consists of: pressure chamber, barrel, nitrogen tank, burst diaphragm, pressure relief valve, pressure transducer, and nozzle.

1. Pressure chamber: The pressure chamber is used to increase the pressure and holds the pressure till the diaphragm is burst. The length of the pressure chamber is .9144 m, with the inside diameter of .0381 m and the outside diameter of .0762. The pressure chamber is made up schedule 80 pipe.
2. Barrel: The barrel function exactly the same way as gun barrel. It is made from schedule 80 pipe with outside diameter of .0254 m, and inside diameter of .0127 m. The barrel length is 0.9144m.
3. Nitrogen tank: The Nitrogen tank was used to supply required pressure to the pressure-chamber. The tank consists of pressure regulator with two high and low pressure gauge and a low-pressure valve. The high pressure gauge reads the pressure inside the tank and the low pressure gauge reads the supplied pressure to the pressure-chamber. The low-pressure valve regulates the output pressure of the tank.
4. Burst diaphragms: In this study one type of burst diaphragms were used. This material is mainly used in fabrication of composite laminate and its main function is vacuum bagging. However, after testing many different Mylars, it was determined that this brand of Mylar gives consistent bursting pressure. This characteristic of the material made it the best possible candidate for burst diaphragm. In order to obtain different velocities, multiple layers of this diaphragm were used. The following table summarizes the burst pressure of the Mylar.

Table 4.3 Bursting Pressure of Diaphragm

No. Layers	1	2	3	4	5	6	7	8
Burst Pressure (psi)	16.7	33.6	44.5	59.1	68.9	82	92.9	104.4

5. Pressure relief valve: The pressure relief valve was used as a safety feature. The pressure relief valve was set at 3.4 MPa, which is the operating pressure of the projectile machine not including safety factor. If for any unknown reason, the pressure inside the chamber increased beyond 3.4 MPa, the relief valve would release the pressure through a 3.81 cm diameter opening and decrease the pressure to that of operating range.
6. Pressure transducer: The operation range of the pressure transducer is 0 to 3.5 MPa. The pressure transducer measures the pressure and records the peak value of the pressure at which the diaphragm burst. Pressure transducer is connected to Attach 10K data acquisition system. It continuously reads and records the pressure inside the pressure chamber.
7. Nozzle: The nozzle is designed to connect the pressure chamber to the barrel. The converging nozzle has diameters of 3.81 cm and 1.27 cm and a length of 50.8 cm. The purpose of the nozzle was to direct the pressure and to increase the air velocity just behind the bullet.

The summary of the operation for the projectile machine is given below:

Impact testing at ballistic rates of strain can be achieved using high-pressure gas gun such as that shown in (see figure 4.4). Typically, a gas such as nitrogen is fed to a chamber located at one end of the barrel. Here a plastic diaphragm restrains the gas. When the gas has reached a

pre-determined value the diaphragm is burst, accelerating a projectile down the barrel to strike a specimen or component supported vertically. The velocity of the impactor was determined just prior to impact using high-speed camera. Generally, the test is not completely destructive but frequently results in large scale-damage and/or target perforation. The gas gun can be used to test large structures and are therefore useful for assessing the high velocity impact response of composite materials.

The program was developed using MATLAB and, the theoretical velocities based on burst pressure of the diaphragms were calculated (see Appendix A). The calculated values for the velocity were then used for the purpose of calibration of the projectile machine and, furthermore to obtain approximate velocity which is required for the penetration of the specimens. The primary objective in developing the program was to design the apparatus, which can satisfy the test conditions and requirements. The focus of the program mainly concerns with the component, which was used in design and the characteristic of each component such as length and diameter and mass was determined using the theoretical results.

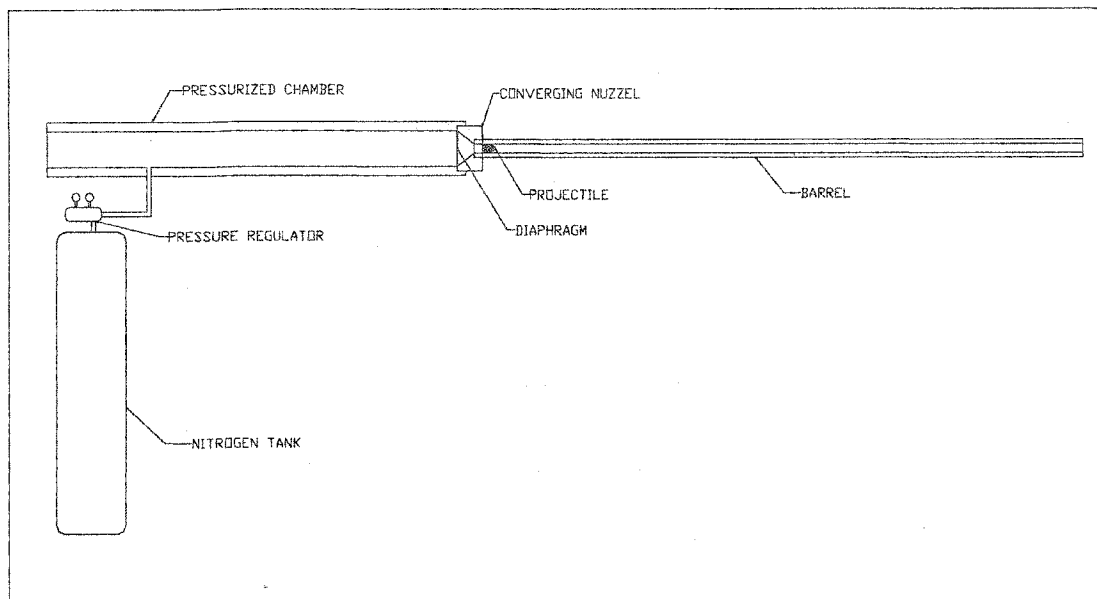


Figure 4.4 Gas gun

CHAPTER 5

EXPERIMENTAL PROCEDURE

5.1 INTRODUCTION

The objective of this study as indicated before, is to increase the high-velocity impact resistance of composite laminates and investigate the effect of stacking sequence. The primary interest is to reduce the amount of deformation caused by impact. Methods for improving the composite resistance to complete penetration without a significant increase in weight or volume is the primary interest of the study, since the increase in weight and volume causes limitations to some applications. The matter has been investigated in terms of energy absorption capability of composite laminates. The effects of different orientation were also considered to reduce the deformation due to impact.

In this study, the experiments are designed to have testing conditions similar to actual ballistic applications. This is accomplished by impacting large specimens instead of the common one dimensional clamped beam configuration. Although in the latter one can visually identify damage modes easily along the length of the beam specimen, the results differ from larger two-dimensional specimens.

5.2 EXPERIMENTAL SETUP AND TEST PROCEDURE

A series of tests were performed on plain graphite composite specimens in order to calibrate the high-speed camera, the projectile machine and the rigidity of the target holding fixture. The test specimens were rigidly clamped between two steel frames. Two steel frames sandwich the laminated composite plate where a total of 16 bolts, at the corners and midsections of the steel frame, were used to clamp the laminate. This was done to insure a rigid mount on all four

edges of the test specimen. The two steel frames were attached to a support structure as shown in figure 5.1. The test specimen was perpendicular to the line of flight of the bullet at the point of impact. Sand bags were located around the structure and the steel frame to provide safety during the impact. Four panels were constructed for each configuration and each panel was impacted with four projectiles, as shown in figure 5.2. The locations for projectile impact were chosen to minimize the effects of previous impact damage and of boundary conditions.

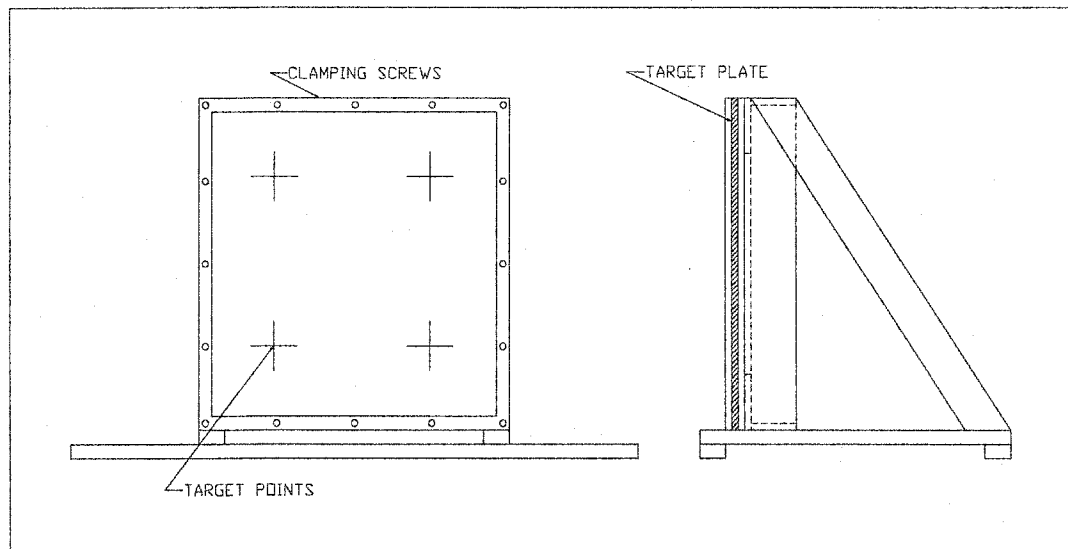


Figure 5.1 Holding fixture

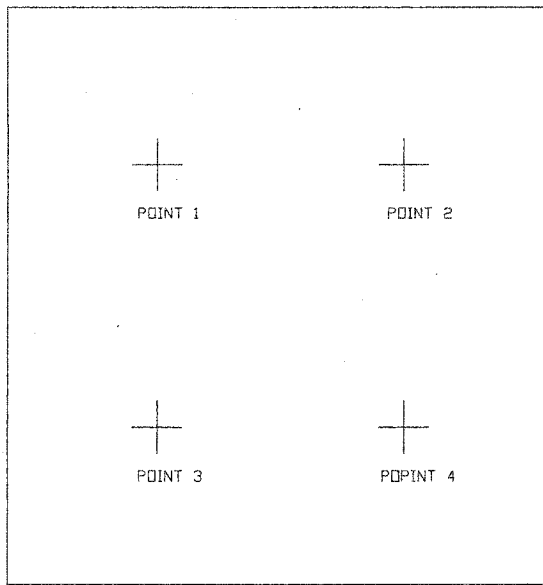


Figure 5.2 Target laminate and impact point

Four impact points per sample were chosen as a balance between the fabrication time and cost, and the ability to get results at each point without an effect on other areas of the sample and to obtain consistent boundary conditions. Although four impact points were chosen for each sample, no overlapping damage was observed. Data were rejected for cases where any overlapping of impact damage occurred.

Testing for each specimen configuration begins with firing a projectile at an estimated velocity that would barely penetrate the specimen. The procedure continues till complete perforation of the specimen occurs, and for the complete penetration the ballistic limit velocity was recorded. In observing the samples the number of firing would be changed as a function of the capability of the specimen to resist penetration.

Ballistic limit velocity testing involves determining the velocity at which there is a 50% probability of specimen penetration. This can be seen as the velocity at which the projectile

just penetrates the composite. Testing involves taking a certain number of shots where the 50% of the tests resulted in projectile complete penetration and 50% of the tests resulted in no penetration. In this work, each sample was tested with the same velocity 8 times and consistently, 4 to 5 shots completely penetrated the sample and 3 to 4 shots, bullets were stuck to the specimens. If all shots are within a specified velocity range (usually 100 m/sec) then the ballistic limit velocity was calculated from the average of these measurements. This type of testing has been widely used by government agencies and armor manufacturers for acceptance testing and material rating.

5.3 HIGH- SPEED CAMERA

The Redlake MASD Motion Scope PCI system has simplified image acquisition for motion analysis. Designed as a PC peripheral for capturing high-speed digital images directly in the PC, The Motion Scope PCI system consists of a high-speed camera, full size PCI camera control and frame store board (onboard memory), installation and user interface software and documentation. The system operates with the “ point&click” windows based application software. Records rate range from 60 through 8000 frames per second, depending on the model. Motion Scope PCI cameras can be started or stopped remotely via a handheld switch or from an external trigger signal generated by an optical, acoustic, or electronic sensor (standard 5 Volt TTL signal, or up to 30 Volt DC signal). Once captured, the images of the event reside on the Redlake MASD Motion Scope PCI boarding the PC until transferred over the computer’s PC bus for display and analysis. Our camera was capable of taking 1000 frames per second with the shutter speed of 8000. The speed on the camera was sufficient for our application and the shutter capability was not utilized.

The Motion Scope PCI 1000 S, digital imaging system was used to record a sequence of digital images of an event at a frame rate of 1000 frames per second. This system stores these images in an image memory on the controller unit. The images can be viewed forward or reverse at selected frame rates, and the time and motion can be analyzed. The trigger mode begins recording when the record button is clicked and continues to record and store images in memory until an external trigger signal is received. The adjustable trigger position (0%-100%) determines how many frames are stored before and after the trigger signal is received.

The lens on the camera head focuses the subject onto a CCD imager. There is a locking ring under the lens to provide coarse focus adjustment. The exposure of each frame is reduced at the higher frame rates, so more illumination would be required as the frame rate increases. The system provides shutter control of image exposures that allows to reduce the time of each frame exposure to eliminate image blurring due to motion. The strobe output is synchronized to the shutter timing, so that it can be used to illumination as well as to eliminate motion blur. The strobe output is enabled at all times during live or record mode. The strobe out put signal goes high when the shutter is open and low when the shutter closes.

The camera head imager must receive enough light to see details of the image, and record the subject at the optimum size, so the significant part of the motion can be seen clearly. The camera was capable of recording a specific event as well as viewing a continues video until an event triggers an end to the sequence. The elapsed recording time depends on the number of frames per second recorded and the number of frames that the memory can store.

The camera records an event until operator gives a stop command or a trigger generated by an external source stops the recording process. The stop command stops the sequence and the frames show the sequence preceding the last frame. There is a delay through the system so the

sequence shows a few frames after the system received the stop command. The playback window has a start frame button so one can go to the frame showing the event, press start frame, which assigns frame 0 to that frame and synchronizes the elapsed time to the event.

The camera was calibrated as follows:

A ruler was suspended and placed in the viewing area of the camera. This was performed so that the number of pixels per centimeter can be calculated. In our measurements, it was determined that 300 pixels represented 2 centimeters. This information was recorded in the software so that when the velocity measurement is taken, the unit would correspond to the unit of velocity. In other words, the camera was capable of giving an output of number of pixels that the bullets had traveled from one frame to the next. By inputting the number of pixels per centimeter, the program could internally convert the number of pixels to the distance traveled by the bullet. By knowing the elapsed time between each frame, given by the software, and knowing how many pixels the bullet has moved from one frame to the next hence the distance in centimeter, we could calculate the velocity.

A shot was taken and the camera recorded the event. A total of 5 consecutive frames were taken and a total of 5 points per image were recorded on the periphery of the bullet in each image. These points were taken from the same area on the bullet in all images. The velocity given by the software of the camera was calibrated to centimeter per second, which was later converted to meter per second. At this point, all that was needed to measure the impact velocity was to take few frames just before impact and identify 5 identical points on the bullet in each image. The software would calculate the velocity of the projectile from one frame to the next. A total of five consecutive frames for each measurement were taken so that the software could

produce four velocities and output these velocities along with the average velocity into an output file.

5.4 EXPERIMENTAL MEASURMENTS

The dial indicator was used and the mid-plane deflections were determined for the various stacking sequence and configurations. The amounts of mid-plane deflections are listed in chapter six in tables (see tables 6.1 through 6.13). The dial indicator was supplied by Mitutoyo, and consisted of two gages. The dial indicator measures the total thickness for the various samples and then determines the overall thickness of the specimens, then the deformed points were measured and the values subtracted from the previous measurements and the deformations were determined.

5.5 PROJECTILES

A round nose cylindrical projectile was used in this study. The mass of the projectile varies between (.04012 ~ .04022) kg, with a density of 8.74 Mg/m^3 and a diameter of 0.0127 m. The material used for the projectile was 660 Bronze. The projectiles are made on a CNC-lathes machine, and the weight variance was less than 0.25% ($\pm 0.1 \text{ g}$).

CHAPTER 6

EXPERIMENTAL RESULTS

6.1 INTRODUCTION

In this chapter the static properties for the unidirectional laminates were calculated using classical lamination theory. The complete development of the theory is given in chapter 3. The developed equations correspond to the linear elastic response of a laminated composite subjected to in-plane loads and bending moments. Individual layers are assumed to be homogeneous, orthotropic, or transversely isotropic and in a state of plane stress. Laminates can be classified according to the stacking sequence and fiber orientation of the individual layers. In this study the specially orthotropic laminates were considered. In this type of laminates $[A_{16}]$ and $[A_{26}]$ are zero, and as a result there is no coupling between in-plane extensional and shear response. It is also important to note that $[D_{16}]$ and $[D_{26}]$ are not necessarily zero for a specially orthotropic laminate. Thus the term specially orthotropic refers to the in-plane response and not the bending response. In this study the two types of specially orthotropic laminates namely cross-ply laminates and angle-ply laminates and the combination of these two were investigated. The complete derivation of the theory and the required equations are given in Appendix C.

6.2 AS-4 RESULTS

The mid-plane deflection was measured using a dial indicator set up. The major and minor radii of the ellipsoid were also measured using a non-destructive Ultrasonic device. The speed of projectile was measured using a high-speed camera and the corresponding impact energy

was calculated. The static in-plane properties of different laminate and experimental results of testing for different laminate lay-ups are listed below:

Stacking sequence $[(45, -45, 0, 0)_2]_S$

$$A = \begin{bmatrix} 22.21 \times 10^7 & 5.053 \times 10^7 & 0 \\ 5.053 \times 10^7 & 6.80 \times 10^7 & 0 \\ 0 & 0 & 5.15 \times 10^7 \end{bmatrix} \quad D = \begin{bmatrix} 104.85 & 38.75 & 5.25 \\ 38.75 & 48.83 & 5.25 \\ 5.25 & 5.25 & 37.47 \end{bmatrix}$$

Table 6.1 Experimental results for $[(45, -45, 0, 0)_2]_S$ laminate

Points	Average velocity [m/s]	Mass [kg]	Major axis (a) [m]	Minor axis (b) [m]	Mid-plane deflection (w_0) [m]	Impact Energy (E) [J]
1	26.50	.04014	.0301	.008	.000535	14.09
2	34.28	.04017	.09192	.017131	.000866	23.60
3	41.60	.04009	.102063	.0264	.001347	34.69
4	48.13	.04011	.118625	.02752	Perforated	46.46

Stacking sequence $[(0, 0, 45, -45)_2]_S$

$$A = \begin{bmatrix} 22.2 \times 10^7 & 5.05 \times 10^7 & 0 \\ 5.05 \times 10^7 & 6.79 \times 10^7 & 0 \\ 0 & 0 & 5.15 \times 10^7 \end{bmatrix} N/m \quad D = \begin{bmatrix} 153.45 & 20.02 & 3.15 \\ 20.02 & 30.21 & 3.15 \\ 3.15 & 3.15 & 22.48 \end{bmatrix} Nm$$

Table 6.2 Experimental results for $[(0, 0, 45, -45)_2]_S$ laminate

Points	Average velocity [m/s]	Mass [kg]	Major axis (a) [m]	Minor axis (b) [m]	Mid-plane deflection (w_0) [m]	Impact Energy (E) [J]
1	26.48	.04014	.033327	.008694	.000518	14.07
2	34.14	.04019	.094185	.015939	.000862	23.42
3	42.12	.04015	.137655	.031358	.001422	35.62
4	48.12	.04016	.139864	.032247	Perforated	46.50

Stacking sequence $[(0,45,-45,0)_2]_S$

$$A = \begin{bmatrix} 22.2 \times 10^7 & 5.05 \times 10^7 & 0 \\ 5.05 \times 10^7 & 6.79 \times 10^7 & 0 \\ 0 & 0 & 5.15 \times 10^7 \end{bmatrix} N/m \quad D = \begin{bmatrix} 132.19 & 28.22 & 4.20 \\ 28.22 & 38.36 & 4.20 \\ 4.20 & 4.20 & 29.03 \end{bmatrix} Nm$$

Table 6.3 Experimental results for $[(0,45,-45,0)_2]_S$ laminate

Points	Average velocity [m/s]	Mass [kg]	Major axis (a) [m]	Minor axis (b) [m]	Mid-plane deflection (w_0) [m]	Impact Energy (E) [J]
1	26.38	.04018	.040055	.008741	.000551	13.98
2	34.63	.04014	.08694	.015886	.000841	24.69
3	41.65	.04015	.119959	.029924	.001393	34.83
4	48.19	.04014	.12473	.030678	Perforated	46.61

Stacking sequence $[(45,-45,0,90)_2]_S$

$$A = \begin{bmatrix} 14.5 \times 10^7 & 5.05 \times 10^7 & 0 \\ 5.05 \times 10^7 & 14.5 \times 10^7 & 0 \\ 0 & 0 & 5.15 \times 10^7 \end{bmatrix} N/m \quad D = \begin{bmatrix} 83.14 & 58.13 & 5.25 \\ 38.75 & 70.54 & 5.25 \\ 5.25 & 5.25 & 37.47 \end{bmatrix} Nm$$

Table 6.4 Experimental results for $[(45,-45,0,90)_2]_S$ laminate

Points	Average velocity [m/s]	Mass [kg]	Major axis (a) [m]	Minor axis (b) [m]	Mid-plane deflection (w_0) [m]	Impact Energy (E) [J]
1	26.27	.04013	.031244	.010921	.000563	13.85
2	34.12	.04014	.082506	.019986	.000869	23.37
3	41.49	.04015	.1016	.031909	.001289	34.56
4	48.29	.04016	.124449	.039716	.001522	48.09
5	58.88	.04020	.125419	.040028	Perforated	69.68

Stacking sequence $[(45, -45, 90, 0)_2]_S$

$$A = \begin{bmatrix} 14.5 \times 10^7 & 5.05 \times 10^7 & 0 \\ 5.05 \times 10^7 & 14.5 \times 10^7 & 0 \\ 0 & 0 & 5.15 \times 10^7 \end{bmatrix} N/m \quad D = \begin{bmatrix} 70.54 & 38.75 & 5.25 \\ 38.75 & 83.14 & 5.25 \\ 5.25 & 5.25 & 37.47 \end{bmatrix} Nm$$

Table 6.5 Experimental results for $[(45, -45, 90, 0)_2]_S$ laminate

Points	Average velocity [m/s]	Mass [kg]	Major axis (a) [m]	Minor axis (b) [m]	Mid-plane deflection (w_0) [m]	Impact Energy (E) [J]
1	26.91	.04016	.03092	.010941	.000565	14.54
2	34.74	.04011	.074385	.018947	.000854	24.20
3	41.48	.04011	.104573	.038986	.00149	34.51
4	48.27	.04015	.11279	.039645	Perforated	46.78

Stacking sequence $[(0, 90, 0, 90)_2]_S$

$$A = \begin{bmatrix} 17.93 \times 10^7 & 0.76 \times 10^7 & 0 \\ 0.76 \times 10^7 & 17.93 \times 10^7 & 0 \\ 0 & 0 & 1.71 \times 10^7 \end{bmatrix} N/m \quad D = \begin{bmatrix} 121.13 & 4.41 & 0 \\ 4.41 & 87.52 & 0 \\ 0 & 0 & 9.98 \end{bmatrix} Nm$$

Table 6.6 Experimental results for $[(0, 90, 0, 90)_2]_S$ laminate

Points	Average velocity [m/s]	Mass [kg]	Major axis (a) [m]	Minor axis (b) [m]	Mid-plane deflection (w_0) [m]	Impact Energy (E) [J]
1	27.16	.04014	.020063	.009886	.000559	14.81
2	34.52	.04015	.075005	.019668	.000899	23.92
3	41.55	.04017	.081325	.022765	Perforated	34.68

Stacking sequence $[(45, -45, 45, -45)_2]_S$

$$A = \begin{bmatrix} 11.06 \times 10^7 & 9.35 \times 10^7 & 0 \\ 8.28 \times 10^7 & 11.06 \times 10^7 & 0 \\ 0 & 0 & 8.60 \times 10^7 \end{bmatrix} N/m \quad D = \begin{bmatrix} 64.35 & 54.36 & 8.40 \\ 54.27 & 64.35 & 8.40 \\ 8.40 & 8.40 & 49.96 \end{bmatrix} Nm$$

Table 6.7 Experimental results for $[(45, -45, 45, -45)_2]_S$ laminate

Points	Average velocity [m/s]	Mass [kg]	Major axis (a) [m]	Minor axis (b) [m]	Mid-plane deflection (w_0) [m]	Impact Energy (E) [J]
1	26.22	.04015	.0132	.007196	.000511	13.80
2	34.55	.04017	.046412	.01656	.00092	23.98
3	41.91	.04017	.070202	.03083	.001434	35.28
4	48.95	.04015	.090167	.043412	.001854	48.05
5	59.22	.04011	.112538	.044318	Perforated	70.33

Figure 6.1 shows the impact points and the corresponding damaged area at the back of the plate. As it is shown, the damaged area is of the form of semi ellipse with major axis much greater than the minor axis. The ratio of major to minor axis (a/b) is between 2.5 to 3.5 for various stacking sequence.

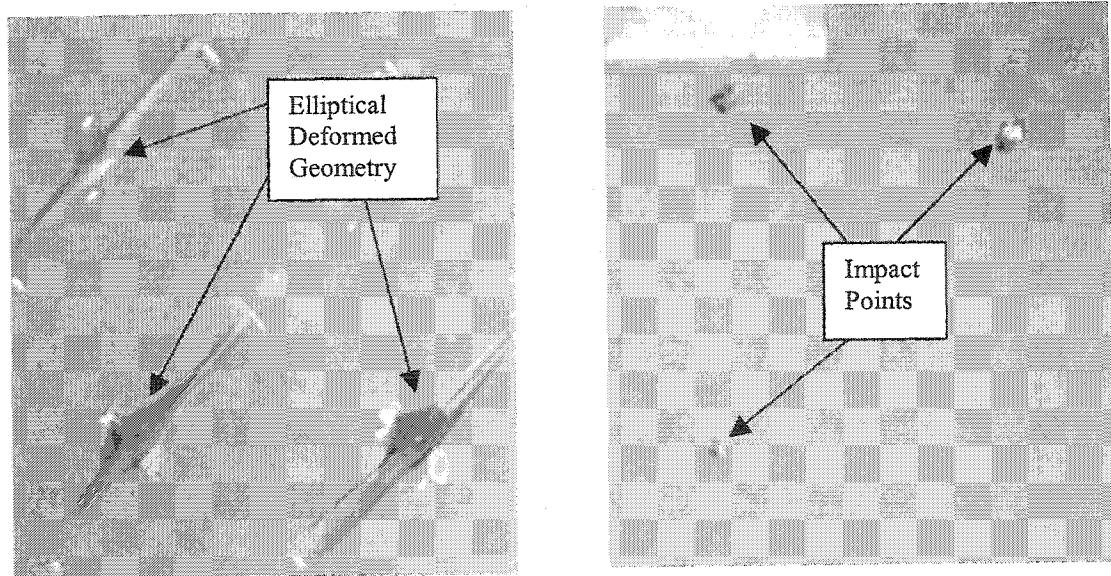


Figure 6.1 AS4 laminated plate after impact

6.3 HYBRID RESULTS

Here the AS4/3051 and IM7/5250 were combined with T1003 Glass/Epoxy (E-Glass) to form the hybrid composites. The mid-plane deflection was measured using a dial indicator set up for each hybrid laminate. The major and minor radii of the ellipsoid were also measured using non-destructive Ultrasonic device for both IM7-Eglass and AS4-Eglass hybrid. The speed of projectile was measured using a high-speed camera and the corresponding impact energy for each laminate was calculated. The static in-plane properties of different hybrid laminate and experimental results of testing for different hybrid laminate lay-ups are listed below:

Stacking sequence $[(45, -45, 0, 90)_2]_S$ E-Glass/AS4

$$A = \begin{bmatrix} 12.06 \times 10^7 & 4.31 \times 10^7 & 0 \\ 4.31 \times 10^7 & 12.06 \times 10^7 & 0 \\ 0 & 0 & 4.44 \times 10^7 \end{bmatrix} N/m \quad D = \begin{bmatrix} 83.88 & 40.64 & 4.71 \\ 40.64 & 73.83 & 4.71 \\ 4.71 & 4.71 & 36.92 \end{bmatrix} Nm$$

Table 6.8 Experimental results for $[(45, -45, 0, 90)_2]_S$ laminate

Points	Average velocity [m/s]	Mass [kg]	Major axis (a) [m]	Minor axis (b) [m]	Mid-plane deflection (w_0) [m]	Impact Energy (E) [J]
1	26.85	.04013	.009152	.005262	.000416	14.47
2	34.23	.04012	.012533	.006539	.000567	23.50
3	41.19	.04018	.018549	.008224	.000688	34.09
4	48.45	.04014	.022681	.011472	.000919	47.11
5	59.35	.04018	.059115	.025949	.001443	70.77
6	68.80	.04016	.072752	.032197	.001717	95.05
7	82.89	.04013	.083362	.033213	Perforated	137.86

Stacking sequence $[(45, -45, 90, 0)_2]_S$

E-Glass/AS4

$$A = \begin{bmatrix} 12.06 \times 10^7 & 4.31 \times 10^7 & 0 \\ 4.31 \times 10^7 & 12.06 \times 10^7 & 0 \\ 0 & 0 & 4.44 \times 10^7 \end{bmatrix} N/m \quad D = \begin{bmatrix} 73.83 & 40.64 & 4.71 \\ 40.64 & 83.89 & 4.71 \\ 4.71 & 4.71 & 36.92 \end{bmatrix} Nm$$

Table 6.9 Experimental results for $[(45, -45, 90, 0)_2]_S$ laminate

Points	Average velocity [m/s]	Mass [kg]	Major axis (a) [m]	Minor axis (b) [m]	Mid-plane deflection (w_0) [m]	Impact Energy (E) [J]
1	26.85	.04018	.010064	.005406	.000408	14.48
2	34.15	.04013	.015319	.00766	.000607	23.40
3	42.18	.04015	.021123	.009372	.00072	35.72
4	48.31	.04022	.025681	.013255	.000995	46.93
5	58.50	.04020	.043813	.022021	.001366	69.50
6	69.02	.04016	.067893	.032981	.001785	95.66
7	81.11	.04017	.082732	.034762	Perforated	132.14

Stacking sequence $[(-45, 45, 90, 0)_2]_S$

E-Glass/AS4

$$A = \begin{bmatrix} 12.06 \times 10^7 & 4.31 \times 10^7 & 0 \\ 4.31 \times 10^7 & 12.06 \times 10^7 & 0 \\ 0 & 0 & 4.44 \times 10^7 \end{bmatrix} N/m \quad D = \begin{bmatrix} 73.83 & 40.64 & -4.71 \\ 40.64 & 83.89 & -4.71 \\ -4.71 & -4.71 & 36.92 \end{bmatrix} Nm$$

Table 6.10 Experimental results for $[(-45, 45, 90, 0)_2]_S$ laminate

Points	Average velocity [m/s]	Mass [kg]	Major axis (a) [m]	Minor axis (b) [m]	Mid-plane deflection (w_0) [m]	Impact Energy (E) [J]
1	26.09	.04018	.010626	.005721	.000422	13.68
2	34.23	.04012	.014385	.007457	.000603	23.50
3	41.48	.04016	.017299	.009298	.000758	34.55
4	48.53	.04013	.022868	.012951	.000993	47.26
5	59.94	.04013	.046527	.023069	.00139	72.09
6	68.93	.04011	.071795	.030813	.001659	95.29
7	82.81	.04013	.081216	.031718	Perforated	137.60

Stacking sequence $[(0, 90, 0, 90)_2]_S$ E-Glass/AS4

$$A = \begin{bmatrix} 14.26 \times 10^7 & 1.01 \times 10^7 & 0 \\ 1.01 \times 10^7 & 14.26 \times 10^7 & 0 \\ 0 & 0 & 2.25 \times 10^7 \end{bmatrix} N/m \quad D = \begin{bmatrix} 107.89 & 10.01 & 0 \\ 10.01 & 7.90 & 0 \\ 0 & 0 & 22.33 \end{bmatrix} Nm$$

Table 6.11 Experimental results for $[(0,90,0,90)_2]_S$ laminate

Points	Average velocity [m/s]	Mass [kg]	Major axis (a) [m]	Minor axis (b) [m]	Mid-plane deflection (w_0) [m]	Impact Energy (E) [J]
1	26.71	.04016	.011883	.005686	.000417	14.33
2	34.11	.04016	.015216	.007597	.000609	23.36
3	41.41	.04017	.019568	.009697	.000761	34.44
4	48.47	.04018	.028715	.014172	.001004	47.20
5	59.42	.04014	.04494	.0223349	.001346	70.86
6	68.99	.04018	.074572	.031187	.001628	95.62
7	77.94	.04012	.103841	.033132	Perforated	121.86

Figure 6.2 shows the impact points and the corresponding damaged area at the back of the plate. It is also shown; the damaged area is of the form of semi ellipse with major axis much greater than the minor axis. The ratio of major to minor axis (a/b) is between 2.5 to 3.0 for various stacking sequence.

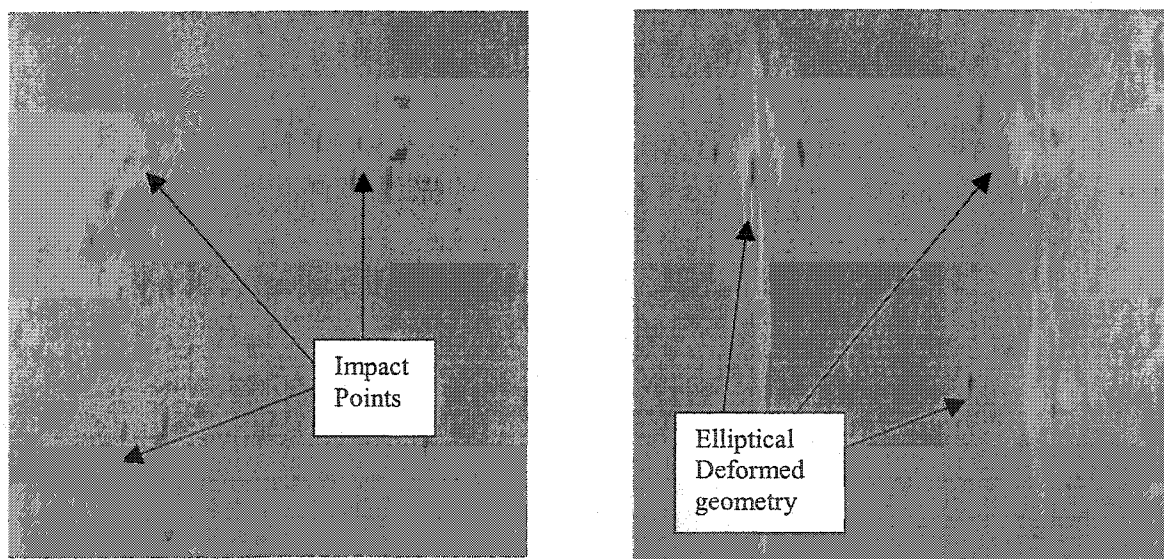


Figure 6.2 AS4/E-Glass laminated plate after impact

Stacking sequence $[(0,90,0,90)_2]_S$

E-Glass/IM7

$$A = \begin{bmatrix} 15.97 \times 10^7 & 0.99 \times 10^7 & 0 \\ 0.99 \times 10^7 & 15.97 \times 10^7 & 0 \\ 0 & 0 & 3.34 \times 10^7 \end{bmatrix} N/m \quad D = \begin{bmatrix} 65.80 & 6.13 & 0 \\ 6.13 & 46.20 & 0 \\ 0 & 0 & 14.24 \end{bmatrix} Nm$$

Table 6.12 Experimental results for $[(0,90,0,90)_2]_S$ laminate

Points	Average velocity [m/s]	Mass [kg]	Major axis (a) [m]	Minor axis (b) [m]	Mid-plane deflection (w_0) [m]	Impact Energy (E) [J]
1	26.26	.04014	.012957	.005356	.000406	13.84
2	34.68	.04015	.016038	.00737	.000601	24.14
3	41.15	.04015	.018609	.009605	.000767	33.99
4	48.90	.04017	.029961	.013398	.000947	48.03
5	59.87	.04018	.044332	.022054	.001317	72.11
6	69.43	.04015	.073854	.031725	.001625	96.77
7	80.84	.04015	.083173	.032741	Perforated	131.19

Stacking sequence $[(90,0,45,-45)_2]_S$

E-Glass/IM7

$$A = \begin{bmatrix} 13.89 \times 10^7 & 4.73 \times 10^7 & 0 \\ 4.73 \times 10^7 & 13.89 \times 10^7 & 0 \\ 0 & 0 & 5.9 \times 10^7 \end{bmatrix} N/m \quad D = \begin{bmatrix} 47.11 & 11.83 & 1.65 \\ 11.83 & 60.12 & 1.65 \\ 1.65 & 1.65 & 16.63 \end{bmatrix} Nm$$

Table 6.13 Experimental results for $[(90,0,45,-45)_2]_S$ laminate

Points	Average velocity [m/s]	Mass [kg]	Major axis (a) [m]	Minor axis (b) [m]	Mid-plane deflection (w_0) [m]	Impact Energy (E) [J]
1	26.82	.04018	.012697	.005416	.000405	14.45
2	34.30	.04016	.016938	.007607	.000608	23.62
3	41.40	.04015	.020854	.009925	.000774	34.41
4	48.33	.04015	.031851	.013318	.000944	46.89
5	59.57	.04013	.045832	.022004	.001327	71.20
6	68.83	.04014	.070854	.030625	.001632	95.08
7	83.59	.04019	.082437	.031069	Perforated	140.41

Figure 6.3 shows the impact points and the corresponding damaged area at the back of the plate. It is also shown; the damaged area is of the form of semi ellipse with major axis much greater than the minor axis. The ratio of major to minor axis (a/b) is between 2.5 to 3.0 for various stacking sequence.

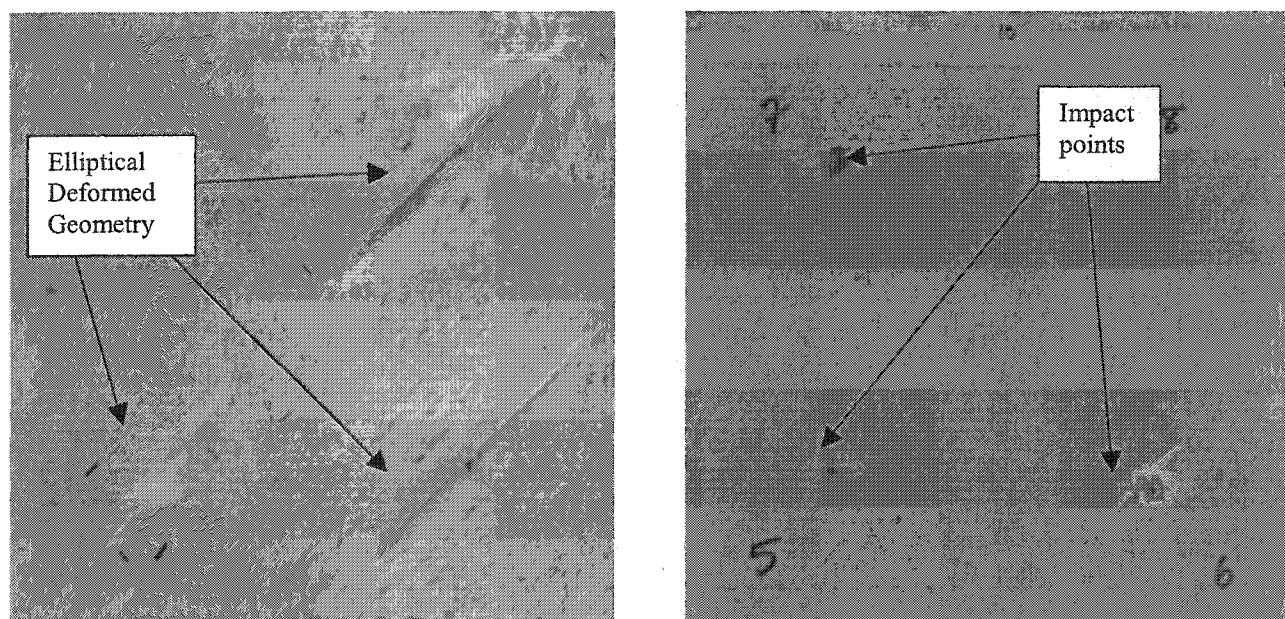


Figure 6.3 IM7/E-Glass laminated plate after impact

From the proceeding results the ballistic limit, which is defined, as the initial velocity of the projectile that results in complete penetration of the target with zero residual velocity, was determined. The ballistic limit velocities were experimentally measured using the high-speed camera and the values are listed in the following table (see table 6.14).

Table 6.14 Experimental results for ballistic limit velocity

<i>Stacking sequence</i>	<i>Material</i>	<i>Velocity (m/s)</i>
$[(45, -45, 0, 0)_2]_S$	AS4	48.13
$[(0, 0, 45, -45)_2]_S$	AS4	48.12
$[(0, 45, -45, 0)_2]_S$	AS4	48.19
$[(45, -45, 0, 90)_2]_S$	AS4	58.88
$[(45, -45, 90, 0)_2]_S$	AS4	48.27
$[(0, 90, 0, 90)_2]_S$	AS4	41.55
$[(45, -45, 45, -45)_2]_S$	AS4	59.22
$[(45, -45, 0, 90)_2]_S$	AS4/E-GLASS	82.89
$[(45, -45, 90, 0)_2]_S$	AS4/E-GLASS	81.11
$[(-45, 45, 90, 0)_2]_S$	AS4/E-GLASS	82.81
$[(0, 90, 0, 90)_2]_S$	AS4/E-GLASS	77.94
$[(0, 90, 0, 90)_2]_S$	IM7/E-GLASS	80.84
$[(90, 0, 45, -45)_2]_S$	IM7/E-GLASS	83.59

CHAPTER 7

DEVELOPMENT OF THE MATHEMATICAL MODEL

7.1 MATHEMATICAL MODEL OF DEFORMED GEOMETRY

When the projectile enters the target, the material is displaced laterally as well as downward, producing in-plane compression with a highly localized deformation gradient as well as out-of plane loading. The deflection w and the geometry of sub laminate delamination were studied after the impact. Based on the experimental results, it was observed that the delamination area is in the form of an ellipse and the out of plane deflection w of that area has a parabolic-like cross-section around the point of impact tapering off to a clamped type boundary condition around the elliptical boundary. Accordingly, the standard elliptic paraboloid equation is modified to relate the out of plane deflection w of the delaminated area to the major and minor axes of elliptical boundary, yielding the following form:

$$w = w_o \left(1 - \frac{x^2}{a^2} - \frac{y^2}{b^2}\right) + w_o \log\left(\frac{x^2}{a^2} + \frac{y^2}{b^2}\right) \quad (7.1)$$

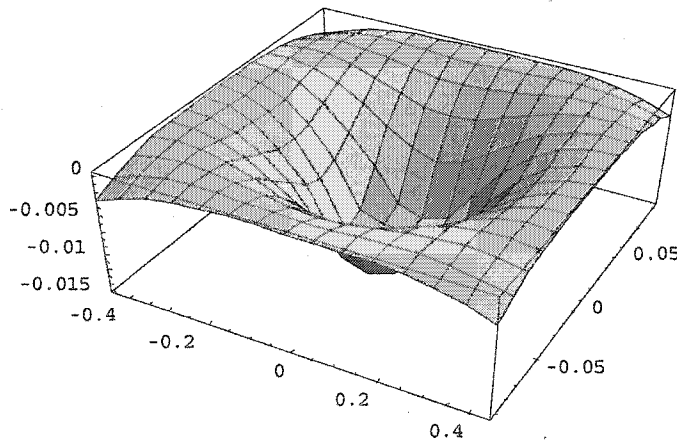


Figure 7.1 the assumed deformed geometry

where w_o is the deflection of the mid plane for the particular laminate and a, b are major and minor axes of an ellipse along directions x and y , respectively. It should be noted that there is a

discontinuity in the material at the point of impact due to the local fiber breakage. Thus, equation (7.1) is not defined at the point of impact but satisfies all other conditions.

Employing the Von Karman strain-displacement relations [61], strain ε and curvature κ are expressed as:

$$\varepsilon = (\varepsilon_x, \varepsilon_y, \gamma_{xy}) = \frac{1}{2} \left(\frac{\partial w}{\partial x} \right)^2, \frac{1}{2} \left(\frac{\partial w}{\partial y} \right)^2, \frac{1}{2} \left(\frac{\partial w}{\partial x} \frac{\partial w}{\partial y} \right) \quad (7.2)$$

$$\kappa = (\kappa_x, \kappa_y, \kappa_{xy}) = \left(-\frac{\partial^2 w}{\partial x^2} \right), \left(-\frac{\partial^2 w}{\partial y^2} \right), \left(-\frac{\partial^2 w}{\partial x \partial y} \right) \quad (7.3)$$

Where subscripts denote the component of strain and curvatures in x, y directions, respectively. Based on the static properties of composite laminate the strain energy of the plate is represented by [61]:

$$U = \frac{1}{2} \iint (\varepsilon^T A \varepsilon + 2\kappa^T B \varepsilon + \kappa^T D \kappa) dx dy \quad (7.4)$$

where A, B and D are the extensional, coupling and flexural stiffness matrices, respectively, for which can be calculated using the classical lamination theory. The complete calculation for the components of the laminated composite is given in (Appendix C). In the following analysis the lay-up of the laminate is symmetric with respect to the mid-plane, hence the effect of the coupling between extensional and bending matrices were considered to be zero. The mathematical model mainly responds to the geometry of the deformation under high velocity impact, and satisfies the required boundary conditions. The deflection which presented in equation (7.1) is then substituted to the equations (7.2) and (7.3), and the results were substituted in to the equation (7.4), the complete derivation of the equations were given in (Appendix B). The strain energy is therefore obtained as:

$$U = \left\{ \left\{ \frac{1}{90a^3b^3} (-60(5b^4(-4+3\pi)D_{11} + a^2(-2b^2(28+3\pi)D_{12} - a^2(20+9\pi)D_{22} + b^2(2+3\pi)D_{66}))w_0^2 + (18b^4(551-205\pi)A_{11} + a^2(10b^2(423\pi-922)A_{12} + 18a^2(551-50\pi)A_{22} + 5b^2(423\pi-922)A_{66}))w_0^4 \right\} \right\} \quad (7.5)$$

The strain energy in the equation (7.5) is derived based on the static properties of the composite laminate. The strain energy mainly consisted of two parts, respectively. One part includes the component of extensional matrices $[A]$ and the other part includes the components of bending matrices $[D]$, which are calculated using the classical lamination theory. The other parameters such as mid-plane deflection and the major and minor axis's are measured experimentally. The kinetic energy of the projectile entering the target is given by:

$$E = \frac{1}{2}mV^2 \quad (7.6)$$

in equation (7.6), m is the mass of the projectile and V is the velocity of the projectile. In this study the mass of the projectile is kept constant and, the erosion of the mass is neglected. It was also observed that the time required for the impact events are extremely short, therefore the effect of the friction forces between the projectile and the composite specimens were considered to be small and, hence was neglected. The following tables compare the strain energy during the impact using the static properties and the kinetic energy of the projectile for different stacking sequence and different materials. Knowing that the values obtained for the kinetic energy of the projectile is different than the values obtained for the strain energy; the dynamic correlation factors were introduced.

Table 7.1 comparisons of the strain energy and kinetic energy for AS4

<i>Stacking Sequence</i>	<i>A Component of U (J)</i>	<i>D Component of U(J)</i>	<i>Total Strain Energy U(J)</i>	<i>Kinetic Energy E(J)</i>
$[(45,-45,0,0)_2]_S$	26.85	28.24	55.09	14.09
$[(45,-45,0,0)_2]_S$	56.27	22.31	78.59	23.60
$[(45,-45,0,0)_2]_S$	101.76	16.85	118.61	34.69
$[(0,0,45,-45)_2]_S$	20.34	13.82	34.16	14.07
$[(0,0,45,-45)_2]_S$	70.00	17.18	87.18	23.42
$[(0,0,45,-45)_2]_S$	100.67	9.09	109.76	35.62
$[(0,45,-45,0)_2]_S$	30.38	23.38	53.75	13.98
$[(0,45,-45,0)_2]_S$	59.30	19.50	78.81	24.69
$[(0,45,-45,0)_2]_S$	93.61	11.29	104.90	34.83
$[(45,-45,0,90)_2]_S$	28.37	18.59	46.97	13.85
$[(45,-45,0,90)_2]_S$	68.39	18.42	86.81	23.37
$[(45,-45,0,90)_2]_S$	101.28	12.56	113.84	34.56
$[(45,-45,0,90)_2]_S$	125.22	11.15	136.36	48.09
$[(45,-45,90,0)_2]_S$	28.33	21.53	49.86	14.54
$[(45,-45,90,0)_2]_S$	67.77	22.16	89.93	24.20
$[(45,-45,90,0)_2]_S$	102.98	11.28	114.26	34.51
$[(0,90,0,90)_2]_S$	28.69	17.69	46.38	14.81
$[(0,90,0,90)_2]_S$	91.31	22.45	113.76	23.92
$[(45,-45,45,-45)_2]_S$	25.00	24.59	49.59	13.80
$[(45,-45,45,-45)_2]_S$	69.24	20.30	89.54	23.98
$[(45,-45,45,-45)_2]_S$	99.63	12.21	111.84	35.28
$[(45,-45,45,-45)_2]_S$	130.71	9.66	140.36	48.05

Table 7.2 comparisons of the strain energy and kinetic energy for AS4/E-Glass

<i>Stacking Sequence</i>	<i>A Component of U(J)</i>	<i>D Component of U(J)</i>	<i>Total Strain Energy U(J)</i>	<i>Kinetic Energy E(J)</i>
[(45,-45,0,90) ₂]s	19.18	30.24	49.43	14.47
[(45,-45,0,90) ₂]s	47.14	39.53	86.67	23.50
[(45,-45,0,90) ₂]s	74.69	42.00	116.69	34.09
[(45,-45,0,90) ₂]s	108.42	34.56	142.99	47.11
[(45,-45,0,90) ₂]s	146.46	18.70	165.16	70.77
[(45,-45,0,90) ₂]s	189.23	17.08	206.31	95.05
[(45,-45,90,0) ₂]s	17.98	32.81	50.79	14.48
[(45,-45,90,0) ₂]s	46.83	38.37	85.20	23.40
[(45,-45,90,0) ₂]s	68.95	39.79	108.74	35.72
[(45,-45,90,0) ₂]s	109.71	33.54	143.25	46.93
[(45,-45,90,0) ₂]s	144.27	23.38	167.66	69.50
[(45,-45,90,0) ₂]s	193.57	18.31	211.88	95.66
[(−45,45,90,0) ₂]s	18.29	31.25	49.53	13.68
[(−45,45,90,0) ₂]s	46.56	38.78	85.34	23.50
[(−45,45,90,0) ₂]s	72.42	38.28	110.71	34.55
[(−45,45,90,0) ₂]s	104.68	32.42	137.10	47.26
[(−45,45,90,0) ₂]s	142.77	22.31	165.09	72.09
[(−45,45,90,0) ₂]s	185.57	20.11	205.68	95.29
[(0,90,0,90) ₂]s	22.17	28.31	50.48	14.33
[(0,90,0,90) ₂]s	53.93	32.20	86.13	23.36
[(0,90,0,90) ₂]s	81.54	31.16	112.71	34.44
[(0,90,0,90) ₂]s	116.16	25.52	141.68	47.20
[(0,90,0,90) ₂]s	149.66	18.28	167.94	70.86
[(0,90,0,90) ₂]s	195.32	16.54	211.87	95.62

Table 7.3 comparisons of the strain energy and kinetic energy for IM7/E-Glass

<i>Stacking Sequence</i>	<i>A Component of U(J)</i>	<i>D Component of U(J)</i>	<i>Total Strain Energy U(J)</i>	<i>Kinetic Energy E(J)</i>
$[(0,90,0,90)_2]_S$	29.07	20.64	49.71	13.84
$[(0,90,0,90)_2]_S$	66.29	21.33	87.62	24.14
$[(0,90,0,90)_2]_S$	92.23	17.97	110.21	33.99
$[(0,90,0,90)_2]_S$	127.12	16.51	143.63	48.03
$[(0,90,0,90)_2]_S$	158.09	10.49	168.58	72.01
$[(0,90,0,90)_2]_S$	204.73	9.05	213.78	96.77
$[(90,0,45,-45)_2]_S$	24.81	26.15	50.95	14.45
$[(90,0,45,-45)_2]_S$	60.60	28.34	88.93	23.62
$[(90,0,45,-45)_2]_S$	88.81	25.51	114.32	34.41
$[(90,0,45,-45)_2]_S$	122.78	23.90	146.68	46.89
$[(90,0,45,-45)_2]_S$	154.68	15.11	169.79	71.20
$[(90,0,45,-45)_2]_S$	201.21	13.08	214.30	95.08

7.2 DYNAMIC CORRELATION TO STATIC PROPERTIES

In the previous section the strain energy was obtained using the assumed deflection function for the deformed geometry in conjunction with Von Karman strain displacement relation. The strain energy consists of two components; the extensional matrix [A] and the bending matrix [D]. These components were correlated to experimental impact energy, which was calculated during the impact of the laminated plates, using regression analysis. Two dynamic correlation factors for each stacking sequence associate to the extensional matrix and the bending matrix components were introduced. The first dynamic correlation factor (c_1) corresponds to the dynamic properties of the extensional matrix, and the second correlation factor (c_2) corresponds to the dynamic properties of the bending matrix. The values for these correlation factors are listed in the following table (see table 7.4).

An existing Genetic Algorithm program was used to determine the two dynamic correlation factors. This program uses the user-defined function and performs the regression analysis to minimize the error (the cost function) between the user-defined model and experimental data. In other words, the equation (7.5), experimentally found kinetic energy and the measured mid plane deflection were used as the input parameters for the GA program. The algorithm simulates the evolution of a series of constants to find the best fit for a given curve (equation 7.5). The GA works by randomly creating solutions to the problem at hand. On average, the randomly generated solutions are usually not very good at first. The major operations used in GA algorithm are; Reproduction, Sorting, Crossover, Mutation and finally Solution and cost function.

Reproduction selects the best individual candidates in the solution's population and duplicates them for the next generation. Then best candidates are sorted from the best solution to the least suitable solution. This process is called sorting. The crossover operation chooses pairs of individuals within the regenerated population to exchange information between the pairs, producing new fitting constants. The next operation is mutation. In this operation, individual constants are randomly selected and their design information are changed to produce solution out of the regenerated population. The final process is the minimization based on a cost function. This cost function is generally an error analysis function such as least square error. The evolution process continues for a certain number of generations and the best final generation is the optimum solution set of constants.

The dynamic correlation factors, determined using the regression analysis, are responsible for the dynamic properties of composite laminates subjected to the impact loading. As indicated before the first dynamic correlation factor converts the extensional stiffness [A], which was

determined statically, to the dynamic in-plane properties under impact. Equally, the second dynamic correlation factor converts the static bending stiffness [D] to the dynamic bending property under impact. The following figures depict the experimental kinetic energy and mathematical model vs. mid-plane deflection.

Table 7.4 Correlation factors for different stacking sequences

<i>Stacking Sequence And /Material</i>	<i>Dynamic Correlation Factor (C_1)</i>	<i>Dynamic Correlation Factor (C_2)</i>	<i>% Error</i>
[(45, -45, 0, 0) ₂] s (AS4)	0.317	0.206	0.362
[(0, 0, 45, -45) ₂] s (AS4)	0.258	0.545	5.492
[(0, 45, -45, 0) ₂] s (AS4)	0.362	0.133	0.100
[(45, -45, 0, 90) ₂] s (AS4)	0.323	0.213	2.816
[(45, -45, 90, 0) ₂] s (AS4)	0.292	0.270	0.680
[(0, 90, 0, 90) ₂] s (AS4)	0.086	0.698	0
[(45, -45, 45, -45) ₂] s (AS4)	0.324	0.208	2.039
[(45, -45, 0, 90) ₂] s (AS4/E-GLASS)	0.427	0.139	6.915
[(45, -45, 90, 0) ₂] s (AS4/E-GLASS)	0.423	0.165	5.236
[(45, 45, 90, 0) ₂] s (AS4/E-GLASS)	0.444	0.131	4.975
[(0, 90, 0, 90) ₂] s (AS4/E-GLASS)	0.412	0.123	7.122
[(0, 90, 0, 90) ₂] s (IM7/E-GLASS)	0.399	0.038	8.032
[(90, 0, 45, -45) ₂] s (IM7/E-GLAS)	0.392	0.110	9.058

Figure 7.2 shows the comparison between the experimental and mathematical results of $[(45, -45, 0, 0) \text{ } 2] \text{ s}$ tested at 3 points with 3 different velocities not including ballistic velocity. As figure indicates, the mathematical curve corresponds to the experimental curve with a list square cumulative error of %0.362.

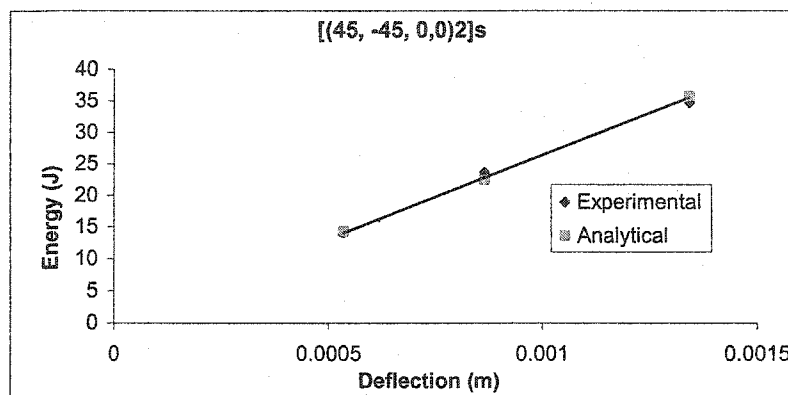


Figure 7.2 Energy comparisons for analytical and experimental for AS4 Plain graphite

Figure 7.3 shows the comparison between the experimental and mathematical results of $[(0, 0, 45, -45) \text{ } 2] \text{ s}$ tested at 3 points with 3 different velocities not including ballistic velocity. As figure indicates, the mathematical curve corresponds to the experimental curve with a list square cumulative error of %5.492.

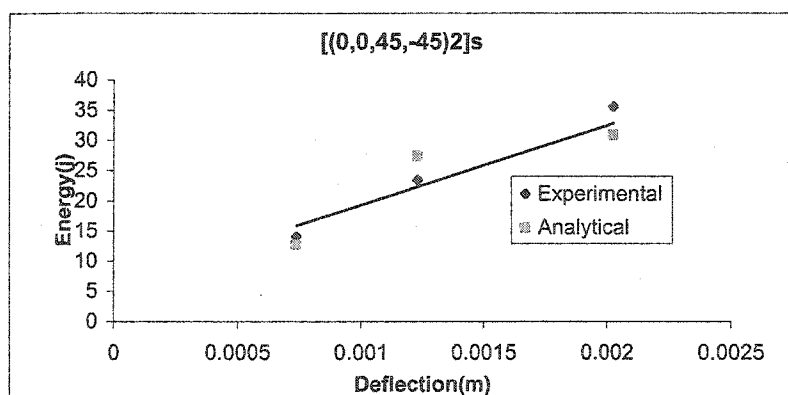


Figure 7.3 Energy comparisons for analytical and experimental for AS4 Plain graphite

Figure 7.4 shows the comparison between the experimental and mathematical results of $[(0, -45, -45, 0)_2]_S$ for AS4 plain-graphite composite laminate tested at 3 points with 3 different velocities not including ballistic velocity. As figure indicates, the mathematical curve corresponds to the experimental curve with a list square cumulative error of %0.1.

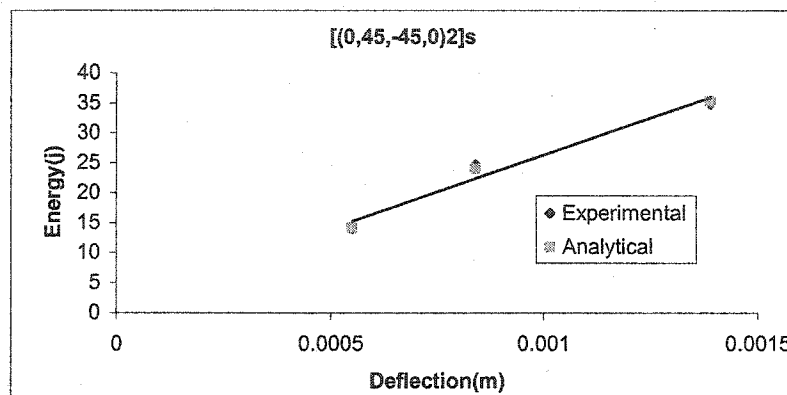


Figure 7.4 Energy comparisons for analytical and experimental for AS4 Plain graphite

Figure 7.5 shows the comparison between the experimental and mathematical results of $[(45, -45, 0, 90)_2]_S$ for AS4 plain-graphite composite laminate, tested at 4 points with 4 different velocities not including ballistic velocity. As figure indicates, the mathematical curve corresponds to the experimental curve with a list square cumulative error of %2.816.

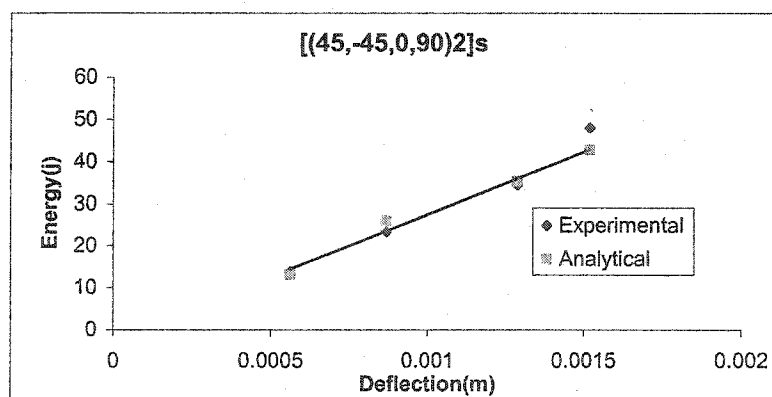


Figure 7.5 Energy comparisons for analytical and experimental for AS4 Plain graphite

Figure 7.6 shows the comparison between the experimental and mathematical results of $[(45, -45, 90, 0)2]s$ tested at 3 points with 3 different velocities not including ballistic velocity. As figure indicates, the mathematical curve corresponds to the experimental curve with a list square cumulative error of %0.680.

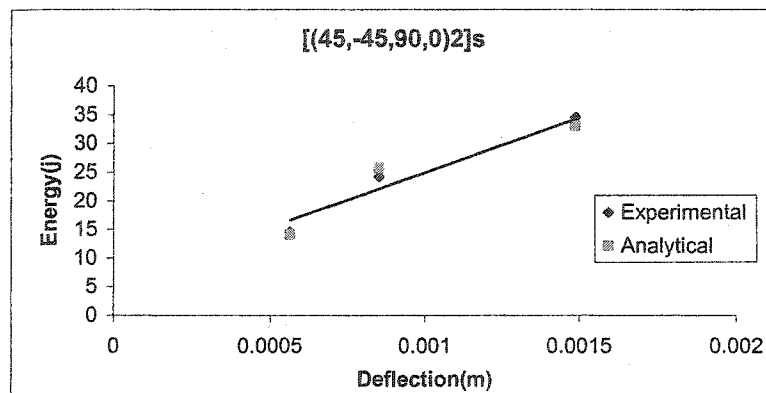


Figure 7.6 Energy comparisons for analytical and experimental for AS4 Plain graphite

Figure 7.7 shows the comparison between the experimental and mathematical results of $[(0, 90, 0, 90)2]s$ tested at 2 points with 2 different velocities not including ballistic velocity. As figure indicates, the mathematical curve corresponds to the experimental curve with a list square cumulative error of approximately zero.

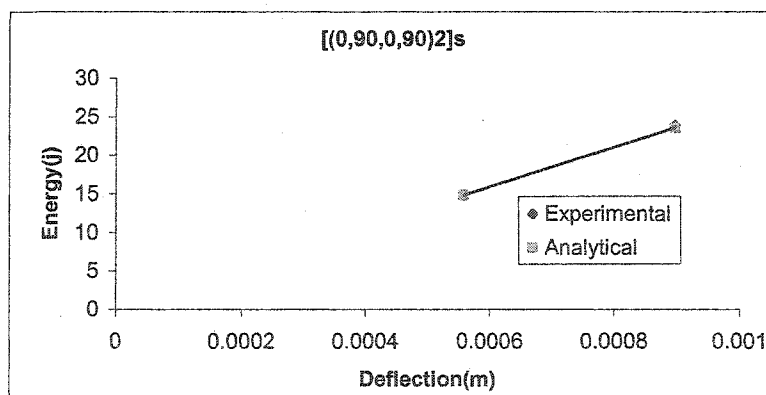


Figure 7.7 Energy comparisons for analytical and experimental for AS4 Plain graphite

Figure 7.8 shows the comparison between the experimental and mathematical results of $[(45, -45, 45, -45)_2]_S$ tested at 4 points with 4 different velocities not including ballistic velocity. As figure indicates, the mathematical curve corresponds to the experimental curve with a list square cumulative error of %2.039.

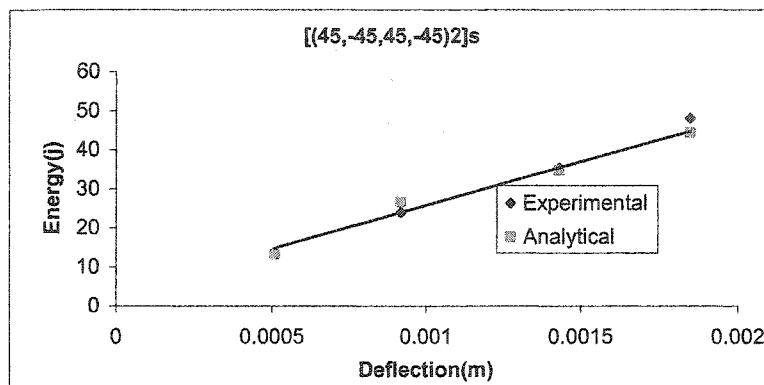


Figure 7.8 Energy comparisons for analytical and experimental for AS4 Plain graphite

Figure 7.9 –7.12 shows the comparison between the experimental and mathematical results of $[(45,-45,0,90)_2]_S$, $[(45,-45,90,0)_2]_S$, $[(-45,45,90,0)_2]_S$, and $[(0,90,0,90)_2]_S$ for AS4/E-Glass composite laminates, tested at 6 points with 6 different velocities not including ballistic velocity. As these figures indicate, the mathematical curve corresponds to the experimental curve with a list square cumulative errors of %6.915, %5.236, %4.975 and %7.122 respectively.

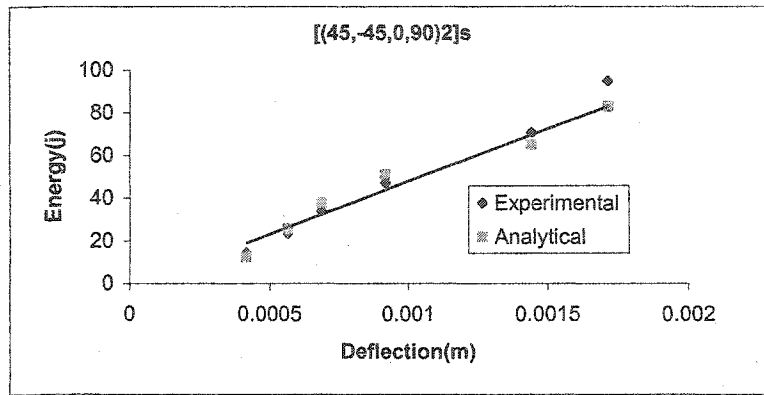


Figure 7.9 Energy comparisons for analytical and experimental for AS4/Eglass hybrid

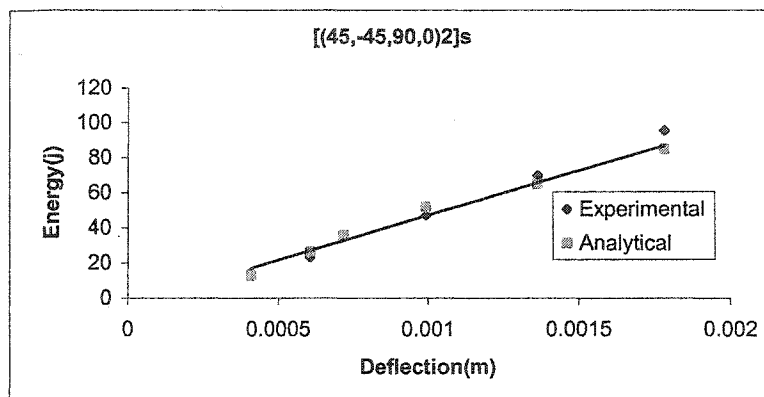


Figure 7.10 Energy comparisons for analytical and experimental for AS4/Eglass hybrid

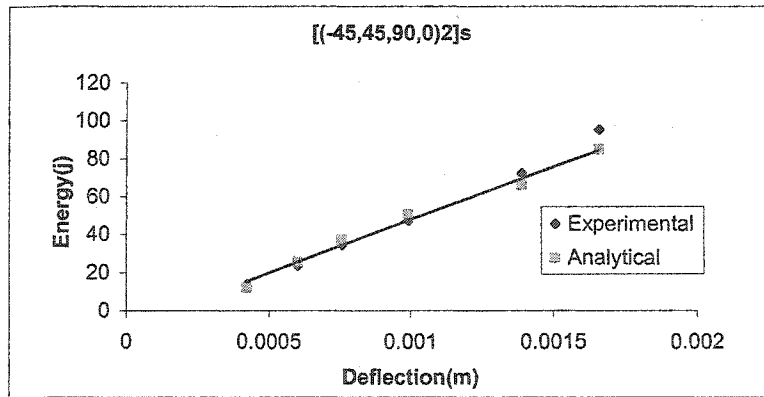


Figure 7.11 Energy comparisons for analytical and experimental for AS4/Eglass hybrid

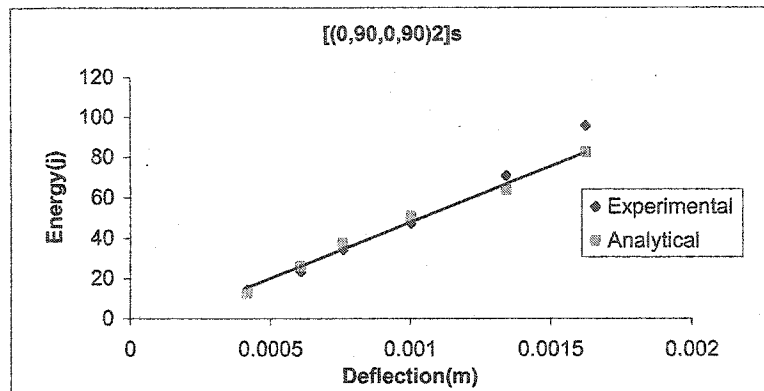


Figure 7.12 Energy comparisons for analytical and experimental for AS4/Eglass hybrid

Figure 7.13 –7.14 shows the comparison between the experimental and mathematical results of $[90,0,45,-45]_2s$, and $[(0,90,0,90)_2]s$ for IM7/E-Glass composite laminates, tested at 6 points with 6 different velocities not including ballistic velocity. As figure indicates, the mathematical curve corresponds to the experimental curve with a list square cumulative errors of %8.032, and %9.058 respectively.

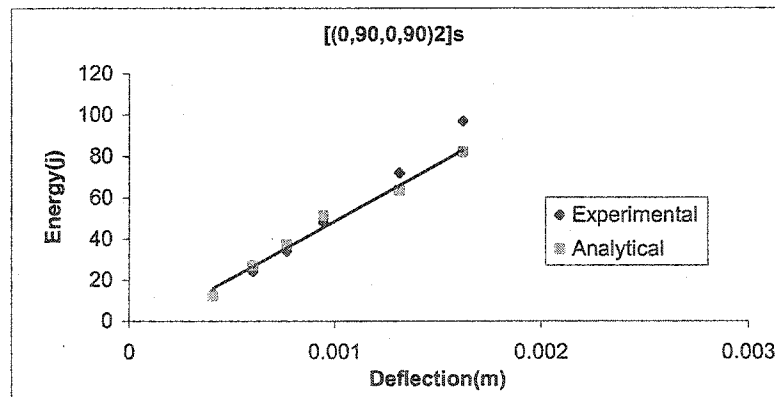


Figure 7.13 Energy comparisons for analytical and experimental for IM7/Eglass hybrid

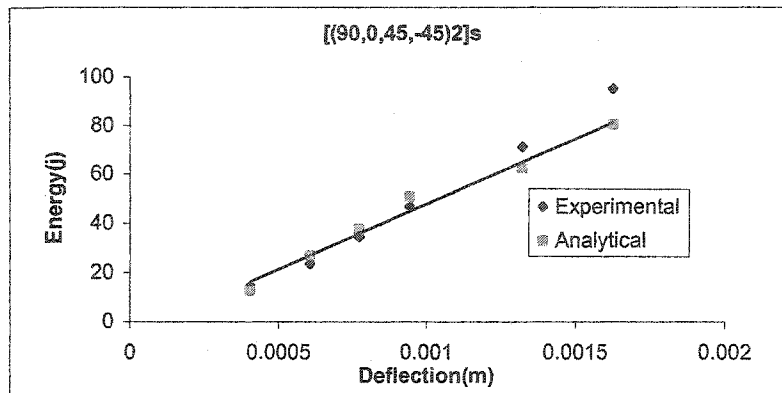


Figure 7.14 Energy comparisons for analytical and experimental for IM7/Eglass hybrid

Figure 7.2 to 7.14 compares the experimental results with the mathematical results for various stacking sequence. Figures 7.2 to 7.14 indicate an excellent agreement between experimental and mathematical results for each stacking sequence. This indicates that our proposed mathematical model could be used in the design of structures that may encounter high-speed impact.

CHAPTER 8

DISCUSSION AND RECOMMENDATIONS

8.1 DISCUSSION

The mathematical model appears to provide a reasonable representation of the deformation of composite laminates during the penetration by a cylindro-hemispherical projectile. Furthermore, the hybrid composites appear to provide more resistance to the impact, whereas the plain composites have less resistance with respect to the higher velocities. The reason can be directed towards the energy absorption capability of the E-Glass, which is capable of absorbing more energy during the impact, and hence less deformation on the back of the Graphite fiber. The ballistic limit velocity for hybrid composites is higher than other materials, which indicates these materials are capable of absorbing more energy during high impact applications.

On the other hand, it was found that, for the same stacking sequence, IM7/E-Glass has shown more resistance to penetration in terms of the absorbed energy and deformation area as compared to the AS4/E-Glass. The delamination is considerably less in hybrid composites than in the plain graphite composites. The amount of the out-of-plane deflection is also smaller in hybrid composites, both in IM7/E-Glass and AS4/E-glass, than in AS4 type composites by an average of 40%.

In studying the plain graphite composites, replacing $\pm 45^\circ$ with 0° had little effect on the energy absorption. However, the sub laminate delamination substantially decreases when ± 45 degree is placed first in the laminate. In other words, the values of major and minor axes are smaller in $[(\pm 45, 0, 0)_2]_S$ than $[(0, 0, \pm 45)_2]_S$ as shown in table 6.1 and 6.2.

In studying the graphite composites, the best orientation in terms of the stacking sequence was found to be $[(45,-45,0,90)_2]_S$ which indicates that this stacking sequence withstands a higher velocity and therefore absorbs more energy during the impact. This is a consequence of replacing the $\pm 45^\circ$ plies orientations in front of the point of the impact. Therefore, the quasi-isotropic orientation $[(45,-45,0,90)_2]_S$ is best for impact resistance if laminate is not combined with E-Glass.

The ballistic-limit velocity prior to the perforation for the Quasi-isotropic laminate was measured as 58.9 m/s. This is a significant increase compared to the other plain graphite samples. The energy required for the complete perforation is approximately 48 % higher in this stacking sequence as compared to other plain Graphite specimens. Table 6.14 summarizes the ballistic limit velocity of plane AS4 and hybrid samples.

It was also found that the energy absorption capability reduces significantly in the cross-ply laminates. The experimental results presented in chapter 6 shows that at a velocity of 41.5m/s complete perforation has occurred. Hence, cross-plied laminates are not suitable candidates for high-speed impact applications. The penetration resistance of the $[(0,90,0,90)_2]_S$ laminate and the energy required for the perforation are approximately 50 % less than for the other plain graphite specimens. It is believed that the increase between the interface angles for the same number of the plies could be the reason for this kind of behavior [80]. Here our experimental results support published data. The experimental results for $[(45,-45,0,0)_2]_S$, $[(0,0,45,-45)_2]_S$ and $[(0,45,-45,0)_2]_S$ graphite composite laminates indicated that it was not possible to establish clearly the influence of the fiber stacking sequence on the energy absorption and the damaged area. The composite laminate with two outer 0° plies exhibited approximately the same amount of damage and energy absorption capability as the laminate with $\pm 45^\circ$ as outer plies.

Measurements of the energy levels of the hybrid composites indicated that the hybrid composites offer the highest resistance to ballistic perforation. The hybrid composites perforated at velocities between 77 and 83 (m/s), whereas graphite composites perforated at velocities between 48 and 59 (m/s). The higher perforation resistance was attributed to the reduced level of delamination generated during the impact, and also the addition of the E-Glass, which was capable of absorbing more energy during the impact. Examination of the data shows that, for the range of impact energies considered here, the level of damage was least in the hybrid composites compare to the graphite composites.

In hybrid composites, the stacking sequence has an effect on energy absorption and the delamination area with respect to the resistance to perforation in the ballistic ranges. In the cross-ply laminates, the resistance to perforation at ballistic limit velocities is less than the resistance to perforation for quasi-isotropic orientation. Also, the damaged-area and minor and major axes, are larger in the cross-plied laminate than the Quasi-isotropic laminate.

As it was indicated before, the change of the material in a hybrid composite affects the growth of the damaged area and also reduces the impact penetration resistance. The results are tabulated in table 6.11 and 6.12 where the size of the major axis is significantly greater in the AS4/E-Glass compared to the IM7/E-Glass. Hence, the IM7/E-Glass hybrid has a higher resistance to penetration. Thus, it can be concluded that cross-plied orientations are not in general suitable when the resistance to penetration is the primary objective, whether plain graphite or hybrid laminate is used. The experimental results for $[(45, -45, 0, 90)_{2s}]$, $[(45, -45, 90, 0)_{2s}]$, and $[(-45, 45, 90, 0)_{2s}]$ AS4/Eglass hybrid composite laminates indicated that the stacking sequence has little effect in energy absorption capability. Replacing 0° plies with 90° plies within the laminate does not affect the impact resistant capability for these orientations as

long as the outer most layers are at 45° and -45° . It can also be concluded from the experimental results here that the Quasi-isotropic orientation has the best impact resistance in plain graphite or hybrid laminates.

The values obtained for the proposed strain energy function was determined using static properties of the laminate by employing classical lamination theory. As it is well documented, CLT makes few assumptions in deriving the stiffness of the material, thus introducing error in the calculation of in plane and bending stiffness of the laminate, please see reference [91] for complete derivation of CLT. Inherent inaccuracies of measuring equipment are other sources of error. Such error could be related to the equipment, which was used to determine the minor and major radii of the delaminated area and the mid-plane deflection. These errors have contributed to the differences between mathematical model and actual kinetic energy during the high-speed impact. However, through the introduction of correlation factors, these errors are minimized and good agreements between experimental and analytical data have been obtained.

8.2 RECOMMENDATIONS

From the analysis, the following guidelines are proposed to improve the impact damage resistance of composite plates.

1. Applying multiple-ply interface angles.
2. Applying small angular differences in fiber orientation for composite laminates.
3. Giving attention to the ply orientation relative to the plate boundaries.
4. Studying the effect of the ply grouping.
5. Studying the effect of ply orientation relative to the fixed axis.

REFERENCES

- [1] Abrate, S, (1991). "Impact on laminated composite materials". *Applied Mechanics Review* 44(4), 155-190.
- [2] Choi, H.Y., and Chang, F., (1991)." A new approach towards understanding damage mechanisms and mechanics of laminated composites due to low velocity impact". *Journal of Composite Materials* 25, 992-1038.
- [3] Cantwell, W.J., Curtis, P., and Morton, J. (1983)." Post impact fatigue performance of carbon fiber laminates with non-woven and mixed woven layers", *Composites*, 14(3), 301-305.
- [4] Cantwell, W.J., Curtis, P.T., and Morton, J., (1986). "An assessment of the impact performance of CFRP reinforced with high strain carbon fibers". *Composite Science and Technology* 25, 133-148.
- [5] Dorey, G., (1984), " Impact and crashworthiness of composite structures". *Structural Impact and Crashworthiness* 1,ed. G. A. O. Davies, Elsevier Applied Science Publishers, London.
- [6] Bradshaw, F.J., Dorey, G., and Sidney, G.R., (1972)." Impact resistance of carbon reinforced plastic", MOD, RAETR 72240.
- [7] Lagace, P.A., and Wolf, E., (1993). "Impact damage resistance of several laminated material systems". *Proceedings of the Structural Dynamics and Materials Conference, AIAA 93*, 1863-1872.
- [8] Cantwell, W.J., and Morton, J., (1991)," The impact resistance of composite materials"-a review. *Composites* 22(5), 347-362.
- [9] Sierakowski, R.L., and Chaturvedi, S.K.(1997), *Dynamic Loading and Characterization of Fiber-Reinforced Composites*. John Wiley & Sons, INC.
- [10] Cantwell, W.J., Morton, J (1989a)." Geometrical effects in the low velocity impact response of CFRP", *Composite Structures* 12(1), 39-60.
- [11] Choi, H.Y., Wang, H.S., and Chang, F., (1992)," Effect of laminate configuration and impactor's mass on the initial impact damage of graphite/epoxy composite plates due to line-loading impact", *Journal of Composite Materials* 26(6), 804-827.
- [12] Novak, R.C., and De Crescente, M.A., (1972)," Impact behavior of unidirectional of resin matrix composites tested in the fiber direction", *Composite Materials (Second Conference)*, ASTM STP 497, 311-323.

- [13] Chamis, C.C., Hanson, M.P., and Serafini, T.T., (1972)," Impact resistance of unidirectional fiber composites", Composite Materials: Testing and Design (Second Conference), ASTM STP 497, 311-323.
- [14] Cantwell, W.J., and Morton, J., (1989b), "Comparison of low and high velocity impact response of CFRP", Composites, 20(6), 545-551.
- [15] Cantwell, W.J., and Morton, J., (1989c)," The influence of varying projectile mass on the impact response of CFRP", Composite Structures, 13, 101-114.
- [16] Cantwell, W.J., and Morton, J., (1990a), "Impact perforation of carbon fiber reinforced plastic", Composites Science and Technology, 38, 119-141.
- [17] Cantwell, W.J., and Morton, J., (1990b)," An assessment of residual strength of an impact-damaged carbon fiber reinforced epoxy", Composites Structures, 14, 303-317.
- [18] Wang, C.J., and Jang, B.Z., (1991)," Deformation and fracture mechanisms of advanced polymer composites under impact loading", Journal of Thermoplastic Composite Materials, 4, 140-172.
- [19] Paine, J.S.N., and Rogers, C.A., (1995)," Observations of the drop-weight impact response of composites with surface bonded nitinol layers", Durability and Damage Tolerance of Composites Symposium, ASME IMEC&E, San Francisco, CA, Nov. 12-18.
- [20] Gillespie, Jr, J.W., and Carlson, L.A., (1987)," Rate dependent mode I interlaminar crack growth mechanisms in graphite/epoxy and graphite/PEEK", Composite Science and Technology, 28, 1-15.
- [21] Oppenheimer, D.W., and Slepetz, J.M., (1975)," Impact damage tolerance of graphite/epoxy sandwich panels", Foreign Object Impact Damage to Composites, ASTM STP 568, 30-48.
- [22] Curtis, P.T., (1984)," An initial evaluation of a high-strain carbon fiber reinforced epoxy", Royal Aircraft Establishment, TR 84004.
- [23] Hedrick, J.C., Niranjan, M.P., and Mc Grath, J.E., (1993)," Toughening of epoxy resin networks with functionalized engineering thermoplastic", Advances in Chemistry, 208, 293-304.
- [24] Haung, Y., Kinloch, A.J., Bertsch, R.J., and Siebert, A.R., (1993), effect on the fracture properties of rubber-modified epoxy polymers, Advances in Chemistry, 208, 189-210.
- [25] Hunston, D.L., et al., (1987), Matrix resin effects in composite delamination: mode I fracture aspects, Toughened Composites, ASTM STP 937, 74-79.
- [26] Williams, J.G., and Rhodes, M.D., (1982)," Effects of resins on impact damage tolerance of graphite/epoxy laminates", ASTM STP 787, 450.

- [27] Wang, H., and Vu-Khan, (1991), "Impact induced delamination in [0₅,90₅0₅] carbon fiber/polyetheretherketone composite laminates", Polymer Engineering and Science31 (18), 1301-1309.
- [28] Chan, W.S., Rogers, C., and Aker, S., (1986), Improvement of edge delamination strength of composite laminates using adhesive layers, Composite Material Testing and Design, 25,992-1038.
- [29] Sun, C.T., and Rechak, S., (1988)," Effect of adhesive layers on impact damage in composite laminates", Composite Material Testing and Design, ASTM STP 972, 97-123.
- [30] Bascom, W.D., Gwoen, S.Y., and Grande, D., (1993)," Multiphase matrix polymers for carbon-fiber composites", Advances in Chemistry, 208, 519-537.
- [31] Hoisington, M.A., and Seferis, J.C., (1993)," Model multi-layer toughened thermosetting advanced composites", Advances in Chemistry, 208, 505-518.
- [32] Rechak, S., AND Sun, C.T., (1990), "optimal use of adhesive layers in reducing impact damage in composite laminates", Journal of Reinforced Plastic and Composites, 9,569-582.
- [33] Jang, B.Z., and Chung, W.C., (1986), "Structure -property relationships in three dimensionally reinforced fibrous composites", Advanced Composites: Latest Development, ASM international, 138-192.
- [34] Su, K.B., (1989)," Delamination resistance of stitched thermoplastic matrix composite laminates", Advances in Thermoplastic Matrix Composite Materials, ASTM STP 1044, 279-300.
- [35] Kang, T.J., and Lee, S.H., (1994)," Effect of stitching on the mechanical and impact properties of woven laminate composite", Journal of Composites Materials, 28(16), 1574-1587.
- [36] Jang, B.Z., Chen, L.C., Wang, C.Z., Lin, H.T., and Zee, R.H., (1989)," Impact resistance and energy absorption mechanics in hybrid composites", Composite Science and Technology, 34, 305-335.
- [37] Adams, D.F., and Miller, A.K., (1975)," An analysis of the impact behavior of hybrid composite materials", Materials Science and Engineering, 19, 245-260.
- [38] Hariss, B., and Bunsell, A.R., (1975)," Impact properties of glass fiber/carbon fiber hybrid composites", Composites, 197-201.
- [39] Manders, P.W., and Bader, M.G., (1981)," The strength of hybrid glass/carbon fiber composites. Part I. Failure strain enhancement and failure mode", Journal of Material Science, 16,2233-2245.

- [40] Dorey, G., Sidney, G.R., and Huchings, J., (1978)," Impact properties of carbon fiber/Kevlar 49 fiber hybrid composites", Composites, 25-32.
- [41] Wardle, M.W., (1982)," Impact damage tolerance of composites reinforced Kevlar aramid fibers", Progress in Science and Engineering of Composites, 1, 837-844.
- [42] Marom, G., Drukker, E., Weinberg, A., and Banbaji, J., (1986), "Impact behavior of carbon/fiber hybrid composites", Composites, 17(2), 150-153.
- [43] Cordova, D.S., and Bhatnager, A., (1987), High performance hybrid reinforced fiber composites, SAMPE technical Conference, Anaheim, California, 4-9.
- [44] Poursartip, A., Riahi, G., Teghtsoonian, E., Chinatambi, N., and Mulford, N., (1987), mechanical properties of PE fiber /carbon fiber hybrid laminates, ICCM-VI and ECCM-II, 1, Elsevier Applied Science, 209-220.
- [45] Hsieh, C.Y., Mount, A., Jang, B.Z., and Zee, R.H., (1990)," Response of polymer composites to high and low velocity impact", 22nd International SAMPE Technical Conference22, 14-27.
- [46] Jenq, S.T., Wang, S.B., and Sheu, L.T., (1992), "A model for predicting the residual strength of GFRP laminates subjected to ballistic impact", Journal of Reinforced Plastic and Composites, 11, 1127-1141.
- [47] Dikshit, S.N., and Sundararajan, G., (1992), "Effect of clamping rigidity of the armour on ballistic performance", Defense Science Journal, 42(2), 117-120.
- [48] Cristescu, H.Y., Malvern, L.E., and Sierakowski, R.L., (1975)," Failure mechanisms in composite plates impacted by blunt-ended penetrators", Foreign Object Impact Damage to Composites, ASTM STP, 568, 159-172.
- [49] Hong, S., and Liu, D., (1989)," On the relationship between impact energy and delamination area", Experimental Mechanics, 29(2), 115-120.
- [50] Strait, L.H., Karasek, M.L., and Amateau, M.F., (1992)," Effects of stacking sequence on the impact resistance of carbon fiber reinforced thermoplastic toughened epoxy laminates", Journal of Composite Materials, 26(12), 1725-1740.
- [51] Hitchen, S.A., and Kemp, R.M.J., (1995)," The effect of stacking sequence on impact damage in a carbon/fiber epoxy composites", Composites, 26(3), 207-214.
- [52] Finn, S.R., He, Y., and Springer, G.S., (1993), "Delaminations in composite plates under transverse impact load, Experimental Results", Composite Structures, 23, 191-204.

- [53] Baker, A.A., Jones, r., and Callinan, R.J., (1985)," Damage tolerance of graphite/epoxy composites", Composite Structures, 4, 15-44.
- [54] Curtis, P.T., and Bishop, S.M., (1984), "An assessment of the potential of woven carbon fiber-reinforced plastics for high performance applications", Composites, 15(4), 259-264.
- [55] Husman, G.E., Whitney, J.M., and Halpin, J.C., (1975)," Residual strength characterization of laminated composites subjected to impact loading", Foreign Object Impact Damage to Composites, ASTM STP, 568, 92-113.
- [56] Suarez, J.A., and Whiteside, J.B., (1975),"comparison of residual strength of composite and metal structures after ballistic damage", Foreign Object Damage to Composites, ASTM STP, 568, 72-91.
- [57] Zee, R.H., and Hsieh, C.Y., (1993)," Energy loss partitioning during ballistic impact of polymer composites", Polymer Composites, 14(3), 265-271.
- [58] Sykes, G.F., and Stoakley, D.M., (1980)," Impact penetration studies of graphite/epoxy laminates", Proc. 12th Nat. SAMPE technical Conference, 482-493.
- [59] Zhu, G., Goldsmith, W., and Dharan, C.H.K., (1992b)," Penetration of laminated Kevlar by projectiles: Experimental Investigation", International Journal of Solid Structures, 29(4), 399-420.
- [60] Czarnecki, G., (1992a), "A preliminary investigation of dual mode fracture sustained by graphite/epoxy laminates impacted by high-velocity spherical metallic projectile", MS Thesis University of Dayton.
- [61] Zhu, G., Goldsmith, W., and Dharan, C.H.K., (1992a), "Penetration of laminated Kevlar by projectiles: Analytical Model", International Journal of Sold Structures, 29(4), 421-436.
- [62] Prevorsek, D.C., Kwon, Y.D., and Chin, H.B., (1994)," Analysis of the temperature rise in the projectile and extended chain polyethylene fiber composite armour during ballistic impact and penetration", Polymer Engineering and Science, 34(2), 141-152.
- [63] Bhatnagar, A., Lin, L.C., Lang, D.C., and Chang, H.W., (1989)," comparison of ballistic performance of composites", 34th International SAMPE Symposium, 1529-1537.
- [64] Kang, T.J., and Lee, S.H., (1994)," Effect of stitching on the mechanical and impact properties of woven laminate composite", Journal of Composite Materials, 28(16), 1574-1587.
- [65] Lin, L.C., and Bhatnager, A., (1992), "Ballistic energy absorption of composites-III", 24th International Technical Conference, 24, 291-306.
- [66] Bless, S.J., and Hartman, D.R., (1989)," Ballistic penetration of S-2 glass laminates", 21st International SAMPE Technical Conference, 21, 852-866.

- [67] Lin, L.C., Bhatnager, A., and Chang, H.W., (1990)," Ballistic energy absorption of composites", 22nd International SAMPE Technical Conference, 1-13.
- [68] Heatherington, J.G., and Rajagopalan, B.P., (1991)," An investigation into the energy absorbed during ballistic perforation of composite armors", International Journal of Impact Engineering, 11(1), 33-40.
- [69] Gupta, N.K., and Madhu, V., (1992), "Normal and oblique impact of a kinetic energy projectile on mild steel plates", International Journal of Impact Engineering, 12(3), 333-343.
- [70] Jenq, S.T., Jing, H.S., and Chung, C., (1994)," Predicting the ballistic limit for plain woven glass/epoxy composite laminate", International Journal of Impact Engineering, 15(4), 451-464.
- [71] Cuniff, P.M., Song, J.W., and Ward, J.E., (1989)," Investigation of high performance fibers for ballistic impact resistance potential", 21st International SAMPE Technical Conference, 840-847.
- [72] Heatherington, J.G., (1992), "The optimization of two component composite armors, International Journal of Impact Engineering", 12(3), 409-414.
- [73] Wright, S.C., Fleck, N.A., and Stronge, W.J., (1993)," Ballistic impact of polycarbonate-An Experimental Investigation", International Journal of Impact Engineering, 13(1), 1-20.
- [74] Walters, W., and Scott, B.R., (1990)," High velocity penetration of Kevlar reinforced laminate", 22nd International SAMPE Technical Conference, 1078-1091.
- [75] Dikshit, S.N., Kutumbarao, V.V., and Sundararajan, G., (1995),"The influence of plate hardness on the ballistic penetration of thick steel plates", International Journal of Impact Engineering, 16(2), 293-320.
- [76] Pageau, G., Vaziri, R., and Poursartip, A., (1991), "An evaluation of metal matrix composites as ballistic protection materials", 22nd International SAMPE Technical Conference, 639-650.
- [77] Azzi, B., Bless, S., and Brar, N.S., (1991)," Force measurements projectiles penetrating fiber reinforced composite targets", 23rd International Technical Conference, 616-623.
- [78] Zee, R.H., Wang, C.J., Mount, A., Jang, B.J., and Hsieh, C.Y., (1991), "Ballistic response of polymer composites", Polymer Composites, 12(3), 196-202.
- [79] Dorey, G., (1974),"Fracture behavior and residual strength of carbon fiber composites subjected to impact loads", AGARD CP 163, Advisory Group for Aerospace Research and Development, 8-1.

- [80] Cantwell, W.J., and Morton, J., (1985b)," Detection of impact damage in CFRP laminates", Composite Structures, 3, 241-257.
- [81] Ross, C.A. and Sierakowski, R.L. (1973)." Studies on the impact resistance of composite plates", Composites, 4, 157-161.
- [82] Cantwell, W.J. (1988). "The influence of target geometry on the high velocity response of CFRP", Composite Structures, 10(3), 247-265.
- [83] Lee, B.L., Song, J.W., and Ward (1994), "Failure of spectra polyethylene fiber-reinforced composites under ballistic impact loading", Journal of Composite Materials, 28(13), 1202-1226.
- [84] Sun, C.T., and Grady, J.E (1988a)." Dynamic delamination fracture toughness of a graphite/epoxy laminate under impact". Composite Science and Technology 31, 55-72.
- [85] Daniel, M. and Liber, T. (1976)." Wave propagation in fiber composite laminates", NASA CR-135086, June.
- [86] Takeda, N. (1980)." Experimental studies of the delamination mechanisms in impacted fiber-reinforced composite plates", Ph.D. dissertation, University of Florida.
- [87] Takeda, N., Sierakowski, R.L., and Malvern, L.E. (1981). "Wave propagation experiments on ballistic ally impacted composite laminates", Journal of Composite Materials, 15, 157-174.
- [88] Hirschbuehler, K.R. (1987). "A comparison of several mechanical tests used to evaluate the toughness of composites", ASTM STP 937, pp. 61-73.
- [89] Peiffer, D.G. (1979)." Impact strength of thick interlaminar composites", Journal of Applied Polymer Science, 24, 1451-1455.
- [90] Malvern, L.E., Sun, C.T., and Liu, D. (1987)," Damage in composite laminates from central impacts at sub perforation speeds", Proceedings of the Symposium in memory of Prof. Bisplinghoff, Editor, P. Hajela, University of Florida Press, Gainesville, FL, pp. 298-312.
- [91] Herakovich, C. T. (1997), Mechanics of Fibrous Composites. J.Wiley, New York.

Appendix A

MATLAB Program

```

gama = 1.4;           % specific for air
mp = .140;           % mass of projectile
R = 287;             % gass constant KJ/kg.K
T1 = 294;             % K
T2 = 294;             % K
a2 = 333;             % m/s2
a1 = sqrt(gama* R * T2); % m/s2
P1 = 101400;          % N/m2
P2 = 861844;          % N/m2
A = 1.26677e-4;       % area of the pipe
d = 0;                % distance in meter
v = 0;                % velocity, initial condition
vp = 0;               % initial velocity of projectile
acc = 0;              % initial acceleration
t = 0;                % time at zero
tbar = 0;              % time average
deltbar = 0;           % incremental average time
delt = .0005;          % time increment
n = 100;
for i=1:n
    acc = ((1-((gama-1)/2)*(a1/a2)*v))^(2*gama/(gama-1)) - ((P1/P2)*(1+((gama-1)/2)*(v^2))
    + gama*v*sqrt(1+(((gama+1)/4)*(v^2))));;
    t = t + delt;
    deltbar = (P2*A*delt)/(mp*a1);
    tbar = tbar + deltbar;
    v = v + acc*deltbar;
    vp = a1*v;
    d = vp*deltbar;
    plot(t,d,'r+');
end

```

```
%plot(t, vp, 'gx');
hold on;
end
```

Appendix B

Derivation of Deflection Function

$$\left(w_0 * \left(1 - \frac{x^2}{a^2} - \frac{y^2}{b^2} \right) + w_0 * \text{Log} \left[\left(\frac{x^2}{a^2} + \frac{y^2}{b^2} \right) \right] \right)$$

Strain = X

$$\partial_x \left(w_0 * \left(1 - \frac{x^2}{a^2} - \frac{y^2}{b^2} \right) + w_0 * \text{Log} \left[\left(\frac{x^2}{a^2} + \frac{y^2}{b^2} \right) \right] \right) // \text{FullSimplify}$$

$$\frac{2x \left(-1 + \frac{1}{\frac{x^2+y^2}{a^2+b^2}} \right) w_0}{a^2}$$

$$1/2 * \left(\frac{2x \left(-1 + \frac{1}{\frac{x^2+y^2}{a^2+b^2}} \right) w_0}{a^2} \right)^2 // \text{FullSimplify}$$

$$\frac{2x^2 \left(-1 + \frac{1}{\frac{x^2+y^2}{a^2+b^2}} \right)^2 w_0^2}{a^4}$$

Strain - Y

$$\partial_y \left(w_0 * \left(1 - \frac{x^2}{a^2} - \frac{y^2}{b^2} \right) + w_0 * \text{Log} \left[\left(\frac{x^2}{a^2} + \frac{y^2}{b^2} \right) \right] \right) // \text{FullSimplify}$$

$$\frac{2y \left(-1 + \frac{1}{\frac{x^2+y^2}{a^2+b^2}} \right) w_0}{b^2}$$

$$1/2 * \left(\frac{2y \left(-1 + \frac{1}{\frac{x^2+y^2}{a^2+b^2}} \right) w_0}{b^2} \right)^2 // \text{FullSimplify}$$

$$\frac{2y^2 \left(-1 + \frac{1}{\frac{x^2}{a^2} + \frac{y^2}{b^2}} \right)^2 w_0^2}{b^4}$$

Strain - XY

$$1/2 * \left(\frac{2x \left(-1 + \frac{1}{\frac{x^2}{a^2} + \frac{y^2}{b^2}} \right) w_0}{a^2} * \frac{2y \left(-1 + \frac{1}{\frac{x^2}{a^2} + \frac{y^2}{b^2}} \right) w_0}{b^2} \right) // \text{FullSimplify}$$

$$\frac{2xy \left(-1 + \frac{1}{\frac{x^2}{a^2} + \frac{y^2}{b^2}} \right)^2 w_0^2}{a^2 b^2}$$

Curvature - X

$$-\partial_x \left(\frac{2x \left(-1 + \frac{1}{\frac{x^2}{a^2} + \frac{y^2}{b^2}} \right) w_0}{a^2} \right) // \text{FullSimplify}$$

$$\frac{2 \left(\frac{2x^2}{\left(\frac{x^2}{a^2} + \frac{y^2}{b^2} \right)^2} + a^2 \left(1 - \frac{1}{\frac{x^2}{a^2} + \frac{y^2}{b^2}} \right) \right) w_0}{a^4}$$

Curvature - Y

$$-\partial_y \left(\frac{2y \left(-1 + \frac{1}{\frac{x^2}{a^2} + \frac{y^2}{b^2}} \right) w_0}{b^2} \right) // \text{FullSimplify}$$

$$\frac{2 \left(\frac{2y^2}{\left(\frac{x^2+y^2}{a^2+b^2} \right)^2} + b^2 \left(1 - \frac{1}{\frac{x^2}{a^2} + \frac{y^2}{b^2}} \right) \right) w_0}{b^4}$$

Curvature - XY

$$-\partial_x \left(\frac{2y \left(-1 + \frac{1}{\frac{x^2+y^2}{a^2+b^2}} \right) w_0}{b^2} \right) // \text{FullSimplify}$$

$$\frac{4a^2 b^2 x y w_0}{(b^2 x^2 + a^2 y^2)^2}$$

Membrane Stiffness, A*

$$\begin{pmatrix} \frac{2x^2 \left(-1 + \frac{1}{\frac{x^2+y^2}{a^2+b^2}} \right)^2 w_0^2}{a^4} & \frac{2y^2 \left(-1 + \frac{1}{\frac{x^2+y^2}{a^2+b^2}} \right)^2 w_0^2}{b^4} & \frac{2xy \left(-1 + \frac{1}{\frac{x^2+y^2}{a^2+b^2}} \right)^2 w_0^2}{a^2 b^2} \\ & \frac{2x^2 \left(-1 + \frac{1}{\frac{x^2+y^2}{a^2+b^2}} \right)^2 w_0^2}{a^4} & \\ & \frac{2y^2 \left(-1 + \frac{1}{\frac{x^2+y^2}{a^2+b^2}} \right)^2 w_0^2}{b^4} & \\ & \frac{2xy \left(-1 + \frac{1}{\frac{x^2+y^2}{a^2+b^2}} \right)^2 w_0^2}{a^2 b^2} & \end{pmatrix} \cdot \begin{pmatrix} A_{11} & A_{12} & 0 \\ A_{12} & A_{22} & 0 \\ 0 & 0 & A_{66} \end{pmatrix} . \begin{pmatrix} // \text{FullSimplify} \end{pmatrix}$$

$$\left\{ \left\{ \frac{4 (b^2 x^2 + a^2 (-b^2 + y^2))^4 (b^8 x^4 A_{11} + a^4 y^2 (a^4 y^2 A_{22} + b^4 x^2 (2 A_{12} + A_{66}))) w_0^4}{a^8 b^8 (b^2 x^2 + a^2 y^2)^4} \right\} \right\}$$

Flexural Stiffness - D*

$$\left(\begin{array}{c} \left(\frac{2x^2}{\left(\frac{x^2}{a^2} + \frac{y^2}{b^2}\right)^2} + a^2 \left(1 - \frac{1}{\frac{x^2}{a^2} + \frac{y^2}{b^2}} \right) \right) w_0 \\ \hline a^4 \\ \left(\frac{2y^2}{\left(\frac{x^2}{a^2} + \frac{y^2}{b^2}\right)^2} + b^2 \left(1 - \frac{1}{\frac{x^2}{a^2} + \frac{y^2}{b^2}} \right) \right) w_0 \\ \hline b^4 \\ \frac{4a^2 b^2 x y w_0}{(b^2 x^2 + a^2 y^2)^2} \end{array} \right).$$

$$\begin{pmatrix} D_{11} & D_{12} & D_{16} \\ D_{12} & D_{22} & D_{26} \\ D_{16} & D_{26} & D_{66} \end{pmatrix} \cdot \begin{pmatrix} \frac{2x^2}{\left(\frac{x^2}{a^2} + \frac{y^2}{b^2}\right)^2} + a^2 \left(1 - \frac{1}{\frac{x^2}{a^2} + \frac{y^2}{b^2}} \right) w_0 \\ \hline a^4 \\ \frac{2y^2}{\left(\frac{x^2}{a^2} + \frac{y^2}{b^2}\right)^2} + b^2 \left(1 - \frac{1}{\frac{x^2}{a^2} + \frac{y^2}{b^2}} \right) w_0 \\ \hline b^4 \\ \frac{4a^2 b^2 x y w_0}{(b^2 x^2 + a^2 y^2)^2} \end{pmatrix} // \text{FullSimplify}$$

$$\left\{ \left\{ \frac{1}{(a b^3 x^2 + a^3 b y^2)^4} \right. \right. \\ \left. \left. \left(4 (b^4 (b^4 x^4 + a^2 b^2 x^2 (b^2 + 2 y^2) + a^4 (-b^2 y^2 + y^4))^2 D_{11} + a^2 (2 b^2 (b^8 x^8 + 4 a^2 b^6 x^6 y^2 - a^4 b^4 x^4 (b^4 - 6 y^4) + 2 a^6 b^2 x^2 y^2 (b^4 + 2 y^4) + a^8 (-b^4 y^4 + y^8)) D_{12} + a^2 (4 b^6 x y (b^4 x^4 + a^2 b^2 x^2 (b^2 + 2 y^2) + a^4 (-b^2 y^2 + y^4)) D_{16} + (b^4 x^2 (-a^2 + x^2) + a^2 b^2 (a^2 + 2 x^2) y^2 + a^4 y^4)^2 D_{22} + 4 a^2 b^4 x y ((b^4 x^2 (-a^2 + x^2) + a^2 b^2 (a^2 + 2 x^2) y^2 + a^4 y^4) D_{26} + a^2 b^4 x y D_{66})) \right) w_0^2 \right\} \right\}$$

STRAIN ENERGY - U

A* component of 'U'

Integrate[

$$\left\{ \left[\frac{4 (b^2 x^2 + a^2 (-b^2 + y^2))^4 (b^8 x^4 A_{11} + a^4 y^2 (a^4 y^2 A_{22} + b^4 x^2 (2 A_{12} + A_{66}))) w_0^4}{a^8 b^8 (b^2 x^2 + a^2 y^2)^4} \right] \right\},$$

{x, -a, a}] // FullSimplify

$$\left\{ \left\{ \frac{1}{30 a^3 b^8 y^3 (b^2 + y^2)^3} \right. \right. \\ \left(\left(b^5 \left(15 b^{11} y + 1728 b^9 y^3 + 6129 b^7 y^5 + 8184 b^5 y^7 + 4768 b^3 y^9 + 960 b y^{11} + \right. \right. \right. \\ \left. \left. \left. 15 (b^2 + y^2)^3 (b^6 - 24 b^4 y^2 - 144 b^2 y^4 - 64 y^6) \operatorname{ArcTan} \left[\frac{b}{y} \right] \right) A_{11} + \right. \\ 5 a^2 \left(2 b^3 \left(3 b^{11} y - 16 b^9 y^3 - 323 b^7 y^5 - 792 b^5 y^7 - 672 b^3 y^9 - 176 b y^{11} + \right. \right. \\ \left. \left. 3 (b^2 + y^2)^3 (b^6 - 8 b^4 y^2 + 48 b^2 y^4 + 64 y^6) \operatorname{ArcTan} \left[\frac{b}{y} \right] \right) A_{12} + \right. \\ a^2 \left(15 b^{12} y - 32 b^{10} y^3 - 15 b^8 y^5 + 216 b^6 y^7 + 288 b^4 y^9 + 144 b^2 y^{11} + 48 \right. \\ \left. y^{13} + 3 b (b^2 + y^2)^3 (5 b^6 - 24 b^4 y^2 + 48 b^2 y^4 - 64 y^6) \operatorname{ArcTan} \left[\frac{b}{y} \right] \right) A_{22} + \\ b^3 \left(3 b^{11} y - 16 b^9 y^3 - 323 b^7 y^5 - 792 b^5 y^7 - 672 b^3 y^9 - 176 b y^{11} + \right. \\ \left. 3 (b^2 + y^2)^3 (b^6 - 8 b^4 y^2 + 48 b^2 y^4 + 64 y^6) \operatorname{ArcTan} \left[\frac{b}{y} \right] \right) A_{66} \left. \right) \left. \right\} w_o^4 \right\}$$

D* component of ' U '

Integrate[

$$\left\{ \left\{ \frac{1}{(a b^3 x^2 + a^3 b y^2)^4} \right. \right. \\ \left(4 \left(b^4 \left(b^4 x^4 + a^2 b^2 x^2 (b^2 + 2 y^2) + a^4 (-b^2 y^2 + y^4) \right) \right)^2 D_{11} + \right. \\ \left. \left. a^2 \right. \right. \\ \left(2 b^2 \left(b^8 x^8 + 4 a^2 b^6 x^6 y^2 - a^4 b^4 x^4 (b^4 - 6 y^4) + 2 a^6 b^2 x^2 y^2 \right. \right. \\ \left. \left. (b^4 + 2 y^4) + a^8 (-b^4 y^4 + y^8) \right) D_{12} + \right. \\ a^2 \left(4 b^6 x y \left(b^4 x^4 + a^2 b^2 x^2 (b^2 + 2 y^2) + a^4 (-b^2 y^2 + y^4) \right) \right. \\ D_{16} + \left(b^4 x^2 (-a^2 + x^2) + a^2 b^2 (a^2 + 2 x^2) y^2 + a^4 y^4 \right)^2 \\ D_{22} + 4 a^2 b^4 x y \left((b^4 x^2 (-a^2 + x^2) + a^2 b^2 (a^2 + 2 x^2) y^2 + a^4 y^4) D_{26} + \right. \\ \left. \left. a^2 b^4 x y D_{66} \right) \right) \left. \right) w_o^2 \right\}, \{x, -a, a\}] // FullSimplify$$

component D of ' U '

$$\left\{ \left\{ \frac{1}{3 a^3 b^4 y^3 (b^2 + y^2)^3} \right. \right. \\ \left(2 \left(b^4 \left(3 b^8 y - 8 b^6 y^3 - 3 b^4 y^5 + 12 b^2 y^7 + 12 y^9 + 3 b^3 (b^2 + y^2)^3 \operatorname{ArcTan} \left[\frac{b}{y} \right] \right) D_{11} + \right. \right. \\ a^2 \left(-2 b^2 \left(3 b^8 y - 8 b^6 y^3 - 27 b^4 y^5 - 36 b^2 y^7 - \right. \right. \\ \left. \left. 12 y^9 + 3 b^3 (b^2 + y^2)^3 \operatorname{ArcTan} \left[\frac{b}{y} \right] \right) D_{12} + a^2 \right. \\ \left. \left(3 b^8 y + 40 b^6 y^3 + 93 b^4 y^5 + 60 b^2 y^7 + 12 y^9 + 3 b^3 (b^2 + y^2)^3 \operatorname{ArcTan} \left[\frac{b}{y} \right] \right) \right. \\ \left. \left. D_{22} + b^5 \left(3 b^5 y + 8 b^3 y^3 - 3 b y^5 + 3 (b^2 + y^2)^3 \operatorname{ArcTan} \left[\frac{b}{y} \right] \right) D_{66} \right) \right) w_0^2 \right\} \right\}$$

Integrate[

$$\left\{ \left\{ \frac{1}{30 a^3 b^8 y^3 (b^2 + y^2)^3} \right. \right.$$

$$\left(\left(b^5 \left(15 b^{11} y + 1728 b^9 y^3 + 6129 b^7 y^5 + 8184 b^5 y^7 + 4768 b^3 y^9 + \right. \right. \right.$$

$$960 b y^{11} + 15 (b^2 + y^2)^3 (b^6 - 24 b^4 y^2 - 144 b^2 y^4 - 64 y^6) \operatorname{ArcTan}\left[\frac{b}{y}\right] \left. \right) \right.$$

$$A_{11} +$$

$$5 a^2 \left(2 b^3 \left(3 b^{11} y - 16 b^9 y^3 - 323 b^7 y^5 - 792 b^5 y^7 - 672 b^3 y^9 - \right. \right. \right.$$

$$176 b y^{11} + 3 (b^2 + y^2)^3 (b^6 - 8 b^4 y^2 + 48 b^2 y^4 + 64 y^6) \operatorname{ArcTan}\left[\frac{b}{y}\right] \left. \right)$$

$$A_{12} + a^2 \left(15 b^{12} y - 32 b^{10} y^3 - 15 b^8 y^5 + 216 b^6 y^7 + 288 b^4 y^9 + \right. \right. \right.$$

$$144 b^2 y^{11} + 48 y^{13} + 3 b (b^2 + y^2)^3 (5 b^6 - 24 b^4 y^2 + 48 b^2 y^4 - 64 y^6) \operatorname{ArcTan}\left[\frac{b}{y}\right] \left. \right)$$

$$\left. \left. \left. \operatorname{ArcTan}\left[\frac{b}{y}\right]\right) A_{22} + \right.$$

$$b^3 \left(3 b^{11} y - 16 b^9 y^3 - 323 b^7 y^5 - 792 b^5 y^7 - 672 b^3 y^9 - \right. \right. \right.$$

$$176 b y^{11} + 3 (b^2 + y^2)^3 (b^6 - 8 b^4 y^2 + 48 b^2 y^4 + 64 y^6) \operatorname{ArcTan}\left[\frac{b}{y}\right] \left. \right)$$

$$A_{66} \left. \right) \left. w_o^4 \right) \} \} +$$

$$\left\{ \left\{ \frac{1}{3 a^3 b^4 y^3 (b^2 + y^2)^3} \right. \right.$$

$$\left(2 \left(b^4 \left(3 b^8 y - 8 b^6 y^3 - 3 b^4 y^5 + 12 b^2 y^7 + 12 y^9 + 3 b^3 (b^2 + y^2)^3 \operatorname{ArcTan}\left[\frac{b}{y}\right] \right) \right.$$

$$D_{11} +$$

$$a^2 \left(-2 b^2 \left(3 b^8 y - 8 b^6 y^3 - 27 b^4 y^5 - 36 b^2 y^7 - 12 y^9 + \right. \right. \right.$$

$$3 b^3 (b^2 + y^2)^3 \operatorname{ArcTan}\left[\frac{b}{y}\right] \left. \right) D_{12} +$$

$$a^2 \left(3 b^8 y + 40 b^6 y^3 + 93 b^4 y^5 + 60 b^2 y^7 + 12 y^9 + \right. \right. \right.$$

$$3 b^3 (b^2 + y^2)^3 \operatorname{ArcTan}\left[\frac{b}{y}\right] \left. \right) D_{22} +$$

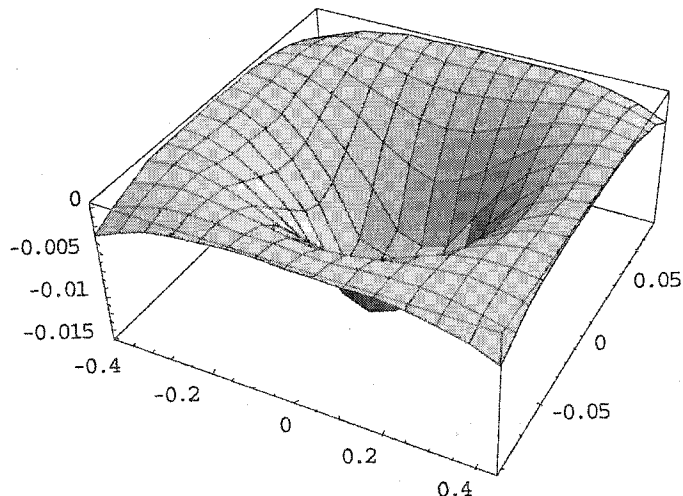
$$b^5 \left(3 b^5 y + 8 b^3 y^3 - 3 b y^5 + 3 (b^2 + y^2)^3 \operatorname{ArcTan}\left[\frac{b}{y}\right] \right) D_{66} \left. \right) \left. w_o^2 \right) \} \},$$

$$\{y, -b, b\} \right] // FullSimplify$$

$$\left\{ \left\{ \frac{1}{90 a^3 b^3} (-60 (5 b^4 (-4 + 3 \pi) D_{11} + a^2 (-2 b^2 (28 + 3 \pi) D_{12} - a^2 (20 + 9 \pi) D_{22} + b^2 (2 + 3 \pi) D_{66})) w_0^2 + (18 b^4 (441 + 120 \text{Catalan} - 205 \pi) A_{11} + a^2 (10 b^2 (-1054 + 144 \text{Catalan} + 423 \pi) A_{12} + 18 a^2 (441 + 120 \text{Catalan} - 50 \pi) A_{22} + 5 b^2 (-1054 + 144 \text{Catalan} + 423 \pi) A_{66})) w_0^4) \right\} \right\}$$

Catalan is Catalan's constant, with numerical value ≈ 0.915966

$$\text{Plot3D}\left[\left(0.01 \left(1 - \frac{x^2}{0.2} - \frac{y^2}{0.009056}\right)\right) + \left(0.01 \log\left(\frac{x^2}{0.2} + \frac{y^2}{0.009056}\right)\right), \{x, -0.4472135, 0.447213\}, \{y, -0.09516301, 0.09516301\}\right]$$



Appendix C

Classical Lamination Theory

Properties for the AS4 Carbon Fiber

Major Modulus	Minor Modulus	Major Poisson's Ratio	Minor Poisons Ratio	Shear Modulus
1.25E+11	9.50E+09	0.3	0.022727	6.50E+09

Transformed Stiffness Matrix

Theta = 0

$$Q = \begin{array}{cc|cc} Q_{11} & Q_{22} & Q_{12} & Q_{66} \\ 1.26261E+11 & 9565217391 & 2869565217 & 6500000000 \\ \hline 1.26261E+11 & 2869565217 & 0 & 0 \\ 2869565217 & 9565217391 & 0 & 6500000000 \\ 0 & 0 & 6500000000 & \end{array}$$

C11	C22	C12	C21	C66	Angle Tata	Thickness
1.263E+11	9565217391	2869565217	2.87E+09	6.5E+09	0	0.0001651
Q16	Q26					
0	0					

Major Modulus	Minor Modulus	Major Poison's	Minor Poisons	Shear Modulus
1.25E+11	9.50E+09	0.3	0.02273	6.50E+09

Transformed Stiffness Matrix

Theta = 90

$$Q = \begin{array}{cc|cc} Q_{11} & Q_{22} & Q_{12} & Q_{66} \\ 9565217391 & 1.26261E+11 & 2869565217 & 6500000000 \\ \hline 9565217391 & 2869565217 & 0 & 0 \\ 2869565217 & 1.26261E+11 & 0 & 6500000000 \\ 0 & 0 & 6500000000 & \end{array}$$

C11	C22	C12	C21	C66	Angle Tata	Thickness
1.263E+11	9565217391	2869565217	2.87E+09	6.5E+09	1.5707963	0.0001651
Q16	Q26					
0.000E+00	0					

Major Modulus	Minor Modulus	Major Poisons	Minor Poisons	Shear Modulus
1.25E+11	9.50E+09	0.3	0.02273	6.50E+09

Transformed Stiffness Matrix

Theta = 45

$$Q = \begin{vmatrix} Q_{11} & Q_{22} & Q_{12} & Q_{66} \\ 41891304348 & 41891304348 & 35391304348 & 32521739130 \\ 41891304348 & 35391304348 & 29173913043 & \\ 35391304348 & 41891304348 & 29173913043 & \\ 29173913043 & 29173913043 & 32521739130 & \end{vmatrix}$$

C11	C22	C12	C21	C66	Angle Tata	Thickness
1.263E+11	9565217391	2869565217	2.87E+09	6.5E+09	0.78539816	0.0001651
Q16	Q26					
2.917E+10	2.9174E+10					

Major Modulus	Minor Modulus	Major Poisons	Minor Poisons	Shear Modulus
1.25E+11	9.50E+09	0.3	0.022727	6.50E+09

Transformed Stiffness Matrix

Theta = -45

$$Q = \begin{vmatrix} Q_{11} & Q_{22} & Q_{12} & Q_{66} \\ 41891304348 & 41891304348 & 35391304348 & 32521739130 \\ 41891304348 & 35391304348 & -29173913043 & \\ 35391304348 & 41891304348 & -29173913043 & \\ -29173913043 & -29173913043 & 32521739130 & \end{vmatrix}$$

C11	C22	C12	C21	C66	Angle Tata	Thickness
1.263E+11	9565217391	2869565217	2.87E+09	6.5E+09	-0.78539816	0.0001651
Q16	Q26					
-2.917E+10	-2.917E+10					

Thickness of the layers for AS4 Carbon-Fiber Reinforced			
	T.B	T.D	T.A
-0.0013208	-4.0887E-07	7.6055E-10	0.0001651
-0.0011557	-3.54354E-07	5.71538E-10	0.0001651
-0.0009906	-2.99838E-07	4.09527E-10	0.0001651
-0.0008255	-2.45322E-07	2.74518E-10	0.0001651
-0.0006604	-1.90806E-07	1.66511E-10	0.0001651
-0.0004953	-1.3629E-07	8.55057E-11	0.0001651
-0.0003302	-8.1774E-08	3.15021E-11	0.0001651
-0.0001651	-2.7258E-08	4.5003E-12	0.0001651
0.0001651	2.7258E-08	4.5003E-12	0.0001651
0.0003302	8.1774E-08	3.15021E-11	0.0001651
0.0004953	1.3629E-07	8.55057E-11	0.0001651
0.0006604	1.90806E-07	1.66511E-10	0.0001651
0.0008255	2.45322E-07	2.74518E-10	0.0001651
0.0009906	2.99838E-07	4.09527E-10	0.0001651
0.0011557	3.54354E-07	5.71538E-10	0.0001651
0.0013208	4.0887E-07	7.6055E-10	0.0001651

Calculated Stiffnesses for the AS4 Carbon Fiber

$[(45, -45, 0, 0), z] s$

$$A = \begin{vmatrix} 222095391.3 & 50534957 & 0 \\ 50534956.52 & 67963774 & 0 \\ 0 & 0 & 51539913 \end{vmatrix}$$

$$B = \begin{vmatrix} 1.81899E-12 & 9.095E-13 & 0 \\ 9.09495E-13 & -1.82E-12 & 0 \\ 0 & 0 & -2.73E-12 \end{vmatrix}$$

$$D = \begin{vmatrix} 104.8493649 & 38.75317 & 5.2516515 \\ 38.75317012 & 48.831749 & 5.2516515 \\ 5.25165146 & 5.2516515 & 37.465433 \end{vmatrix}$$

$[(0,0,45, -45)_2] s$

$$A = \begin{vmatrix} 2.22E+08 & 50534957 & 0 \\ 50534957 & 67963774 & 0 \\ 0 & 0 & 51539913 \end{vmatrix}$$

$$B = \begin{vmatrix} -3.64E-12 & 1.251E-12 & 0 \\ 1.251E-12 & 1.819E-12 & 0 \\ 0 & 0 & 0 \end{vmatrix}$$

$$D = \begin{vmatrix} 153.44945 & 20.01941 & 3.15099088 \\ 20.01941 & 30.210692 & 3.15099088 \\ 3.1509909 & 3.1509909 & 22.4759203 \end{vmatrix}$$

$[(0,45, -45,0)_2] s$

$$A = \begin{vmatrix} 222095391.3 & 50534956.52 & 0 \\ 50534956.52 & 67963773.91 & 0 \\ 0 & 0 & 51539913.04 \end{vmatrix}$$

$$B = \begin{vmatrix} 0 & -3.29692E-12 & 0 \\ -3.29692E-12 & -4.54747E-13 & 0 \\ 0 & 0 & 1.59162E-12 \end{vmatrix}$$

$$D = \begin{vmatrix} 132.1869109 & 28.21543014 & 4.201321168 \\ 28.21543014 & 38.35740483 & 4.201321168 \\ 4.201321168 & 4.201321168 & 29.03383206 \end{vmatrix}$$

$[(45, -45,0,90)_2] s$

$$A = \begin{vmatrix} 1.45E+08 & 50534957 & 0 \\ 50534957 & 145029583 & 0 \\ 0 & 0 & 51539913 \end{vmatrix}$$

$$B = \begin{vmatrix} 1.819E-12 & 9.095E-13 & 0 \\ 9.095E-13 & -5.46E-12 & 0 \\ 0 & 0 & -2.7285E-12 \end{vmatrix}$$

$$D = \begin{vmatrix} 83.142539 & 38.75317 & 5.25165146 \\ 38.75317 & 70.538575 & 5.25165146 \\ 5.2516515 & 5.2516515 & 37.4654328 \end{vmatrix}$$

$[(0,90,45, -45)_2] \text{ s}$

$$A = \begin{vmatrix} 145029582.6 & 50534957 & 0 \\ 50534956.52 & 145029583 & 0 \\ 0 & 0 & 51539913 \end{vmatrix}$$

$$B = \begin{vmatrix} -1.45519E-11 & 1.251E-12 & 0 \\ 1.25056E-12 & 1.364E-12 & 0 \\ 0 & 0 & 0 \end{vmatrix}$$

$$D = \begin{vmatrix} 102.3333725 & 20.01941 & 3.1509909 \\ 20.01941016 & 81.326767 & 3.1509909 \\ 3.150990876 & 3.1509909 & 22.47592 \end{vmatrix}$$

$[(45, -45, 90, 0)_2] \text{ s}$

$$A = \begin{vmatrix} 145029582.6 & 50534956.52 & 0 \\ 50534956.52 & 145029582.6 & 0 \\ 0 & 0 & 51539913.04 \end{vmatrix}$$

$$B = \begin{vmatrix} 0 & 9.09495E-13 & 0 \\ 9.09495E-13 & -3.63798E-12 & 0 \\ 0 & 0 & -177.177065 \end{vmatrix}$$

$$D = \begin{vmatrix} 70.53857535 & 38.75317012 & 5.25165146 \\ 38.75317012 & 83.14253886 & 5.25165146 \\ 5.25165146 & 5.25165146 & 37.46543283 \end{vmatrix}$$

$[(45, -45, 45, -45)_2] \text{ s}$

$$A = \begin{vmatrix} 110660070 & 93489669.57 & 0 \\ 82829952.2 & 110660069.6 & 0 \\ 0 & 0 & 85909426 \end{vmatrix}$$

$$B = \begin{vmatrix} -1.819E-12 & 9.09495E-13 & 0 \\ 9.0949E-13 & -3.63798E-12 & 9.095E-13 \\ 0 & 9.09495E-13 & 9.095E-13 \end{vmatrix}$$

$$D = \begin{vmatrix} 64.3492967 & 54.36463676 & 8.4026423 \\ 54.2677825 & 64.3492967 & 8.4026423 \\ 8.40264234 & 8.402642336 & 49.956693 \end{vmatrix}$$

$[(0,90,0,90)_z]$ s

$$A = \begin{vmatrix} 179399095.7 & 7580243.478 & 0 \\ 7580243.478 & 179399095.7 & 0 \\ 0 & 0 & 17170400 \end{vmatrix}$$

$$B = \begin{vmatrix} 1.45519E-11 & -3.41061E-13 & 0 \\ -3.41061E-13 & 1.36424E-12 & 0 \\ 0 & 0 & 0 \end{vmatrix}$$

$$D = \begin{vmatrix} 121.1266147 & 4.407943521 & 0 \\ 4.407943521 & 87.51604532 & 0 \\ 0 & 0 & 9.984659945 \end{vmatrix}$$

Properties for the IM7 Carbon Fiber

Major Modulus	Minor Modulus	Major Poisson's	Minor Poisson's	Shear Modulus
2.55E+11	1.47E+10	0.32	0.018447	2.48E+10

Transformed Stiffness Matrix

Theta = 0

Q11	Q22	Q12	Q66
2.56514E+11	14787290244	4731932878	248000000000

$$Q = \begin{vmatrix} 2.56514E+11 & 4731932878 & 0 \\ 4731932878 & 14787290244 & 0 \\ 0 & 0 & 248000000000 \end{vmatrix}$$

C11	C22	C12	C21	C66	Angle Tata	Thickness
2.57E+11	1.48E+10	4.73E+09	4.73E+09	2.48E+10	0	0.000098425
Q16	Q26					
0	0					

Major Modulus	Minor Modulus	Major Poisson's	Minor Poisson's	Shear Modulus
2.55E+11	1.47E+10	0.32	0.01845	2.48E+10

Transformed Stiffness Matrix

Theta = 90

Q11	Q22	Q12	Q66
14787290244	2.56514E+11	4731932878	24800000000

$$Q = \begin{vmatrix} 14787290244 & 4731932878 & 0 \\ 4731932878 & 2.56514E+11 & 0 \\ 0 & 0 & 24800000000 \end{vmatrix}$$

C11	C22	C12	C21	C66	Angle Tata	Thickness
2.57E+11	1.48E+10	4.73E+09	4.73E+09	2.48E+10	1.570796	0.000098425
Q16	Q26					
0.00	0					

Major Modulus	Minor Modulus	Major Poisson's	Minor Poisson's	Shear Modulus
2.55E+11	1.47E+10	0.32	0.01845	2.48E+10

Transformed Stiffness Matrix

Theta = 45

Q11	Q22	Q12	Q66
94991343630	94991343630	70191343630	65459410752

$$Q = \begin{vmatrix} 94991343630 & 70191343630 & 60431732069 \\ 70191343630 & 94991343630 & 60431732069 \\ 60431732069 & 60431732069 & 65459410752 \end{vmatrix}$$

C11	C22	C12	C21	C66	Angle Tata	Thickness
2.57E+11	1.48E+10	4.73E+09	4.73E+09	2.48E+10	0.79	0.000098425
Q16	Q26					
6.04E+10	6.04E+10					

Major Modulus	Minor Modulus	Major Poisson's	Minor Poisson's	Shear Modulus
2.55E+11	1.47E+10	0.32	0.01845	2.48E+10

Transformed Stiffness Matrix

Theta = -45

$$Q = \begin{vmatrix} Q_{11} & Q_{22} & Q_{12} & Q_{66} \\ 94991343630 & 94991343630 & 70191343630 & 65459410752 \\ 94991343630 & 70191343630 & -60431732069 & \\ 70191343630 & 94991343630 & -60431732069 & \\ -60431732069 & -60431732069 & 65459410752 & \end{vmatrix}$$

C11	C22	C12	C21	C66	Angle Tata	Thickness
2.57E+11	1.48E+10	4.73E+09	4.73E+09	2.48E+10	-0.7854	0.000098425
Q16	Q26					
-6.04E+10	-6E+10					

Thickness of the layers for IM-7			
	T.B	T.D	T.A
-0.0007874	-1.45312E-07	1.6114E-10	0.000098425
-0.000688975	-1.25937E-07	1.21093E-10	0.000098425
-0.00059055	-1.06562E-07	8.67676E-11	0.000098425
-0.000492125	-8.71873E-08	5.81629E-11	0.000098425
-0.0003937	-6.78124E-08	3.52791E-11	0.000098425
-0.000295275	3.87499E-08	1.81163E-11	0.000098425
-0.00019685	-2.90624E-08	6.67443E-12	0.000098425
-0.000098425	-9.68748E-09	9.5349E-13	0.000098425
0.000098425	9.68748E-09	9.5349E-13	0.000098425
0.00019685	2.90624E-08	6.67443E-12	0.000098425
0.000295275	4.84374E-08	1.81163E-11	0.000098425
0.0003937	6.78124E-08	3.52791E-11	0.000098425
0.000492125	8.71873E-08	5.81629E-11	0.000098425
0.00059055	1.06562E-07	8.67676E-11	0.000098425
0.000688975	1.25937E-07	1.21093E-10	0.000098425
0.0007874	1.45312E-07	1.6114E-10	0.000098425

Properties for the E-Glass

Major Modulus	Minor Modulus	Major Poisson's	Minor Poisson's	Shear Modulus
3.90E+10	9.50E+09	0.3	0.073077	6.50E+09

Transformed Stiffness Matrix

Theta = 0

$$Q = \begin{vmatrix} Q_{11} & Q_{22} & Q_{12} & Q_{66} \\ 39874164373 & 9712937475 & 2913881243 & 6500000000 \\ 39874164373 & 2913881243 & 9712937475 & 0 \\ 2913881243 & 9712937475 & 0 & 6500000000 \\ 0 & 0 & 0 & 6500000000 \end{vmatrix}$$

C11	C22	C12	C21	C66	Angle Tata	Thickness
3.987E+10	9.71E+09	2.91E+09	2.91E+09	6.5E+09	0	0.0002667
Q16	Q26					
0	0					

Major Modulus	Minor Modulus	Major Poisson's	Minor Poisson's	Shear Modulus
3.90E+10	9.50E+09	0.3	0.073077	6.50E+09

Transformed Stiffness Matrix

Theta = 90

$$Q = \begin{vmatrix} Q_{11} & Q_{22} & Q_{12} & Q_{66} \\ 9712937475 & 39874164373 & 2913881243 & 6500000000 \\ 9712937475 & 2913881243 & 39874164373 & 0 \\ 2913881243 & 39874164373 & 0 & 6500000000 \\ 0 & 0 & 0 & 6500000000 \end{vmatrix}$$

C11	C22	C12	C21	C66	Angle Tata	Thickness
3.987E+10	9.71E+09	2.91E+09	2.91E+09	6.5E+09	1.57079633	0.0002667
Q16	Q26					
0.00	0					

Major Modulus	Minor Modulus	Major Poisons	Minor Poisons	Shear Modulus
3.90E+10	9.50E+09	0.3	0.073077	6.50E+09

Transformed Stiffness Matrix

Theta = 45

Q11	Q22	Q12	Q66
20353716083	20353716083	13853716083	10939834841

$$Q = \begin{vmatrix} & 20353716083 & 13853716083 & 7540306724 \\ 20353716083 & & 20353716083 & 7540306724 \\ & 7540306724 & 7540306724 & 10939834841 \end{vmatrix}$$

C11	C22	C12	C21	C66	Angle Tata	Thickness
3.987E+10	9.71E+09	2.91E+09	2.91E+09	6.5E+09	0.78539816	0.0002667
Q16	Q26					
7.54E+09	7.54E+09					

Major Modulus	Minor Modulus	Major Poisons	Minor Poisons	Shear Modulus
3.90E+10	9.50E+09	0.3	0.073077	6.50E+09

Transformed Stiffness Matrix

Theta = -45

Q11	Q22	Q12	Q66
20353716083	20353716083	13853716083	10939834841

$$Q = \begin{vmatrix} & 20353716083 & 13853716083 & -7540306724 \\ 13853716083 & & 20353716083 & -7540306724 \\ & -7540306724 & -7540306724 & 10939834841 \end{vmatrix}$$

C11	C22	C12	C21	C66	Angle Tata	Thickness
3.987E+10	9.71E+09	2.91E+09	2.91E+09	6.5E+09	-0.7853982	0.0002667
Q16	Q26					
-7.54E+09	-7.5E+09					

Thickness of the layers for E-Glass			
	T.B	T.D	T.A
-0.0021336	-1.06693E-06	3.20594E-09	0.0002667
-0.0018669	-9.24676E-07	2.4092E-09	0.0002667
-0.0016002	-7.82418E-07	1.72628E-09	0.0002667
-0.0013335	-6.4016E-07	1.15717E-09	0.0002667
-0.0010668	-4.97902E-07	7.01893E-10	0.0002667
-0.0008001	-3.55644E-07	3.60431E-10	0.0002667
-0.0005334	-2.13387E-07	1.32791E-10	0.0002667
-0.0002667	-7.11289E-08	1.89701E-11	0.0002667
0.0002667	7.11289E-08	1.89701E-11	0.0002667
0.0005334	2.13387E-07	1.32791E-10	0.0002667
0.0008001	3.55644E-07	3.60431E-10	0.0002667
0.0010668	4.97902E-07	7.01893E-10	0.0002667
0.0013335	6.4016E-07	1.15717E-09	0.0002667
0.0016002	7.82418E-07	1.72628E-09	0.0002667
0.0018669	9.24676E-07	2.4092E-09	0.0002667
0.0021336	1.06693E-06	3.20594E-09	0.0002667

AS4/E-Glass Hybrid & IM7/E-Glass Hybrid Properties

Thickness for the layers of Hybrid (AS-4, E-Glass)			
	T.B	T.D	T.A
-0.00173	-8.5016E-07	2.03728E-09	0.0002667
-0.00146	-7.07902E-07	1.41398E-09	0.0002667
-0.00119	-5.65644E-07	9.04498E-10	0.0002667
-0.00093	-4.23386E-07	5.08837E-10	0.0002667
-0.00066	-1.90806E-07	1.66511E-10	0.0001651
-0.0005	-1.3629E-07	8.55057E-11	0.0001651
-0.00033	-8.1774E-08	3.15021E-11	0.0001651
-0.00017	-2.7258E-08	4.5003E-12	0.0001651
0.000165	2.7258E-08	4.5003E-12	0.0001651
0.00033	8.1774E-08	3.15021E-11	0.0001651
0.000495	1.3629E-07	8.55057E-11	0.0001651
0.00066	1.90806E-07	1.66511E-10	0.0001651
0.000927	4.23386E-07	5.08837E-10	0.0002667
0.001194	5.65644E-07	9.04498E-10	0.0002667
0.001461	7.07902E-07	1.41398E-09	0.0002667
0.001727	8.5016E-07	2.03728E-09	0.0002667

Thickness for the layers of Hybrid (IM-7, E-Glass)			
	T.B	T.D	T.A
-0.0014605	-7.07902E-07	1.41398E-09	0.0002667
-0.0011938	-5.65644E-07	9.04498E-10	0.0002667
-0.0009271	-4.23386E-07	5.08837E-10	0.0002667
-0.0006604	-2.81128E-07	2.26996E-10	0.0002667
-0.0003937	-6.78124E-08	3.52791E-11	0.000098425
-0.000295275	-4.84374E-08	1.81163E-11	0.000098425
-0.00019685	-2.90624E-08	6.67443E-12	0.000098425
-0.000098425	-9.68748E-09	9.5349E-13	0.000098425
0.000098425	9.68748E-09	9.5349E-13	0.000098425
0.00019685	2.90624E-08	6.67443E-12	0.000098425
0.000295275	4.84374E-08	1.81163E-11	0.000098425
0.0003937	6.78124E-08	3.52791E-11	0.000098425
0.0006604	2.81128E-07	2.26996E-10	0.0002667
0.0009271	4.23386E-07	5.08837E-10	0.0002667
0.0011938	5.65644E-07	9.04498E-10	0.0002667
0.0014605	7.07902E-07	1.41398E-09	0.0002667

Calculated stiffnesses for Hybrid Composites

$[(45, -45, 0, 90)_2]_S$ AS4/E-Glass

$$\begin{aligned}
 A &= \begin{vmatrix} 120677895.7 & 43155151.09 & 5.58794E-09 \\ 43155151.09 & 120677895.7 & 5.58794E-09 \\ 5.58794E-09 & 5.58794E-09 & 44374772.33 \end{vmatrix} \\
 B &= \begin{vmatrix} -1.81899E-12 & 9.09495E-13 & 0 \\ 9.09495E-13 & 0 & 0 \\ 0 & 0 & 0 \end{vmatrix} \\
 D &= \begin{vmatrix} 83.87383704 & 40.63574669 & 4.708756607 \\ 40.63574669 & 73.83176643 & 4.708756607 \\ 4.708756607 & 4.708756607 & 36.91530843 \end{vmatrix}
 \end{aligned}$$

$[(45, -45, 90, 0) \text{ z}] \text{ s AS4/E-Glass}$

$$A = \begin{vmatrix} 120677895.7 & 43155151.09 & 5.58794E-09 \\ 43155151.09 & 120677895.7 & 5.58794E-09 \\ 5.58794E-09 & 5.58794E-09 & 44374772.33 \end{vmatrix}$$

$$B = \begin{vmatrix} 1.81899E-12 & 9.09495E-13 & 0 \\ 9.09495E-13 & -5.45697E-12 & 0 \\ 0 & 0 & 0 \end{vmatrix}$$

$$D = \begin{vmatrix} 73.83176643 & 40.63574669 & 4.708756607 \\ 40.63574669 & 83.88818581 & 4.708756607 \\ 4.708756607 & 4.708756607 & 36.91530843 \end{vmatrix}$$

$[(-45, 45, 90, 0) \text{ z}] \text{ s AS4/E-Glass}$

$$A = \begin{vmatrix} 120677895.7 & 43155151.09 & 0.00E+00 \\ 43155151.09 & 120677895.7 & 0.00E+00 \\ 0.00E+00 & 0.00E+00 & 44374772.33 \end{vmatrix}$$

$$B = \begin{vmatrix} 1.81899E-12 & 9.09495E-13 & 0 \\ 9.09495E-13 & -5.45697E-12 & 0 \\ 0 & 0 & 0 \end{vmatrix}$$

$$D = \begin{vmatrix} 73.83176643 & 40.63574669 & -4.708756607 \\ 40.63574669 & 83.88818581 & -4.708756607 \\ -4.708756607 & -4.708756607 & 36.91530843 \end{vmatrix}$$

$[(0, 90, 0, 90) \text{ z}] \text{ s AS4/E-Glass}$

$$A = \begin{vmatrix} 142599068.1 & 10007178.76 & 0 \\ 10007178.76 & 142599068.1 & 0 \\ 0 & 0 & 22453600 \end{vmatrix}$$

$$B = \begin{vmatrix} 3.63798E-12 & -6.82121E-13 & 0 \\ -6.82121E-13 & -8.18545E-12 & 0 \\ 0 & 0 & 9.09495E-13 \end{vmatrix}$$

$$D = \begin{vmatrix} 107.8929991 & 10.00090071 & 0 \\ 10.00090071 & 79.00155331 & 0 \\ 0 & 0 & 22.32800833 \end{vmatrix}$$

$[(0,90,0,90)_2]$ s IM7/E-Glass

A=	159710924.3	9942980.968	0
	9942980.968	159710924.3	0
	0	0	33395920
B=	0	6.82121E-13	0
	6.82121E-13	-4.54747E-12	0
	0	0	-4.54747E-13
D=	65.80302332	6.125772268	0
	6.125772268	46.20375731	0
	0	0	14.24426802

$[(90,0,45, -45)_2]$ s IM7/E-Glass

A=	138966898.4	47384966.79	0
	47384966.79	138966898.4	0
	0	0	59020555.82
B=	-4.54747E-12	-2.27374E-13	0
	-2.27374E-13	3.63798E-12	0
	0	0	4.54747E-13
D=	47.11353626	11.82524198	1.64726324
	11.82524198	60.12374932	1.64726324
	1.64726324	1.64726324	16.62901555

Note:

T.A, T.B, and T.D values were used to calculate the matrices associated with each stacking sequence namely $[A]$, $[B]$, and $[D]$.

$$T.A = \sum_{k=1}^n (h_k - h_{k-1})$$

$$T.B = \frac{1}{2} \sum_{k=1}^n (h_k^2 - h_{k-1}^2)$$

$$T.D = \frac{1}{3} \sum_{k=1}^n (h_k^3 - h_{k-1}^3)$$

Where n is the total number of layers.

The following equation is used to determine transverse Poisson's ratios from other material constants.

$$\nu_{21}E_{11} = \nu_{12}E_{22}$$

The components of the reduced stiffness matrix for an orthotropic material in terms of engineering constants are as follows:

$$C_{11} = \frac{E_{11}}{1 - \nu_{12}\nu_{21}} \quad C_{12} = \frac{\nu_{12}E_{22}}{1 - \nu_{12}\nu_{21}} \quad C_{22} = \frac{E_{22}}{1 - \nu_{12}\nu_{21}} \quad C_{66} = G_{12}$$

The transformed reduced stiffness matrix in terms of engineering constants is:

$$Q_{11} = C_{11} \cos^4 \theta + 2(C_{12} + 2C_{66}) \sin^2 \theta \cos^2 \theta + C_{22} \sin^4 \theta$$

$$Q_{22} = C_{11} \sin^4 \theta + 2(C_{12} + 2C_{66}) \sin^2 \theta \cos^2 \theta + C_{22} \cos^4 \theta$$

$$Q_{12} = (C_{11} + C_{22} - 4C_{66}) \sin^2 \theta \cos^2 \theta + C_{12} (\sin^4 \theta + \cos^4 \theta)$$

$$Q_{66} = (C_{11} + C_{22} - 2C_{12} - 2C_{66}) \sin^2 \theta \cos^2 \theta + C_{66} (\sin^4 \theta + \cos^4 \theta)$$

$$Q_{16} = (C_{11} - C_{12} - 2C_{66}) \sin \theta \cos^3 \theta + (C_{12} - C_{22} + 2C_{66}) \sin^3 \theta \cos \theta$$

$$Q_{26} = (C_{11} - C_{12} - 2C_{66}) \sin^3 \theta \cos \theta + (C_{12} - C_{22} + 2C_{66}) \sin \theta \cos^3 \theta$$

Associated matrices for corresponding composite laminates:

[A]: Extensional or membrane stiffness

[D]: Flexural or bending stiffness

[B]: Coupling between membrane and bending behavior

Component of extensional matrix [A]

$$A = \begin{bmatrix} A_{11} & A_{12} & A_{16} \\ A_{21} & A_{22} & A_{26} \\ A_{16} & A_{26} & A_{66} \end{bmatrix} \quad \text{Where } A_{12} = A_{21}$$

Component of bending matrix [D]

$$D = \begin{bmatrix} D_{11} & D_{12} & D_{16} \\ D_{21} & D_{22} & D_{26} \\ D_{16} & D_{26} & D_{66} \end{bmatrix} \quad \text{Where } D_{12} = D_{21}$$

Component of coupling matrix [B]

$$B = \begin{bmatrix} B_{11} & B_{12} & B_{16} \\ B_{21} & B_{22} & B_{26} \\ B_{16} & B_{26} & B_{66} \end{bmatrix} \quad \text{Where } B_{12} = B_{21}$$